The Emission and Application of Patterned Electromagnetic Energy on Biological Systems

by

Nirosha J. Murugan

Thesis submitted in partial fulfillment

of the requirements for the degree of

Doctor of Philosophy (Ph.D.) in Biomolecular Sciences

The Faculty of Graduate Studies

Laurentian University

Sudbury, Ontario, Canada

THESIS DEFENCE COMMITTEE/COMITÉ DE SOUTENANCE DE THÈSE
Laurentian Université/Université Laurentienne
Faculty of Graduate Studies/Faculté des études supérieures

Title of Thesis Titre de la thèse	The Emission and Application of Patterned Electromagnetic Energy on Biological Systems
Name of Candidate Nom du candidat	Murugan, Nirosha
Degree Diplôme	Doctor of Philosophy
Department/Program Département/Programme	Biomolecular Sciences
Date of Defence Date de la soutenance	March 31, 2017

APPROVED/APPROUVÉ

Thesis Examiners/Examinateurs de thèse:

Dr. Michael Persinger
(Supervisor/Directeur(trice) de thèse)

Dr. Rob Lafrenie
(Committee member/Membre du comité)

Dr. Abdelwahab Omri
(Committee member/Membre du comité)

Dr. Irena Cosic
(External Examiner/Examinateur externe)

Dr. John Lewko
(Internal Examiner/Examinateur interne)

Approved for the Faculty of Graduate Studies
Approuvé pour la Faculté des études supérieures
Dr. David Lesbarrères
Monsieur David Lesbarrères
Dean, Faculty of Graduate Studies
Doyen, Faculté des études supérieures

ACCESSIBILITY CLAUSE AND PERMISSION TO USE

Abstract

From the assembly of intricate biomolecules to the construction of tissues and organs from homogenous embryonic cells, patterns permeate throughout biological systems. Whereas molecules govern the multiform signalling pathways necessary to direct anatomy and physiology, biophysical correlates are inextricably paired to each and every chemical reaction – yielding a constant interplay between matter and energy. Electromagnetic energies represented as propagating photons or electromagnetic fields have shown to contain complex information that is specific to their paired molecular events. The central aim of this thesis was to determine whether these biophysical signatures or patterns can be obtained from biomolecules and subsequently be used in lieu of the chemical itself within a molecular cascade to elicit desired effects within biological systems. The findings presented here show that using a novel bioinformatics tool, namely the Cosic Resonant Recognition Model (RRM), biomolecules (proteins) can recognize their particular targets and vice versa by dynamic electromagnetic resonance. We also show using fundamental units of energies that this dynamic electromagnetic resonance is within the visible spectrum and can be used to define molecular pathways such as the ERK-MAP pathway, or distinctive viral proteins that mark certain pathogens such as Zika or Ebola viruses. Further findings presented herein show that these electromagnetic patterns derived from biomolecules can be detected using modern technologies such as photomultiplier tubes, and as every signature is unique to that system, can be used to identify insidious systems such as cancers from healthy populations. Furthermore, it is now possible to capture these unique electromagnetic signatures of biomolecules, parse the signals from the noise, and re-apply these patterns

back onto systems to elicit effects such as altered proliferation rates of cancers or regenerative systems. The series of theoretical models and investigations outlined here clearly profiles the predominant electronic nature of the living matrix and its constituents, which lays the groundwork for reshaping our knowledge of cellular mechanisms that ultimately drive physiology, medicine and the development of effective diagnostic, preventative or therapeutic tools.

Keywords: Cosic Resonance Recognition Model, Biophoton, Electromagnetic Fields, Spectral Analysis, Phototherapy, Cancer, Planaria

Acknowledgements

I would like to express my special appreciation and thanks to my supervisor and mentor Dr. Michael A. Persinger for giving me the key to open the doors to critical thinking, discovery, and most importantly academic freedom. Your never ending efforts to integrate the natural sciences and the endless fight in front and behind the scenes to help students like me get the academic freedom to pursue the most challenging ideas/concepts that develop our society will be cherished and will never be forgotten.

I would also like to give special thanks to my thesis committee members, Dr. R.M. Lafrenie and Dr. A. Omri and internal & external reviewers Dr. Irena Cosic and Dr. J.H. Lewko for your comments and guidance in the development of my dissertation and academic progress. Dr. Lafrenie, you have offered me not just your lab to explore the abstract but also advice on how to flourish within the scientific community, and for that I am forever grateful.

To the Neuroscience Research Group (NRG) I owe my deepest gratitude. Each and everyone one of you (past/present) have helped shape me as a scientist and as an academic explorer. Thank you for working with me, laughing with me, discussing ideas, and critically evaluating my work. You are a special group of people who will help make this world be a better and more effective place. Specifically, I would like to thank Dr. Linda St. Pierre, thank you for being there for me, “ripping the Band-Aid off”, and fighting the close-minded, giving us the opportunity to explore and discover. You and Dr. Persinger are the reason I am continue this scholarly adventure, thank you. The most important

NRG member, Nicolas Rouleau, thank you for being my partner in this scientific exploration. Your dedication, persistence and unbelievable intellect has pushed me and this dissertation to be the best it/I can be. Thank you. You will always be my complementary spin and fill my orbital shell.

Lastly, I would not be here today, with this Doctorate without the early academic foundation laid by my grandfather Dr. K. Arumuguthas. Thank you for the many decades of patience allowing me to grow and learn. Thank you also to my loving parents, Mrs. Nirmala Murugan and Mr. Murugan Palaniandy and my genius brother, Kavinaath Murugan. It is because of your sacrifices and support that I am successful today.

Without such a team behind me, I doubt that I would be in this place today. Thank you.

Table of Contents

List of Tables

List of Figures

List of Abbreviations

Abbreviation	Meaning
4D	Four dimensional
AsPC-1	Pancreatic cell line
B16-BL6	Murine melanoma cell line
cFOS	Proto-oncogene
CRAF	proto-oncogene serine/threonine-protein kinase
CREB	CAMP responsive element binding protein
Cz	longitudinal fissure, central region
DAC	Digital to analogue converter
EIIP	Electron-ion interaction pseudopotential
ELF	Extremely low frequency
EM	Electromagnetic
EMF	Electromagnetic field
ERK	Extracellular signal regulated kinases
ERK1	Extracellular signal–regulated kinases 1
ERK2	Extracellular signal–regulated kinases 2
HBL100	Epithelial cell line
HEK-293	Human embryonic kidney cells 293
HRas	Human renin-angiotensin system protein
IR	Infrared
JAK	Janus kinase
LED	Light emitting diode
LTP	Long term potentiation
MAPK	Mitogen-activated protein kinases
MCF-7	Breast cancer cell line
MDA-MB-231	Breast cancer cell line
MEK1	Mitogen-activated protein kinase 1

MEK2	Mitogen-activated protein kinase 2
NCBI	National Center for Biotechnology Information
PET	Positron emission tomography
PLA2	Phospholipases A2
PMT	Photomultiplier tube
QEEG	Quantitative electroencephalography
RRM	Resonant recognition model
SPD	Spectral profile density
STAT	Signal transducer and activator of transcription
TRK	Tyrosine kinases
UV	Ultraviolet
VEGF	Vascular endothelial growth factor
ZV	Zika virus

Scientific Notation

A	Ampere
B	Strength of magnetic field
c	Speed of light
cc	Cubic centimeter
D	Dalton
DU	Dobson unit
E	Energy
eV	Electron volt
f	Frequency
f_{rrm}	Resonant Recognition Frequency
G-	Giga-
ħ	Modified Plank's constant
hv	Energy
Hz	Hertz

I	Current
J	Joule
K	Cosic constant
k	Boltzmann Constant
k-	Kilo-
lx	Lux
m-	Milli-
n-	Nano-
p-	Pico-
q	Charge
Ry	Rydberg constant
s	Second
T	Tesla
u-	Micro-
V	Voltage
v	Velocity
W	Watt
γ	Gamma
Δfs	Spectral increment
ε	Molar absorptivity
Λ	Effect size
λ	Wavelength
Ω	Ohm

Chapter 1

Introduction

1.0- A Novel Perspective on Biomolecules

Our modern approach to medical intervention is based upon a crude model of pharmacodynamics which, in an attempt to affect precise targets, often impairs or destroys entire systems. Toxicity, side-effects, and general iatrogenic complications are symptoms of an ailing medical industry. We are in desperate need of a new set of technologies which identify, target, and influence biomolecular substrates and their cellular hosts with atomic precision. Alternative strategies to traditional pharmacological solutions may eliminate unintended side effects, and better adapt to the changing needs of individual patients and avoid over-prescription often leading to those side effects.

Recent developments in bioinformatics have generated new methods to computationally infer properties of molecules or entire pathways involved with insidious cascades such as those associated with cancer (Cosic 1995, Karbowski et al. 2015, Persinger et al. 2015). The amino acid sequence of a protein, for example, can be converted and reduced to its charge profile, computationally transformed into a discrete energy and wavelength value, and harnessed to suppress or enhance activity within cells associated with the said protein. Using electromagnetic fields and light generating

apparati, biophysical and energetic properties of proteins can be targeted systematically to promote growth, cellular differentiation, migration, hormone-release, cognitive patterns, behavioural responses, or any event resultant of physiology.

At a fundamental level, atoms, molecules, compounds, and cells operate by a synchronized exchange of charged molecules. The electromagnetic signature of an atom is like a fingerprint – absolutely singular in its presentation. So too are the aggregate electromagnetic signatures of molecules and cells (Oschman, 2015). A sophisticated study involving measurements of electromagnetic emissions from biological material would contribute to an ever-expanding compendium of bioelectromagnetic “fingerprints” which, if re-directed and applied to the cell, could influence molecular targets with maximum precision.

2.0- The Electromagnetic Spectrum

All life on earth has evolved in the presence of a continuous flux of natural electromagnetic fields. These fields are a result mostly from solar radiation, enhanced substantively by earth-bound electromagnetic disturbances such as thunderstorms (Vozoff 1991). The electromagnetic field that arise naturally from our terrestrial home, the geomagnetic field which is known to drive all biological systems that dwell on its surface, is generated by the swirling molten iron at its core (Glatzmaier & Roberts, 1995) In addition to these natural sources, an exponential growth of anthropogenic electromagnetic fields borne of technological developments particularly in wireless communication over the last century now blanket the earth, coupled to a vast and

continuously expanding network of electric power distribution systems. Together, the electromagnetic environment and its influence upon biological systems can be described as complex and multiform.

The natural electromagnetic environment covers a very wide frequency spectrum, from steady-state (static) electric and magnetic fields to very energetic gamma rays, often of galactic origin at frequencies of 10^{23} Hz. The spectrum of electromagnetic energy can be classified based on its ascending frequency (*f,* measured in hertz, Hz) or decreasing wavelength (*λ*, measured in meters, m). This inverse relationship of frequency and wavelength, two fundamental properties of electromagnetic waves, can be related using the Universal Wave equation $\lambda = v/f$, where f is frequency, λ is a wavelength, and the phase speed (v) is the speed of light (3.0×10^8 m/s). Any wave pattern can thus be described in terms of the independent transmission of sinusoidal constituents travelling at a constant speed. Along with frequency and wavelength, all electromagnetic waves are typically constitute a third physical property known as photon energy (*E, measured in electron volts, eV or joules, J*). In terms of modern quantum theory, electromagnetic radiation is the flow of photons through space at speed of light. Each photon contains a certain amount of energy, which increases with growing frequency. In other words, photon energy is directly proportional to the wave frequency, therefore the relationship between the three fundamental properties of electromagnetic waves (frequency, wavelength and photon energy) can be best illustrated by the Plank-Einstein Relation: $E = h \cdot c/\lambda$, where E is energy, Plank's constant (*h*) is 6.26×10^{-34} J·s and *c* is the speed of light. The "behaviour" or physical expression of any electromagnetic wave depends on its wavelength. When a given electromagnetic wave interacts with atoms and molecules, its

interactions also depend on the amount of energy per quantum (photon) it carries. It is because of this that the electromagnetic spectrum is typically broadly classified into 8 regions, radio wave, microwave, terahertz, infrared, visible, ultraviolet, X-rays, and gamma rays.

2.1- The Anatomy of Electromagnetic Fields

The anatomy of the electromagnetic (EM) wave or field can be dissected into its fundamental components - the electric and magnetic fields. A unique feature of EMFs is that the time-varying electric and magnetic fields interact with another at right angles and together are perpendicular to the direction of the charged particles carrying the wave. Electromagnetic waves also differ from mechanical waves in that they do not require a physical medium to propagate. This means that though electromagnetic waves can travel through the three states of matter, they can also move through a vacuum. That said, the mechanisms by which EM waves interact with the environment are dependent on their presentation with respect to time, that is to say their frequencies. From this emerges two types of EM classifications, steady state (static) and time varying fields. In a static EM field, the flux lines, which are theoretical lines of force do not change over time and remain largely fixed; except for a slow decay over time, which is due to the normal forces of entropy. They are a result of the interaction between the magnetic flux lines and induced electric fields. The lifetime of a resultant electric current in any system is contingent on the electrical properties (i.e. resistance, capacitance, and inductance) of the medium producing the magnetic field (Fahidy, 1999). Static magnetic fields exert their effects on

biological systems by altering the orientation of asymmetrically distributed charges on cells (Rohen, 2003).

Time-varying fields by definition change over time. Typical EMFs are often time varying fields, as the resultant change in the magnetic field is associated with a changing electric field and *vice versa* (Weinberg, 1995). Time varying fields fall under two major categories: non-propagating (near-fields) and propagating (far-fields), referring to the distance the EM wave travels through space. An example of a non-propagating wave would be that of the EM fields generated from a rotating static magnetic source (e.g. bar magnet) spinning along its central axis. The wave-like phenomenon if one were to record the intensity of the magnetic field at some distance away from the rotating bar magnet would not be a true wave. Induced from the shifting of charged particles within the medium, it is directly proportional to electric current within the medium – this is the property of electromagnetic induction. In a propagating field, the EM wave is free to radiate far distances without the continuing influence of the moving charges that produced them. These waves rely on the dualist property of photons, being both matter and energy; they contain their own momentum related to their wavelength (as per the de Broglie equation) as they are their own particle, their own medium. That is, the wave is the light particle itself moving physically perpendicular to its direction of motion.

The effects of electromagnetic fields upon chemical compounds and biological systems depends upon the wave's frequency and it's intensity. EMFs of high frequency/short wavelengths (i.e. high ultra-violet, x-rays, γ -rays) are often called ionizing radiation as the packet of photons within these waves possess high energies to disrupt and break chemical bonds and induce radioactive decay. It is this dispersal of charged

and uncharged subatomic components that accelerate radial reactions, inhibit/interfere with chemical reactions and damage living cells beyond the damage resulting from simple heating, and can induce systemic health hazards in an organism .(EMFs of visible or lower frequencies/longer wavelengths (i.e., low ultraviolet, visible light, infrared, microwaves, and radio waves) are called non-ionizing radiation, because the waves do not possess enough energy to strip atoms and molecules from tissues or subatomic particles. These extremely low frequency sources will be the prime subject of this dissertation.

2.2- The Basics of Photons and Light

Simply stated, light is nature's most common method of transferring energy through space. Despite vast advances in the natural sciences, no definition for light satisfies the many contexts in which it impinges upon and affects its innumerable targets. Light from the Sun warms the Earth, drives global weather patterns (Svensmark & Friis-Christensen, 1996), and initiates the life-sustaining process of photosynthesis (Monteith 1972). Microorganisms as well as plants exploit it as an energy source, catalyzing chemical reactions, forcing the ejection of electrons from materials. Though the physicist might be interested in the physical properties of light, the artist is concerned with its influence upon the aesthetic appeal of an object. The earliest examples of human ‘civilisation’ are rock paintings, nestled deep in the recesses of the earth, where the power of artificial light made the paintings dance (Brodrick 1948). Through the sense of sight, light is a primary tool for perceiving the world and often communicating within it. On the

grandest scale, light's interactions with matter have helped shape the very structure of the Universe. Indeed, from cosmological to atomic scales, photonic processes are ubiquitous.

Light refers to the many different forms of packets that electromagnetic energy takes. Quantum mechanics derive Newtonian mechanics, based on the properties of physical matter. Light, too, has a 'physical property' and is simultaneously a particle and pure energy, and the quasi-physical particle that carries electromagnetic information and which fundamental forces act upon is the photon (Cohen-Tannoudji et al., 1992). Organized as a field, which is best conceptualized as a series of points within space-time; photons mediate EMFs and their resultant processes. As quantized particles travelling at c, their influences are quite distinct. Whether photons take the form of γ-rays, X-rays, microwaves, radio waves or visible light, they are always fundamentally made of the same constituents and only differ as a function of amount of energy (i.e. frequency). As particle-waves, photons travel as oscillating bodies where the wavelength of a given photon is proportional to its energy.

This dual particle-wave property imbues the photon with singular characteristics (Engel et al. 2007). First, it displays regular mechanical properties of energy transfer that catalyze chemical reactions. Photodissociation, or photolysis, involves breaking chemical bonds, often to induce a downstream biological effect (Shinke. 1995). By providing an exogenous energy source, photons essentially substitute endogenous electric or molecular sources of energy within cells, further propagating their signals by stimulating biomolecular cascades (Electrons, 2011). However, photons can also display physical properties. That is, their capacity to influence directly physical, chemical, and biological

systems that rely upon non-local and coherent properties. Photons simultaneously operate as particles and waves, thus they have a capacity to induce effects that appear to violate assumptions of causality. For instance, whereas two matter-waves made up of H_2O might interfere with each other on the surface of bulk water, a single photon can interfere with itself. Patterns of oscillation are therefore subject to unexpected interactions with matter.

Photons, unlike sound waves travelling as air particles, exhibit heterogeneous polarizations that are not uniformly oriented with respect to the direction of the propagation (Beijersbergen et al., 1992). Rather, forcing a uniform polarisation (polarized light) is often required in order to affect certain functions. Lasers are an example of light with a single, continuous state of polarisation. Polarising devices result in single-frequency, phase-correlated photons, becoming amplified and target selective (Beth, 1935). The versatility of the photon arises from its particle-wave duality and the various manipulations of its shape and trajectory imbue it with potential for application in innumerable medical contexts given the multitude of unique molecular pathways, each needing its own modulation in order to elicit bio-relevant effects.

Photons can be generated readily by changing the energy level of an electron within an atom. The most common electromagnetic signature in the Universe is the 21 cm “hydrogen” line which is generated constantly across the cosmos by the changing energy levels of neutral hydrogen. Light is a product of atomic and chemical change. It is no surprise that light would be expected to change atomic and chemical structure in turn and that these changes could be biologically relevant (Oschman, 2015, Popp 2002). By manipulating the temporal characteristics of pulsed light, its intensity, frequency, phase,

polarity, and directional application, we can harness the universal energy transferring characteristics of light to achieve practical ends in the biomedical field.

2.3- Biological Systems and Electromagnetic Fields

James C. Maxwell's electromagnetic theory and equations best describe the classic generation of EMFs, which illustrate that both an electric and a magnetic fields result when a charged particle is set into motion at a constant velocity (Maxwell, 1881). The fundamental source that drives any cellular activity is the cell membrane potential which is entirely dependent upon the motion of charged particles. This disparity in ionic charges at the cell membrane, which serves as both an insulator and diffusion barrier, is the primary source by which cellular systems generate electromagnetic fields endogenously (Dotta et al., 2011). In 1968, using theories of nonlinear physics, thermodynamics and quantum mechanics, Herbert Fröhlich proposed his seminal hypothesis, which posited that living systems can generate electromagnetic fields if the cellular components exhibit electrically polar charges that display movement (Frohlich1968; Del Giudice et al. 1988). He defined this state of 'electric polarity' as a condition where electric charges generate electromagnetic fields when they vibrate. It is no surprise, therefore, that the membrane depolarization of neuronal cells during action potentials can induce EMF generation with frequencies of up to 10 kHz (Collings et al., 2001). According to Fröhlich's theory, polar macromolecules such as proteins or nucleic acids, major organelles such as microtubules composed of polar heterodimer subunits, or mitochondria which create hydrogen ion gradients to generate ATP can also generate

EMFs within the range of 100-1000 GHz extending up to terahertz within cells that are not involved in active cell membrane depolarization like the neuron (Frohlich 1972; Mavromatos 2011).

So, how does one measure EMF from living systems? It is important to be cognisant that the vibrational frequency of electrically polar systems (*e.g.* macromolecules and organelles) is equal to the resultant frequency of the generated EMF. As expected, the techniques used to measure the fields depends on the type of field generated and frequency of inquiry. Near field, or non-propagating EMFs, which are only measurable near the cellular components that generate them, are measured using special sensors derived from nanotechnologies. For example, Jelinek and colleagues (1981) have measured vibrations and resulting EMF generation in the kHz range associated with the synchronized M phase of mitosis in *Saccharomyces cerevisiae* (yeast) observed using platinum micro-wire. Other methods of direct measurements of cellular EMF techniques include the detection of a cell's propagating or radiative EMF. Spectroscopic techniques such as Raman or Brillouin spectroscopy are typically used to accomplish the measurement of the state of the cell by its EMF signature (Yeun & Liu 2012; Jat 1998). Pokorny et al. (2001) have shown that >2 Hz EMF are emited from cells during cell replication, specifically during the elongation of mitotic spindles during anaphase.

Since living systems such as cells readily generate EMFs through electrically polarized charges, they must then be able to interact with externally applied charges or EMFs. Fröhlich proposed the existence of a selective resonant interaction of similar frequencies of biomolecular EMFs between endogenous systems (Fröhlich, 1972).

Fröhlich Resonance is one of the mechanisms that cellular systems may use to communicate with one another beyond those involving chemical means. With respect to exogenously applied EMFs, plenty of literature aims to widen the understanding of how applied EMFs affect biological systems (Adey 1981; Goodman 1991, Berg 1995, Kavet 1996) . However, there are several inconsistencies in the results and misapprehensions concerning the effects. Although EMFs with intermediate-to-high frequency ranges (kHz-GHz) have been shown to arrest growth in normal (Czyz et al. 2004)) and malignant cells (Mashevich et al., 2003), extremely-low frequency EMFs (0.1-100 Hz) are of greater interest, owing to their increasing anthropogenic footprint and their ability to penetrate deeper into tissues by interacting with ionic flux characteristics of the cell (Giladi et al., 2008; Krison et al. 2004).

ELF-EMF research in the biological fields was initiated by Galvani's ground breaking bioelectric studies in the late 18th century (Kipnis 1987). The research conducted since then has shown that EM fields can act at the cellular level and affect various cellular functions including DNA synthesis, protein expression/activity, metabolic activity, and cell proliferation and differentiation (Rodan *et al.*, 1978; Lohmann *et al.*, 2003; Lohmann *et al.*, 2000; Byus, *et al.*, 1987; Volkow *et al.*, 2011). Focusing on these areas of ELF-EMF effects, opposing views, reduced reliability and inconsistent reproducibility are often result because of a general lack of understanding of the synergistic effects of EMF intensity, frequency, and temporal presentation. For example, Morabito and colleagues have shown that exposure to a 50 Hz, 0.1-1.0 mT ELF-EMF elicits redox and trophic response in rat cortical neurons, and induce oxidative stress in mouse cerebellum (Morabito et al.

2010). However ELF-EMF exposure of 50 Hz frequency applied at a varied intensity was shown to illicit no markers of oxidative stress within the same model organism.

Another property of ELF-EMF research which is often overlooked and which drives effects in biological systems is the pattern of the applied field. Murugan et al. persuasively presented evidence for the importance of applied pattern upon the dissolution of planaria, which are commonly regarded as otherwise immortal (Murugan et al. 2013). By applying a frequency-modulated EMF, they observed complete dissolution of the worm whereas the reverse application of the effective sequence induced cancellation of the effect. This would prove Frohlich's theory of resonant interaction of similar frequencies, which is driven by the pattern. Further understanding of the pattern emitted and its subsequent application onto a dysfunctional system using the appropriate temporal window and EMF parameters can lead to the emergence of new techniques in modern medicine – specialized electromagnetic medicine.

2.4- Photons and Biological Systems

Photosynthesis is the most fundamental and basic association between light and living systems. Research into light-harvesting complexes, which capture photons and divert the resulting energy into photosynthetic reaction centers, has revealed how natural systems harness light energy. As a result, this has pushed chemical biologists and physicist to devising artificial light-harvesting antennae for practical applications such as sustainable energy production. Other avenues of light and biological systems stem from bioflourescence and bioluminescence (Hasting et al. 2006), observed for example in

some species of jellyfish and firefly. One observes the link between light and biology from within these light sensitive proteins (luciferases), which emit light in response various physiological stimuli from the organisms (Nakatsu et al. 2006). However, hoaning in on the derivation of this dual-particle wave, the fundamental basis light is a product of changing states within atoms, compounds, and their aggregates.

Harnessing the natural potential of light as an experimental tool, scientists have applied the photophysical properties of proteins into the development of small-molecule dyes commonly used in biological research (New, 2016). Though fluorescent proteins, light green fluorescent proteins (GFP) have become indispensable for tracking molecular targets within a cell or organism, scientists have also found other ways to use light to control or interrogate biological systems (Tslen, 1998). The emerging field of optogenetics utilizes physics, organics, and photochemistry to use photoactive compounds to trigger chemical reactions (Deisseroth 2001). Application of these reactions to create 'caged' biomolecules that are activated by a pulse of light has allowed temporal precision in turning a particular biological process on (or off) whereas advances in laser technology have enabled increasingly precise spatial resolution to the applied beams (Kramer et al. 2013; Muller & Weber 2013). Though these techniques can lead to many advancements in biological science, they require a system to be predisposed to photosensitive proteins or genetic modifications that may not be feasible for many applications.

Recently, several researchers have shown that biological systems are capable of naturally emitting electromagnetic waves in the optical range of the spectrum that we call visible or near-visible light (Popp, 2002; Dotta et al. 2014). These light emissions from biological sources are termed biophotons. Biophotons are non-thermal in origin and range

in energy from 10^{-19} to 10^{-18} J with wavelength bandwidths from UV to IR (~180nm - 1500nm). Though biophoton emissions from biological tissues are a form of bioluminescence, they occur at lower energy thresholds and are spontaneous in that they do not require exogenous sources of stimulation (Popp 1997, Scott et al., 1991).

Many explanations of biophoton generation rely on physical fundamentals and suggest two phases: 1) excitation and 2) relaxation. Additional energy to an atomic system excites electrons in their resting orbits and pushes them to higher energy orbitals. When the electrons fall back down and leave the excited state (relaxation phase), energy is re-emitted in the form of a photon; and if the emission source is a biological unit, we call this biophoton emission (Bialynicki-Birula 1994). The wavelength (and its equivalent frequency) of the photon is determined by the difference in energy between the two states. These emitted photons form the emission spectrum. Several researchers have measured continuous emissions of biophotons from the living cells of plants (Mansfield 2005; Creath & Schwartzz 2004 Kobayashi et al. 2007) animals (Galle 1992) and humans (Devraj et al 1997; Sun et al. 2010). The sources of these biophotons remains a basis of consternation to researchers, but it has been shown that biophotons can result from chemical reactions that release reactive elements such as reactive nitrogen species (RNS) or reaction oxygen species (ROS) (Bokkon et al., 2010). The biologically relevant excited species, are mostly generated within the mitochondrial respiratory chain. The production is accomplished through the excitation of electrons of a single oxygen and carbonyl species (R=O), through the redox/radical process of hydrogen peroxide (equation 1).

$$2O^{-}_{2} + 2H^{+} \rightarrow H_2O_2 + {}^{1}O_2 \quad \textbf{(1)}$$

$${}^{1}O_2 \rightarrow {}^{3}O_2 + h\nu \quad \textbf{(2)}$$

When the excited species from these sources return to its ground state energy is released in the form of biophotons (equation 2). This concept is supported through the proportional production of biophoton emission with increased oxygen within a system. [Tilbury & Quickenden, 1988; Hideg *et al.*, 1991ab]. Along with the mitochondria, lipid peroxidation has also been implicated as a source of biophoton emission, which can subsequently be absorbed by chromospheres (e.g. porphyrin ring or flavinic rings) found embedded within the lipid sources such as the plasma membrane (Thar and Kühl, 2004). In 2009, Bokkon suggested that the release and absorption of biophotons, also known as resonance energy transfer, is the mechanism by which biomolecules, such as aromatic amino acids (e.g. tyrosine, tryptophan) can induce conformational changes to generate downstream signal transduction (Bokkon 2009).

The advent of photonic detectors such as the photomultiplier tube (PMT) have provided increasing evidence to suggest that biological systems emit light in the form of biophotons which are highly coupled to cellular processes. Tilbury and Quickenden (1988) distinctively showed biophotons emitting from *E. coli* bacteria which were coupled to the varying stages of *E. coli* growth. They found the bacteria emit biophotons within the UV range (210-210nm) during gthe rowth phase, which shifted to the visible range (450-620nm) during exponential growth. Also, Ohya and colleagues (2002) have shown that distinct profiles of biophoton emission can be used as a marker of early cellular stress within red bean plants. They suggested that these changes in biophotonic profiles can be used as measure of early detection of damage within agricultural crops without any intrusive measures or harvest damage, which can increase agricultural productivity.

Since cells and tissues are able to emit electromagnetic radiation within the visual spectrum and, as is the case with EMFs, have resonant interactions with exogenous sources from the same spectrum of light, they should therefore be able to alter the internal workings of the cell, and subsequently the organism's physiology. Since we know that biophotons from cells are wavelength dependant (Dotta et al., 2014), the application of light must follow the same energy specificity. The advent of light-emitting diodes (LED) allows for this specificity. For example, Liebmann *et al.* (2010) have shown applying light at wavelengths of 412-426 nm (blue) at high intensities can induce cellular toxicity and damage in human epithelial cells, whereas light at 632-940 nm (orange to infrared) applied at the same intensity produces no effect. Furthermore, the application of light with just a 30 nm shift (435nm) in wavelength can reduce cell proliferation and differentiation without inducing cellular markers (Dotta et al., 2014). Developing the idea of applied effects of light and EMF to humans, several studies have shown that pulsed patterns of these physical forces can alleviate several neurophysical ailments (e.g. depression, Golden et al., 2005) if the application is tuned to the appropriate brain structure (Saroka et al., 2014;). Since the visible spectrum has the same properties as for EMFs as described earlier, the same parameters such as temporal application, intensity and wavelength are crucial when attempting to induce precise effects.

3.0- Cosic's Model of Resonance in Proteins

As seen with applications of EMFs and/or light it is the information within the applied field, or what can be broadly termed the pattern, that elicits any specific effect

within a biological system. These processes within biology arise from very specific and selective interactions with biomolecules. Given the physical assumptions and properties of quanta of light, it follows there must be a biophysical link that targets the specificity of these biomolecules using fields derived from subsections of the electromagnetic spectrum.

Amongst the classic macromolecules, proteins are the major contributors that drive cellular processes (Nakai & Kanehisa 1992). The great diversity and versatility of protein sequences derive from the properties of the twenty different amino acid side chains that may exist in a protein molecule and reflects the wide range of bioactivity of the formed protein molecules. However, proteins can only express their biological functioning after folding into their three-dimensional structure, determined by the primary amino acid sequence of the polymer. This linear sequence is the information-containing element that allows proteins to interact with other biomolecules and thus maintains homeostasis within living organisms. If one could delineate the mechanisms of information-containing sequence expression, then protein manipulation could occur at-will to turn off or on biomolecular reactions within deleterious systems such as viruses or cancers.

There have been many attempts to discover the rules central to coding biological function into the sequence of amino acids within the protein. Typical approaches deal with either homology characterization of specific features of the primary and secondary structure of proteins (Zhang et al., 2008) or molecular modeling of protein tertiary structure (de Trad et al., 2002) . Although such approaches permit a significant insight into protein structure and active site location, they still do not provide sufficient knowledge

about the informational, structural and physicochemical parameters crucial to the selectivity of protein interactions.

Irena Cosic ingeniously developed a physical and mathematical model, coined the Resonant Recognition Model (RRM), which extracts information from within a protein's amino acid sequence using digital signal processing methods (Cosic et al. 1991, Cosic 1995, Cosic et al. 2016). The basis of this model is to treat the primary sequence of proteins as a signal, and use signal extraction methods such as Fourier transforms to reveal bio-information hidden within the sequence itself. The RRM is comprised of two stages. The first involves the transformation of the linear amino acid sequence into a numeral sequence or a digital signal. A physical parameter value known as an electron-ion interaction pseudopotential (EIIP) represents each of the 20 individual amino acids (Nair & Sreenadhan 2006). This value represents the average energy stages of all the valence electrons within a given amino acid, thus determining its electronic property. In the second stage of the RRM, the converted numerical sequence of amino acids are then subjected to wavelet transformation, extracting the spatial pattern information, or the frequency domains that are pertinent to biological functioning. Cosic explains that the peaks in these spectral outputs of the signals reflect common frequency domains of a protein's functional group, and through extensive cross-spectral analysis of numerous proteins, she has shown that one peak characteristic frequency (RRM frequency) exists for a group of proteins sharing similar functioning (Cosic 1994; Trad et al., 2002).

Enumerating the amino acid sequence using the delocalization of electrons from these molecules illustrates the concept that the charges moving along the protein backbone induces transient polarizations of the side groups resulting attractive and

repulsive forces between parts of a given molecule and resonance of the whole molecule itself (Nair & Sreenadhan, 2006). These oscillations can be transmitted through polar media such as water at considerable distances (10 – 100nm) and interfere with oscillations of other molecules. As mentioned earlier, Fröhlich's Resonance Theory suggests that two molecules that possess the same frequency can interact with one another with high specificity by virtue of coherent frequencies. As such, this gives rise to the premise that singular proteins oscillating at one frequency, can interact with other biomolecules resonating at the same frequency.

With respect to the RRM, characteristic frequencies derived from linear amino acid sequences can be categorized into clusters or subgroups of macromolecules that share common spectral characteristics. Since the *recognition* arises from the matching of frequencies within the distribution of energies of free electrons along the interacting proteins, it has been termed resonant recognition of proteins. This model assumes that characteristic frequencies are responsible for the resonant recognition between macromolecules at a distance (Cosic 1995). Therefore, these frequencies have to represent oscillations of some physical field that can propagate through water dipoles. One prospect is that this field is electromagnetic in nature. In other words, electromagnetic fields give a foundation by which biomolecules such as proteins can interact with one another to induce conformational changes to stimulate or inhibit signal processes within cellular systems.

4.0- Thesis hypothesis and objectives

Coupled to every biomolecular pathway is an equivalent and proportional transfer of energy which can be measured and quantified. Molecules, characterized by chemical binding sites, are ultimately spatial distributions of charges which exert forces upon electrically chiral objects within aqueous media. It is therefore feasible that physical interventions – involving applications of electromagnetic fields, light, and other forces – and chemical interventions involving pharmaceuticals are equally valid when attempting to modulate biomolecular pathways. Indeed, photostimulation and applications of electromagnetic fields have demonstrated promising results in biomedical fields which typically involve the administration of chemical compounds to treat disease.

Hypothesis

There is a general desire among biophysicists to observe and influence living systems from the aforementioned perspective. However, a level of increased precision is currently required to safely and effectively apply biophysical techniques as adjuvant, additive, or replacement therapies for diseases normally treated by traditional pharmaceutical techniques. Applying emerging bioinformatics models to the structure and function of biomolecules should, in principle, allow us to design biophysical techniques sufficient to treat disease by targeting precise molecular pathways within tissues and cells. Further, an understanding of how biophysical correlates such as photon emissions are paired to molecular events would further elucidate the relationship between the

transfer of energy between particles along a pathway and its epiphenomenal structures. Studying both the electromagnetic emissions of biological systems and their capacities to be modulated by forms of targeted electromagnetic energy could approximate a powerful use of biophysics to treat diseases which are currently resistant to typical therapeutics.

Objectives

The objective of this work is to measure biophoton emissions as well as their unique patterns of presentation resultant of molecular events within living systems and to re-apply these patterns as electromagnetic fields or pulsed light to elicit the same molecular events. The first chapter will address how the amino acid sequences of proteins involved in molecular pathways, such as MAP-ERK, can be reduced to their charge profiles, converted to spatial increments using Cosic's Resonant Recognition Model (RRM), and applied as light to activate said proteins. Chapter 2 will be confirm that the Cosic wavelengths which are coupled to biomolecules (e.g. proteins), can be used in a detection method to discriminate between systems that express malfunctioning proteins. In chapters 3 and 4, the viral proteins that drive the insidious diseases processes associated with viruses such as Ebola and Zika, will be converted into punctate wavelengths and patterns of light using the Cosic RRM, which can be related to their particular geographical prevalence. Once a foundation has been laid which suggests that biological systems emit electromagnetic energy that can be mapped using a bioinformatics tool, subsequent chapters will assess data collected by photomultiplier tubes coupled to wavelength-specific filters which were subjected to advanced forms of

statistical analysis to predict molecular classifications paired to known biochemical events. In other words, emissions of electromagnetic energy will be computed based upon sequencing data and then reapplied to biological systems to alter their regeneration, proliferation rates, or even more dynamic processes such as learning. To truly understand how a phenomenon affects dynamic systems, interference methods often prove useful. As a result, the last chapter assess how exogenously applied materials (such as copper foils) alter magnetic flux lines or light patterns, to produce varying effects when applied to biological systems. In general, the work serves as a validation of the RRM method as well as a justification for the application of biophysical techniques involving electromagnetic radiation to medicine on the basis of photon-protein interactions. It will also show that applied light or electromagnetic fields can also influence processes within simple systems, up to complex systems such as cognitive functioning in humans.

References

Adey, W. R. (1981). Tissue interactions with nonionizing electromagnetic fields. Physiological reviews, 61(2), 435-514.

Beijersbergen A.L., Spreeuw M.W., Woerdman, J.P. (J1992). "Orbital angular momentum of light and the transformation of Laguerre-Gaussian laser modes". Physical Review A. 45 (11): 8186–9.

Beth, R.A. (1935). "Direct detection of the angular momentum of light". Phys. Rev. 48 (5): 471.

Berg, H. (1995). Possibilities and problems of low frequency weak electromagnetic fields in cell biology. Bioelectrochemistry and bioenergetics, 38(1), 153-159.

Bialynicki-Birula, I. (1994). "On the wave function of the photon". Acta Physica Polonica A. 86: 97–116.

Bokkon, I. (2009). Visual perception and imagery: a new molecular hypothesis. BioSystems. 96, 178-184.

Bókkon, I., Salari, V., Tuszynski, J. A., & Antal, I. (2010). Estimation of the number of biophotons involved in the visual perception of a single-object image: Biophoton intensity

can be considerably higher inside cells than outside. Journal of Photochemistry and Photobiology B: Biology, 100(3), 160-166.

Brodrick, A. H. (1948). Prehistoric painting. Central Institute of Art and Design.

Byus, C. V., Pieper, S. E., & Adey, W. R. (1987). The effects of low-energy 60-Hz environmental electromagnetic fields upon the growth-related enzyme ornithine decarboxylase. Carcinogenesis, 8(10), 1385-1389.

Cohen-Tannoudji, C., Dupont-Roc, J., Grynberg, G., & Thickstun, P. (1992). Atom-photon interactions: basic processes and applications (pp. 427-36). New York: Wiley.

Cosic, I., Cosic, D., & Lazar, K. (2016). Environmental light and its relationship with electromagnetic resonances of biomolecular interactions, as predicted by the Resonant Recognition Model. International Journal of Environmental Research and Public Health, 13(7), 647.

Cosic, I., Hodder, A. N., Aguilar, M. I., Hearn, M. T. W. (1991) Resonant Recognition model and protein topography. The FEBS Journal. 198 (1), 113-119.

Cosic, I. (1995). Macromolecular bioactivity: is it resonant interaction between macromoleculars? – Theory and Application. IEEE Transactions on Biomedical Engineering. 41 (12), 1101-1114.

Cohen, S., & Popp, F. A. (1997). Biophoton emission of the human body. Journal of Photochemistry and Photobiology B: Biology, 40(2), 187-189.

Creath, K., & Schwartz, G. E. (2004). Biophoton images of plants: Revealing the light within. The Journal of Alternative & Complementary Medicine, 10(1), 23-26.

Czyz, J., Guan, K., Zeng, Q., Nikolova, T., Meister, A., Schoenborn, F., & Wobus, A. M. (2004). High frequency electromagnetic fields (GSM signals) affect gene expression levels in tumor suppressor p53-deficient embryonic stem cells. Bioelectromagnetics, 25(4), 296-307.

de Trad, C. H., Fang, Q., & Cosic, I. (2002). Protein sequence comparison based on the wavelet transform approach. Protein engineering, 15(3), 193-203.

Deisseroth, K. (2011). Optogenetics. Nature methods, 8(1), 26-29.

Del Giudice, E., Doglia, S., Milani, M., Vitiello, G. (1988). Spontaneous symmetry breaking and electromagnetic interactions in biological systems. Physica Scripta. 38, 505-507.

Devaraj, B., Usa, M., & Inaba, H. (1997). Biophotons: ultraweak light emission from living systems. Current Opinion in Solid State and Materials Science, 2(2), 188-193.

Dotta, B. T., Buckner, C. A., Cameron, D., Lafrenie, R. F., Persinger, M. A. (2001) Biophoton emissions from cell cultures: biochemical evidence for the plasma membrane as the primary source. Gen Physiol Biophys. 30 (3), 301-309.

Dotta, B. T., Murugan, N. J., Karbowski, L. K., Lafrenie, R. M., Persinger, M. A. (2004). Shifting wavelengths of ultraweak photon emissions from dying melanoma cells: their chemical enhancement and blocking are predicted by cosic's theory of resonant recognition model for macromolecules. Naturwissenschaften. 101 (2), 87-94.

Electrons, P. (2011). Force: Quantitative Single-Molecule Measurements from Physics to Biology Claridge, Shelley A.; Schwartz, Jeffrey J.; Weiss, Paul S. ACS Nano, 5(2), 693-729.

Engel G.S., Calhoun T.R., Read E.L., Ahn T.E., Mančal T., Cheng T.C., Blankenship R.E. Fleming G.R. (2007) "Evidence for wavelike energy transfer through quantum coherence in photosynthetic systems". Nature 446, 782-786

Fahidy, T.Z. (1999). The Effect of Magnetic Fields on Electrochemical Processes, In: 5, Modern Aspects of Electrochemistry, No. 32, B.E. Conway, J.O.M. Bockris and R.E. White Eds., Kluwer/Plenum, New York.

Frohlich, H. (1968). Long-range coherence and energy storage in biological systems. Int. J. Quantum Chem, 2(5), 641-649.

Frohlich, H. (1972). Selective long range dispersion forces between large systems. Physics Letters. 39A, 153-155.

Galle, M. (1992). Population density-dependence of biophoton emission from Daphnia. Recent Advances in Biophoton research and its Applications, 345-355.

Glatzmaier G.A., Roberts P.H (1995). A three-dimensional convective dynamo solution with rotating and finitely conducting inner core and mantle. Phys. Earth Planet. Inter., 91, 63-75

Goodman, R., & Shirley-Henderson, A. (1991). Transcription and translation in cells exposed to extremely low frequency electromagnetic fields. Journal of Electroanalytical Chemistry and Interfacial Electrochemistry, 320(3), 335-355.

Hall, G. (2008). Maxwell's electromagnetic field and special relativity. Philosophical Transactions of the Royal Society. 366, 1849-1860.

Hastings, J. Woodland. "Aglow in the Dark: The Revolutionary Science of Biofluorescence. By Vincent Pieribone and David F Gruber. Belknap Press. Cambridge (Massachusetts): Harvard University Press. $24.95. xii+ 263 p; ill.; index. ISBN: 0–674–01921–0. 2005." The Quarterly Review of Biology 81.4 (2006).

Hideg, E., Kobayashi, M., Inaba, H. (1991a). The raf red induced slow component of delayed light from chloroplast is emitted from photosystem ii. Evidence from emission spectroscopy. Photosynth Res. 29, 107-112.

Hideg, E., Scott R. Q., Inaba, H. (1991b). Spectral resolution of long term (0.5-50s) delayed fluorescence from spinach chloroplasts. Arch Biochem Biophys. 285, 371-372.

Hideg, E., Kobayashi, M., Inaba, H. (1992). Delayed fluorescence and ultraweak light emission from isolated chloroplasts (comparison of emission spectra and concentration dependence). Plant Cell Physiol. 33, 689-693.

Jalinek, F., Cifra, M., Pokorny, J., Vanis, J., Simsa, J., Hasek, J., Frydlova, I. (2009) Measurement of electrical oscillations and mechanical vibrations of yeast membrane around 1 kHz. Electromagn Biol Med. 28 (2), 223-232.

Jat K.L. (1998) Analytical Calculation of Stimulated Brillouin Scattering in Magnetic Fields Applied to n-InSb1. Phys. Stat. Sol. (b) 209, 485

Karbowski, L. M., Murugan, N. J., Persinger, M. A. (2015). Novel cosic resonance (standing wave) solutions for components of the JAK-STAT cellular signalling pathway: a convergence of spectral density profiles. FEBS Open Bio. 5, 245-250.

Kavet, R. (1996). EMF and current cancer concepts. Bioelectromagnetics, 17(5), 339-357.

Kipnis, N. (1987). Luigi Galvani and the debate on animal electricity, 1791–1800. Annals of science, 44(2), 107-142.

Kobayashi, M., Sasaki, K., Enomoto, M., & Ehara, Y. (2007). Highly sensitive determination of transient generation of biophotons during hypersensitive response to cucumber mosaic virus in cowpea. Journal of experimental botany, 58(3), 465-472.

Kramer, R. H., Mourot, A., & Adesnik, H. (2013). Optogenetic pharmacology for control of native neuronal signaling proteins. Nature neuroscience, 16(7), 816-823.

Liebmann, J., Born, M., Kolb-Bachofen, V. (2010). Blue-light irradiation regulates proliferation and differentiation in human skin cells. J invest Dermatol. 130 (1), 259-269.

Lohmann, C. H., Schwartz, Z., Liu, Y., Guerkov, H., Dean, D. D., Simon, B., & Boyan, B. D. (2000). Pulsed electromagnetic field stimulation of MG63 osteoblast-like cells affects differentiation and local factor production. Journal of Orthopaedic Research, 18(4), 637-646.

Lohmann, C. H., Schwartz, Z., Liu, Y., Li, Z., Simon, B. J., Sylvia, V. L., ... & Boyan, B. D. (2003). Pulsed electromagnetic fields affect phenotype and connexin 43 protein

expression in MLO-Y4 osteocyte-like cells and ROS 17/2.8 osteoblast-like cells. Journal of orthopaedic research, 21(2), 326-334.

Mansfield, J. W. (2005). Biophoton distress flares signal the onset of the hypersensitive reaction. Trends in plant science, 10(7), 307-309.

Mashevich, M., Folkman, D., Kesar, A., Barbul, A., Korenstein, R., Jerby, E., & Avivi, L. (2003). Exposure of human peripheral blood lymphocytes to electromagnetic fields associated with cellular phones leads to chromosomal instability. Bioelectromagnetics, 24(2), 82-90.

Mavromatos, N. E. (2011). Quantum coherence in (Brain) microtubules and efficient energy and information transport. Journal of Physics: Conference Series. 329, 1-31.

Maxwell, J. C. (1881). A treatise on electricity and magnetism (Vol. 1). Clarendon press.

Monteith J.L. (1972) Solar Radiation and Productivity in Tropical Ecosystems. J. App Eco. 9:3, pp 747-766

Morabito, C., Guarnieri, S., Fano, G., Mariggio, M. A. (2010). Effects of acute and chronic low frequency electromagnetic field exposure on PC12 cells during neuronal differentiation. Cell Physiol Biochem. 26, 947-958.

Müller, K., & Weber, W. (2013). Optogenetic tools for mammalian systems. Molecular BioSystems, 9(4), 596-608.

Murugan, N. J., Karbowski, L. M., Lafrenie, R. M., Persinger, M. A. (2013) Temporally-patterned magnetic fields induce complete fragmentation in planaria. PLOS One. 8 (4), e61714, 1-6.

Nair, A. S., & Sreenadhan, S. P. (2006). A coding measure scheme employing electron-ion interaction pseudopotential (EIIP). Bioinformation, 1(6), 197-202.

Nakai, K., & Kanehisa, M. (1992). A knowledge base for predicting protein localization sites in eukaryotic cells. Genomics, 14(4), 897-911.

Nakatsu, T., Ichiyama, S., Hiratake, J., Saldanha, A., Kobashi, N., Sakata, K., Kato, H. (2006). Structural basis for the spectral difference in lucifersase bioluminescence. Nature. 440, 372-376.

New, E. J. (2016). Harnessing the Potential of Small Molecule Intracellular Fluorescent Sensors. ACS Sensors, 1(4), 328-333.

Ohya, T., Yoshida, S., Kawabata, R., Okabe, H., & Kai, S. (2002). Biophoton emission due to drought injury in red beans: possibility of early detection of drought injury. Japanese journal of applied physics, 41(7R), 4766.

Oschman, J. L. (2015). Energy medicine: The scientific basis. Elsevier Health Sciences.

Persinger, M. A., Murugan N. J., Karbowski L. M. (2015). Combined spectral resonances of signalling proteins' amino acids in the ERK-MAP pathway reflect unique patterns that predict peak photon emissions and universal energies. Int. Lett. Chem. Phys. Astron. 4, 10–25.

Pokorny, J., Hasek, J., Jelinek, F., Saroch, J., Palan, B. (2001). Electric activity of yeast cells in the M phase. Electro Magnetobiol. 20, 371-396.

Popp, Fritz-Albert, et al. "Evidence of non-classical (squeezed) light in biological systems." Physics letters A 293.1 (2002): 98-102.

Rodan, G. A., Bourret, L. A., & Norton, L. A. (1978). DNA synthesis in cartilage cells is stimulated by oscillating electric fields. Science, 199(4329), 690-692.

Schinke, R. (1995). Photodissociation dynamics: spectroscopy and fragmentation of small polyatomic molecules (No. 1). Cambridge University Press.

Sun, Y., Wang, C., & Dai, J. (2010). Biophotons as neural communication signals demonstrated by in situ biophoton autography. Photochemical & Photobiological Sciences, 9(3), 315-322.

Svensmark H., Friis-Christensen E. (1997) Variation of cosmic ray flux and global cloud coverage – a missing link in solar-climate relationships. J. Atoms. And Sol.-Terres. Phys. 48:11, pp 1225-1232

Thar, R., Kühl, M., 2004. Propagation of electromagnetic radiation in mitochondria? J. Theor. Biol. 230, 261–270.

Tilbury, R. N., Quickenden, T. I. (1988) Spectral and time dependence studies of the ultraweak bioluminescence emitted by the bacterium Escherichia coli. Photochem Photobiol. 47, 145-150.

Volkow, N. D., Tomasi, D., Wang, G. J., Vaska, P., Fowler, J. S., Telang, F., ... & Wong, C. (2011). Effects of cell phone radiofrequency signal exposure on brain glucose metabolism. Jama, 305(8), 808-813.

Vozoff K. (1991) The Magnetotelluric Method. Electromagnetic Methods in Applied Geophysics: pp. 641-712. eISBN: 978-1-56080-268-6, doi: 0.1190/1.9781560802686

Weinberg, S. (1995). The Quantum Theory of Fields. 1. Cambridge University Press. pp. 15–17. ISBN 0-521-55001-7.

Yuen C., Liu Q. (2012) Magnetic field enriched surface enhanced resonance Raman spectroscopy for early malaria diagnosis. J Biomed Opt. (1):017005. doi: 10.1117/1.JBO.17.1.017005.

Zhang, T. L., Ding, Y. S., & Chou, K. C. (2008). Prediction protein structural classes with pseudo-amino acid composition: approximate entropy and hydrophobicity pattern. Journal of theoretical biology, 250(1), 186-193.

Chapter Transition: From Principle to Proof

As discussed in the previous chapter, matter and energy can often be treated as interchangeable. To demonstrate how biomolecules are inextricably linked to energy equivalencies, we employed Cosic's Resonance Recognition Model (RRM) as a bioinformatic tool. Our approach first involved converting sequences of amino acids which constitute the polypeptide chains that fold to form complex biomolecules that define the ERK-MAP pathway into pseudopotentials. This conversion allowed us to effectively treat linear sequences of amino acids as linear sequences of charges with electronic properties. Using the spectral analysis technique, we were able to identify intrinsic periodicities expressed within the charge sequences which were predictive of photon wavelengths which could theoretically be observed using photomultiplier tubes. Predictions were then tested empirically to demonstrate the predictive validity of the RRM method. Not only did we identify peak wavelengths which were congruent with our predictions, but we were also about to quantify the precise energy associated with spatial increments which defined key periodicities along the pseudopotential chain. The following chapter discusses the literature surrounding the broader issues which relate to scientific exploration and how RRM has been applied previously. The chapter demonstrates that bioinformatics tools such as RRM can be predictive of real life observations in the form of quanta of released energy which are proportional to spatial increments held within biomolecules which make up living systems.

Chapter 2

Combined Spectral Resonances of Signaling Proteins' Amino Acids in the ERK-MAP Pathway Reflect Unique Patterns That Predict Peak Photon Emissions and Universal Energies

(Original Research)

Persinger M.A., Murugan N.J., Karbowski L.M.

[Published in *International Letters of Chemistry, Physics and Astronomy*]
Vol. 43, pp. 10-25, 2015

Abstract

The duality of matter-energy as particle-waves was applied to the classic ERK-MAP signaling pathways between the plasma cell membrane and the nucleus and was tested with Cosic's Resonance Recognition Method. Spectral analyses of sequences of pseudopotentials that reflect de-localized electrons of amino acids for the 11 proteins in the pathway were computed. The spectral power density of the terminal protein (cFOS) was shown to be the average of the profiles of the precursor proteins. The results demonstrated that in addition to minute successive alterations in molecular structure wave- functions and resonant patterns can also describe complex molecular signaling pathways in cells. Different pathways may be defined by a single resonance profile. The separations between the peaks of wavelengths from Cosic's predictions for photon emissions in the visible spectrum that define the ERK-MAP pathway were within the range of 10^{-20} J. This quantity has been shown to be a fundamental unit of energy within the universe. The involvement of photon patterns indicates that non-local effects could accompany the serial causality (locality) assumed to connect molecular pathways.

Introduction

The substance or subject matter of Science is based upon enumeration. The patterns of these numbers in space-time determine the concepts that define phenomena. The simplified constructs for understanding the immense variations of those measurements constitute the models of perception and understanding. Scientists have usually assumed that the greater the congruence between predictions from a model and the characteristics of the phenomenon being measured, the more accurate and valid are the presumptions of the model.

For example, to explain the retrograde motion of the planet Mars from the reference of the earth as the center of the universe Ptolemy was required to add epicycles or additional subcircles upon the geocentric orbital circles. Copernicus' heliocentric system accommodated the retrograde phenomena by recognizing the different distances of the earth's and Mars' orbits with respect to their relative positions within their orbits. Although both systems predicted the phenomenological and observational aspects of Mars' retrograde motion, the system of Copernicus was ultimately demonstrated to be more consistent with the larger body of measurements.

The two major components for human reasoning, perception, and description of reality have been space and time. Discrete increments of space are allocated to matter or particles.

The spatial patterns of these units of matter or particles determine their function. Discrete increments of time are allocated to complex waves and fields. The temporal patterns of these fields and waves determine their function. The combinations of these

qualitatively discrete categories into a blending field, such as defined by Minkowski's four-dimensional manifold of space-time representation that became instrumental to relativity theories, accommodate the simultaneous dualism of de Broglie matter waves whereby a unit particle, such as an electron, could be either a particle or a wave.

The contemporary approach for molecular biology is serial causality in order to accommodate the demands of locality. Consequently for information or a change in stimulus characteristics to move from one boundary, such as the plasma cell membrane, to an internal boundary, such as the nuclear membrane, a series of spatial interfaces must occur. These interfaces which usually involve the addition or removal of an atomic or molecular component, such as a phosphate group or a proton, occur through a succession of different proteins. These signaling pathways, or more accurately "networks", are aggregates of molecular sequences that could be defined as fields in four-dimensional space.

Starting with some component (A) within the plasma cell membrane, A affects B and B affects C….N until the terminus (the nucleus) is reached. The "information" contained within that series affects the dynamics of the nucleus to initiate transcription and consequently to control the entire cell. The whole of the different proteins within this succession are often described as signaling pathways. For many of the signaling pathways that have been preserved in life forms for the last few billion years the numbers of proteins range from about 8 to 15.

Traditionally molecules with similar spatial patterns (structure) are assumed to exhibit similar functions and molecules of markedly dissimilar structures share minimal functions. However Irena Cosic (Cosic, 1994) observed marked discrepancies for this

central assumption. She addressed this discrepancy by assigning each amino acid with a calculated pseudopotential value based upon the characteristics of de-localized electrons. When these sequence values were spectral analyzed through Fast Fourier Transforms the resulting spectral power densities (SPDs) predicted the wavelength and hence the frequency of the potential photons that can be measured to be emitted from that molecule.

Subsequent experiments by Dotta et al. (2014) showed that during the habituation to ambient temperatures melanoma cells that had been removed from standard incubation conditions (37 °C) shifted power densities across the visible spectrum. Protein enhancers or suppressors for components of the cell whose peak wavelength had been predicted by Cosic's model of Resonance Recognition for Molecules (RRM) increased or decreased the photon radiant flux densities from those cells within the range of accuracy discern by the filters employed in the measurements.

In a manner similar to the difference between Ptolemy's and Copernicus' explanations for the retrograde motions of Mars, we predicted that there may be two models for the accurate prediction of the intercalation between components of signaling pathways in living cells. Both involve transmission of energy. The molecular approach presumes this transmission is completed by discrete addition or removal of matter (a molecule or proton/electron). The Cosic approach assumed that the energy is distributed through the resonance field created by the spatial pattern of the amino acids that constitute the proteins. The accompanying oscillating field could be electromagnetic in nature.

One process would involve the sequential exchange of a quantity of energy from molecule to molecule. The other would involve the summation and averaging of the spectral power density of the spatial order of the amino acids that constitute these proteins. Like the de Broglie matter-waves both manifestations could exist. Whereas the former would require locality to be effective, the latter, if photons were directly involved, could allow the introduction of non-local processes or “entanglement” (Aczel, 2002) within the cell between the outer (plasma cell membrane) and inner (nuclear membrane) boundaries. Here we present quantitative evidence for this possibility.

TRANSFORMATON OF THE MAP-ERK PATHWAY TO COSIC’S SERIAL PSEDUOPOTENTIALS

The signaling pathway presently designated as MAPK (Mitogen-activated protein kinases), originally labeled as ERK (extracellular signal-regulated kinases) is a “chain” of proteins that mediates changes or “information” from a receptor on the cell’s surface to the DNA within the nucleus of the cell. In general the sequence of proteins (mass in kDaltons in parentheses) from the surface of the cell to the nucleus are: VEGF (234 kD), TRK (348 kD), HRas (191 kD), CRAF (640 kD), MEK1 (395 kD), MEK2 (402 kD), ERK1 (362 kD), ERK2 (343 kD), CREB (343 kD), cFOS (383 kD) and PLA2 (808 kD). The meaning of each acronym can be found elsewhere (Albert et al., 2002).

The latter two proteins, cFOS and PLA2 (phospholipase A2) are considered to act in different spaces but to be determined by the components of the pathway. CFOS affects the nucleus while PLA2 involves more cytoplasmic activity. The molecular component

that is shared in the serial sequence from a matter-molecular perspective is the addition of a phosphate group to the neighboring protein that could be considered an aggregate equivalent of a Grotthuss-like chain.

To discern the spatial spectral power density of the amino acid sequence of each of these components of the pathway, each amino acid for each molecule was assigned the pseudopotential value as described by Cosic (Cosic, 1994; Cosic, 2014). The pseudo potential is the estimated electron-ion interaction potential (EIIP) that describes the average energy states of all valence electrons for each amino acid. The formula has been published (Cosic, 1994). What may be important from an astronomical perspective, particularly if Ernst Mach's ideas (Persinger & Koren, 2014) are considered, is contribution of the change of momentum of the delocalized electrons in the interaction.

Because spectral analyses with the algorithm we employed (SPSS-16 PC) required equal case numbers and the different proteins exhibit different lengths of amino acids, all proteins whose lengths were less than the longest one in the pathway were extended by sequential adding of the values (a type of "statistical PCR, or polypeptide chain reaction) so that all sequences were equal length. Spectral analyses were then completed. The real spatial "frequency" was obtained by dividing 0.38 nm by the spectral frequency unit produced by the software. The value of 0.38 nm was considered to be the average width of an amino acid.

For theoretical aesthetics we assumed that a feasible distance for de-localized electrons involving an average bond length (L) of ~0.25 nm would be π•L (~0.8 nm). The SPD for each of the 11 proteins were plotted as a function of the real spatial frequency for the range <0.8 nm. This interval contained 50 successive spectral power densities

each separated by 0.001 base frequency units or Δf. To test the concept of shared endpoints we employed canonical correlation. The last two components of the MAPK-ERK pathway, cFOS and PLA2 were designated as the dependents and the remaining variables were considered the predictors or covariates.

Dependant	Precursors (Independent)
cFOS +0.65	VEGF 0.41
	TRK 0.43
	H-Ras 0.07
	C-Raf -0.02
PLA2	MEK1 -0.14
	MEK2 0.40
	ERK1 0.43
	ERK2 0.60
	CREB -0.26

Table 1. Loading (correlation) coefficients for each protein within the ERK-MAP pathway upon the primary root extracted by canonical correlation for the two terminal components (cFOS and PLA2) of the pathway.

The results are shown in Table 1. The only statistically significant ($p < .01$) root extracted for the canonical correlation indicated that the spatial spectral density of cFOS, the one protein associated with nuclear changes, and PLA2, the protein associated with cytoplasmic activity, were negatively correlated (“loaded”) on the root. There is additional evidence from classical biomolecular interpretations that the activity of the two proteins were negatively correlated such that as one increases the other decreases.

However most biomolecular methodologies do not often differentiate time course and hence the reciprocal relationship, if it occurred within the millisecond range for example, would not be differentiated. To discern this dynamic the temporal increment (Δt) of the measurement must be less than the intrinsic frequency of the fluctuation. With larger Δts the measurer would observe only an increase in both protein activities.

The resonance pattern for cFOS was significantly associated with that of VEGF (the first protein in the signaling pathway) as well as TRK, MEK2, ERK1, and ERK2. On the other hand the resonance pattern of PLA2 was negatively correlated with the resonance pattern of those proteins. The resonance patterns for H-Ras, C-Raf, MEK1 and CREB were not significantly correlated with the patterns of either cFOS or PLA2.

The correlogram or scattergram of the relationship between the spatial resonance or spectral densities of the dependent variables (cFos and PLA2) and the precursors of the root is shown in Figure 1. This was completed by multiplying the unstandardized discriminant function coefficient score for each variable for the dependent variables (and adding the constant) and by multiplying the specific coefficient for each of the independent variables to obtain that function. The Pearson correlation was $r = 0.67$ ($p < .001$). The data are represented as standardized scores.

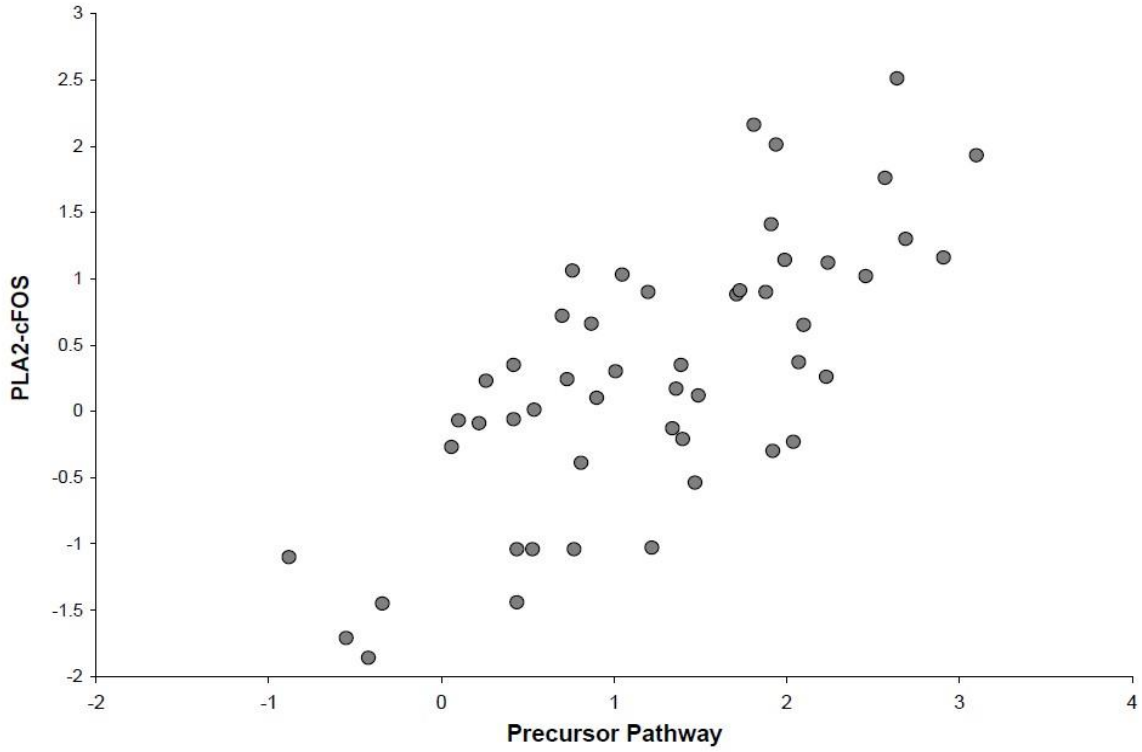

Figure 1. Scattergram of the correlation between the combination of the spectral power densities (SPDs) of two dependent variables (cFOS and PLA2) on the vertical axis and the SPDs for the precursor pathway proteins (horizontal axis) extracted in the first root.

WEIGHTED LINEAR ADDITION OF SPECTRAL DENSITY PATTERNS (SPDs) OF PRECURSORS PREDICT SPDS OF TERMINAL PROTEIN

Considering the negative correlation between the two proteins (cFOS, and PLA2) whose positions are often allocated at the end of the causal sequences between changes in membrane activity and induction of alterations in DNA function, multiple regression (step wise) analyses were completed for each independently. For cFOS multiple regression with cFOS as the dependent variable and the SPDs for each of the 9

precursors proteins as independent variables, resulted in a strong multiple r (r = 0.79) that was statistically significant [$F_{(5,45)}$ = 15.18, p < .001; 59% of variance explained].

The congruence between the predicted SPDs for each spectral frequency unit (Δf) for cFOS and the actual value for the cFOS molecule itself is shown in Figure 2. The equation including the partial regression coefficients (partial slopes) was 0.74(ERK2) - 0.51(MEK1) - 0.57(ERK1) +0.24(VEGF) +0.17(Hras) +0.02. To ensure the specificity of the congruence of the spectral increments (Δfs), because there may have been a mild phase shift for the different proteins, lag/lead analyses were completed. With the second lag as the dependent variable for cFOS, the SPDs for ±3 spectral units or Δfs for each molecule were entered as predictor variables. There was no statistically significant increase in the accuracy of the prediction (multiple r = 0.83).

When the SPDs for PLA2 was employed as the dependent variable and the SPDs of the same nine variables were entered by the stepwise procedure only one variable entered: ERK2 [$F_{(1,49)}$ = 10.69, P < .01; 18% of the variance explained]. When cFOS was added to list of predictor variables, the multiple R [$F_{(2,48)}$ = 12.01, p < .001] value increased to MR = 0.58 (31% of the variance explained). The equation was -.58(cFOS) - 0.24(ERK2) + 0.06 and indicated that in terms of shared numerical variance the resonance characteristics of PLA2 were affected by that of cFOS.

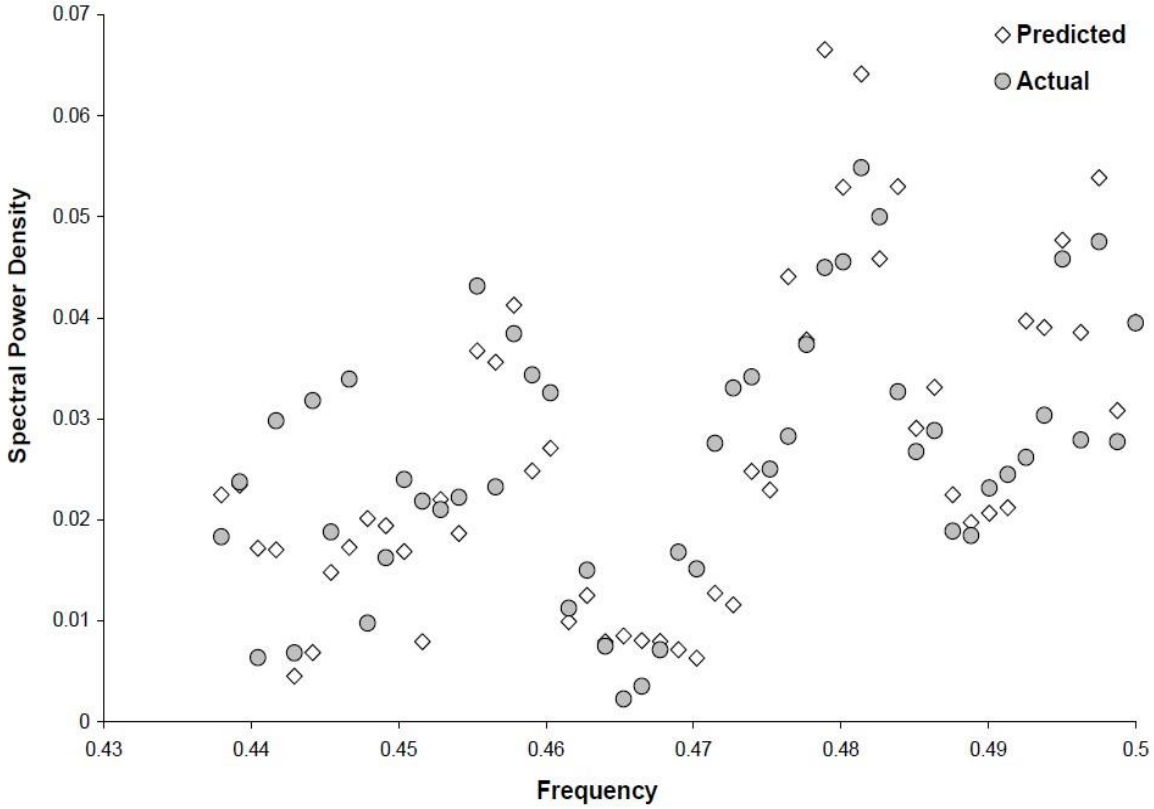

Figure 2. Spectral Power Densities (SPDs) as a function of numerical frequency for the actual cFOS protein molecule (closed circles) and the predicted SPDs (open diamonds) based upon weighted linear combinations of the SPDs of antecedent proteins in the pathway.

Even when ± 3 lag/leads for the Δfs for the SPDs for each protein (except cFos) were added as potential predictor variables the multiple r (0.57) did not change significantly. However when cFOS and its ±3 lags were added, the predicted multiple r increased to 0.88 [$F_{(6,39)}$ = 23.14, p < .001; 75% of variance explained]. The equation was cFOS, lead 1 unit (- 0.63), VEGF (0.61), cFOS, lagged 2 units (-1.12), CREB, lagged 3

units (-0.50), Hras (0.45), ERK2 (-0.24) + 0.08 (constant). The results are shown in Figure 3.

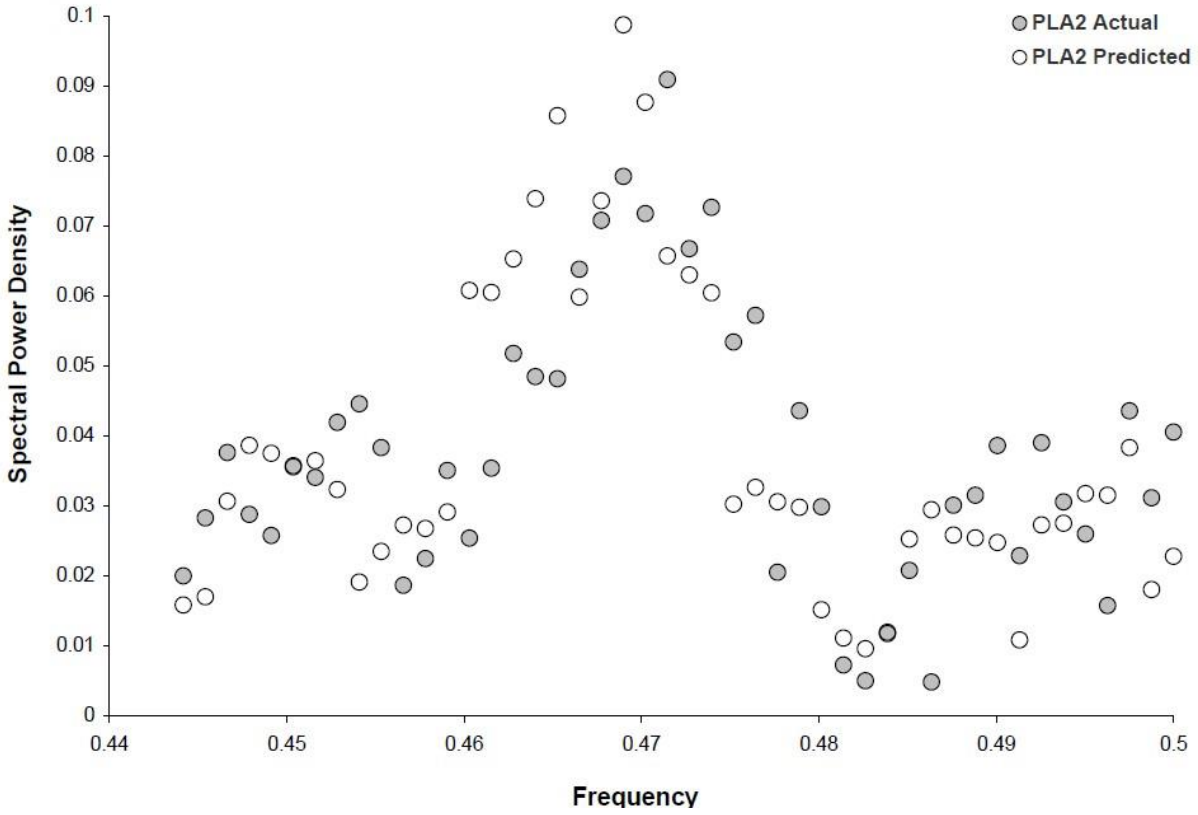

Figure 3. The correlogram of the predicted Spectral Power Density values (open circles) for Phospholipase (PLA2) protein and the actual SPD values (closed circles) for that protein.

To verify that the spectral composition of the average of the SPDs for cFOS and PLA2 were indeed independent with respect to their constituent (precursor) proteins in the pathway, the mean of the SPDs for cFOS and PLA2 were entered as dependent variables. No equation was generated with a pin (probability to enter) level of $p < 0.05$

from the eight precursor variables. In effect this aggregate average, although its components were significantly associated with the SPDs for the precursor molecules in the pathway, were not revealing. The orthogonal (“antiparallel”) association between these two terminal proteins in combination functionally cancelled or “occluded” the conspicuous relationship with the precursors.

There are four major indications from these results. First, the relationship between the proteins within a classic “signaling pathway” that leads to cFOS effects on the nucleus produce a combined resonance pattern that overlaps with the specific resonance pattern of the cFOS molecule. This suggests that molecular pathways can display wave-like properties where components can be decomposed and re-composed into an aggregate that reflects the whole. In other words, the whole is a composite of the weighted mean of the parts.

The second conclusion is that the spectral increments are relatively precise for the central component of the pathway. Adding the lag or lead values (each equivalent to a hypothetical change of $\Delta f = 0.001$ for the spectral increments of the precursor molecules did not significantly change their final correlation (similar resonance pattern) with the cFOS molecule. Hence the likelihood that “random” variables entered the equation could be considered minimal.

Third the PLA2 component which has often been paired according to traditional biomolecular interpretations with cFOS is not independent of cFOS. Its SPD is required to accommodate PLA2’s resonance. In addition, the components from the precursor molecules may be phase shifted by about 0.003 nm of an equivalent wavelength (in nm) or one or two SPD frequency units (0.001). This would be equivalent to $3 \cdot 10^{-12}$ nm which

approaches the Compton λ ($2.42 \cdot 10^{-12}$ m) for an electron. These results indicate that the SPD for the Rydberg-derived pseudopotentials of amino acids in the traditional terminal proteins, cFOS and PLA2 displayed distinct resonance patterns. As shown in Figure 4, the SPDs profiles for the two proteins are negatively correlated (r = -0.60), or, from a wave perspective, almost maximally out of phase.

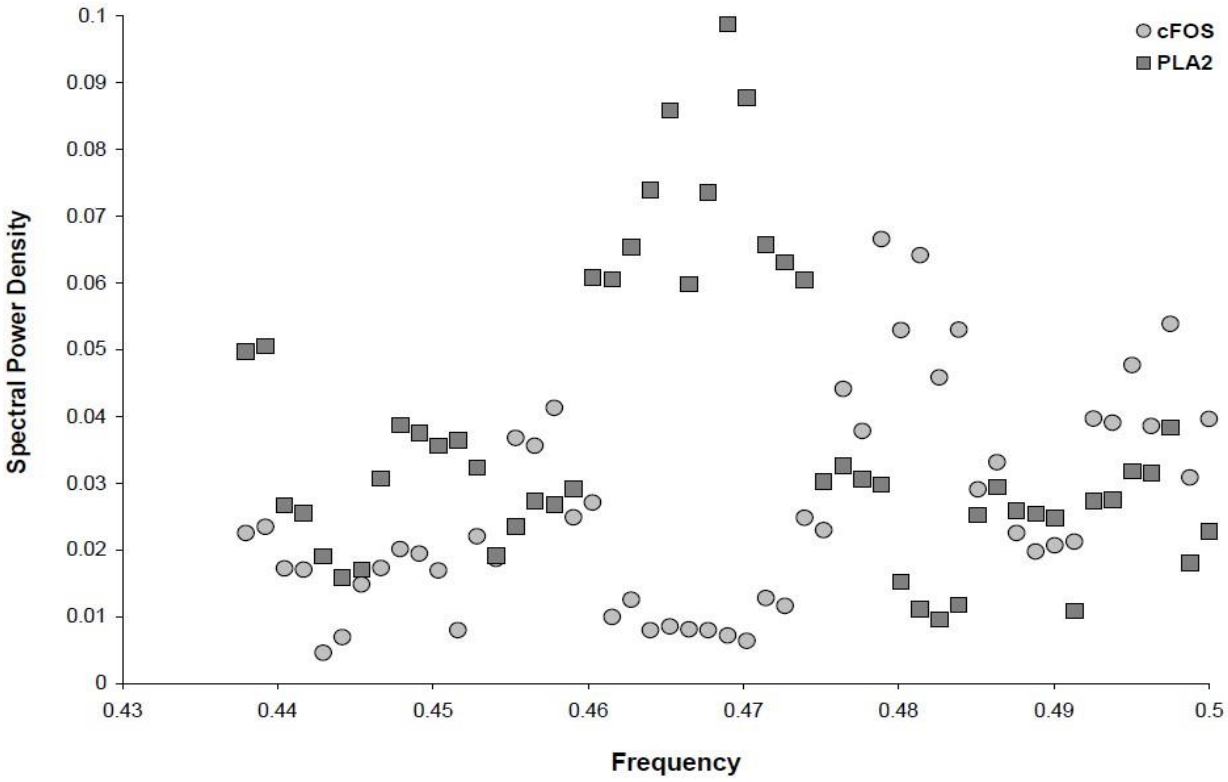

Figure 4. Overlap of the Spectral Power Densities for the cFOS (light circles) and PLA2 (dark squares) molecules according to Cosic's method as a function of base frequency for distances of <0.8 nm to accommodate de-localized electrons.

PREDICTIONS OF PEAK PHOTON EMISSION FROM RESONANCE PATTERNS OF SIGNALING PATHWAYS

According to Cosic (Cosic, 1994; Cosic, 2014), each specific biological function within a protein (or DNA) is characterized by one frequency that in turn predicts a peak wavelength for photon emissions. From an aggregate or field perspective specific biological functions of a "serial" pathway might be described by a specific spectral profile or pattern of peak frequencies. According to Cosic, the peak wavelength λ for photon emission, which we have demonstrated to be valid through direct experimental manipulation is:

$$\lambda = K \cdot f_{rrm} \quad (1),$$

where K is the constant 201 and f_{rrm} is the numerical frequency obtained from the spectral analysis.

For the peak SPD for cFOS, which could be predicted by the weighted linear combination of the precursor proteins in the ERK-MAP pathway, the peak numerical frequencies were .458 (.455-.460), 0.481 (0.476-0.484) and 0.498 (.497-0.498). The central value (0.481) was more than two standard deviations above the central tendency (mean) for the sequence. The other two peaks were more than one standard deviation above the mean.

According to the Cosic formula (1), the peak wavelength (λ) for photons for the cFOS protein would be 438.9 nm, 417.9 nm, and 403.6 nm, respectively. By dividing

these values into the velocity of light in a vacuum, frequencies are obtained. These frequencies multiplied by Planck's constant ($6.626 \cdot 10^{-34}$ J·s) resulted in energies that were 4.52, 4.76, and $4.92 \cdot 10^{-19}$ J, respectively. From a theoretical perspective what is much more important is difference in energies between the power peaks. They would be $2.4 \cdot 10^{-20}$ J and $1.6 \cdot 10^{-20}$ J which is within the range of the second shell energies associated with the movement of protons through water (DeCoursey, 2002) and is considered to be a fundamental energetic unit across hyper-dimensional space (Persinger et al., 2008).

On the other hand, the peak numerical frequency for PLA2 was 0.465 (range 0.460 to 0.474). There was a smaller peak around 0.438. The associated photon wavelengths would be 432 nm and 458 nm. The corresponding energies are $4.6 \cdot 10^{-19}$ J and $4.34 \cdot 10^{-19}$ J. The difference between these two corresponding energies is $2.6 \cdot 10^{-20}$ J.

THE ASTROBIOLOGICAL SIGNIFICANCE OF 10^{-20} JOULE PHASE SHIFT INCREMENTS WITHIN RESONANCE PATTERNS

The occurrence of specific peaks of predicted wavelengths within the ultraviolet boundary of the visible spectrum from the combined SPDs of the molecules that reflect the SPD profile of cFOS has local and non-local applications. Cosic had stated that the frequencies predicted by the RRM could represent oscillations of some physical field which propagates through water dipoles. This field could be electromagnetic in nature. Both theoretical and empirical (Dotta et al., 2014) approaches support her contention.

This “electromagnetic nature” may be intrinsic to the physical chemistry of water and its interactions with solutes. The division of the magnetic moment of a proton ($1.41 \cdot 10^{-26}$ A·m^2) by the unit charge ($1.6 \cdot 10^{-19}$ A·s) results in a term of diffusion ($0.88 \cdot 10^{-7}$ m^2·s^{-1}). When applied to the average viscosity of water ($6.3 \cdot 10^{-4}$ kg·m^{-1}·s^{-1}) for biological temperatures the force would be $5.54 \cdot 10^{-11}$ kg·m·s^{-2}. If this force were applied across the distance of two O-H bonds ($1.92 \cdot 10^{-10}$ m) that would constitute the water molecule, the energy would be ~$1.1 \cdot 10^{-20}$ J. If that force was applied over the estimated width of an amino acid the energy would be ~$2 \cdot 10^{-20}$ J (Persinger, 2014). This value is within the range of the differences in energy between the peak photon emissions from the cFOS complex as predicted by the Resonance Recognition Model.

The possibility that fundamental quantities of energy that operate cellular mechanisms are the same as those found anywhere in the universe and hence relates the processes found within both astronomical and cellular phenomena has been primary ignored by modern perspectives. However this consistency would be consistent with Ernst Mach’s concept of Prominence of the Universe or his principle that the behaviour of any component of the universe, presumably no matter how small, is determined by all of its parts. The concept is also consistent with the assumption that a physical field can exist anywhere.

We (Persinger, 2010) have suggested that the description of the whole, in this case the consideration of the universe as a single spatial and temporal unit, simplifies the required geometries and mathematical descriptions, to basic equations. For example the mass of the universe 10^{52} kg multiplied by its width 10^{26} m and the square of the intrinsic Puthoff frequency (10^{86} s^{-2}) results in a force of 10^{164} N. The force per smallest unit (a

Planck's voxel of ~10-10^5 $m^{-3)}$ when all of these units within the volume of the universe (10^{78} m3) are considered, i.e., 10^{183} Planck's voxels in the universe, results in a force of 10^{-19} N per voxel. If this force is applied across the most fundamental wavelength of the universe, the 10^{-1} m displayed by neutral hydrogen, the energy is ~10^{-20} J. Inclusion of specific coefficients for thee above constituents does not change the order of magnitude for the solution.

The 10^{-20} J solution as a basic unit of energy transmission within the living physical-chemical system has been shown within several levels of discourse by Persinger (2014) For example the ~10^{-12} N of electric force between two potassium ions whose single layer of approximately 10^7 ions over the plasma membrane surface solves for its resting potential, results in 10^{-20} J when the distance between any two potassium ions, about 10 nm, is considered. Effectively the energy ($1.9 \cdot 10^{-20}$ J) axon's action potential, that can be inferred by $1.6 \cdot 10^{-19}$ A·s multiplied by the net change in voltage ($\Delta V = 1.2 \cdot 10^{-1}$ V), is a conservation of that energy transformed from statics to dynamics.

The 10^{-20} J order of magnitude as a discrete amount of energy is associated singular shifts in the bond angle of receptor proteins that allows sequestering of the ligands. The hinge motion associated with sequestering the agonist for glutamate binding is associated with $1.5 \cdot 10^{-20}$ J. The energy difference between phosphorylated and unphosphorylated subunits of phenylanine hydroxylase was in the order of $1.8 \cdot 10^{-20}$ J.

When we measured photon emissions from melanoma cells directly by sensitive photomultiplier units the estimated unit of energy was 10^{-20} J per cell (Dotta et al., 2011). We found that the most parsimonious process that would have produced this "quantity" would have been narrow phase modulations in the range of the width of a plasma cell

membrane that is about 10 to 20 nm, for photons within the visible wavelength particularly near the ultraviolet boundary for the visible wavelengths.

These observations are congruent with the analyses of the RRM frequencies reported here for the ERK-MAP pathway. Although the peak frequencies that could be associated with this specific pathway occurred within the visible, near-ultraviolet, range, the difference in energies between these peaks were in the order of 10^{-20} J. We suggest that this increment of energy either transports or is the unit of energy, which, when presented as temporal patterns, defines the biological functions of the pathway in a manner analogous to Cosic's concept that a specific frequency for a single molecule describes its biological function.

From an astronomical perspective, this indicates that the unit energies that either influence or determine the "information" which defines the boundaries of the cell's structure and function are the same or similar to those that might define the structures and functions of all matter. The relevance of astronomical concepts and principles in cell biology, particularly when addressing the ubiquitous and recalcitrant manifestations such as cancer and malignancy, could be much more important than imagined. Persinger and Lafrenie (Persinger & Lafrenie, 2014), applying the innovative and integrative work of Michael Levin (Levin, 2012), have shown quantitative evidence that "cancer" cells may reflect a more universal phenomena coupled to sources of variance related to Cosmic Microwave Background (CMB) energies and to the quantities by which bits of information dissipate into or appear from entropy.

The convergence may be more apparent than anticipated. According to Cosic (Cosic, 1994) the conductive electron transfer produced by the difference in free electron potentials at the N and C terminals of a protein can be expressed as a pseudopotential that is 0.128 Ry or $2.78 \cdot 10^{-19}$ J or 1.74 V. The maximum velocity from this energy difference would then be:

$$V_{max} = \sqrt{} (2q \cdot V \cdot m\text{-}1) \textbf{ (1),}$$

Where q is the unit charge, V is the potential difference estimated from the pseudopotential, and m is the mass of the electron. The solution is $7.87 \cdot 10^{5}$ $m \cdot s^{-1}$. For a packet of energy, such as might be contained within an electron, to move across a quintessential cell with a diameter of ~10 μm, approximately $1.27 \cdot 10^{-11}$ s would be required. The equivalent frequency is $0.78 \cdot 10^{11}$ Hz. The energy associated with that frequency, obtained by multiplying by Planck's constant ($6.626 \cdot 10^{-34}$ J·s) is $5.21 \cdot 10^{-23}$ J. The temperature equivalent of this value from the Boltzmann constant of $1.38 \cdot 10^{-23}$ $J \cdot T^{-1}$ where T is °K, would be 3.7 °K which is within the range of Cosmic Microwave Background energies. One possible interpretation for this convergence is that the upper limit of Cosic velocity is the interface for access to or from entropy-related energies within the CMB as predicted by Persinger and Lafrenie (2014).

ELECTROMAGNETIC TRANSFORMS AND EXPERIMENTAL VERIFICATION

Murugan et al (2016) found that spring water (containing near physiological patterned ion concentrations) exposed for several days in darkness while being exposed to physiologically- patterned (frequency and phase-modulated) magnetic fields within the microTesla range displayed conspicuous photon emissions. The peak wavelengths of those emissions suggested energy associated with that exposure had been “represented” or “stored” within the organization of water. Each of the serial point durations of the voltages that comprised the magnetic temporal patterns were 3 msec. This value had been selected because of the empirical demonstration of its efficacy for producing powerful biological effects on both organisms and cells. The value had been derived from the nearest integer solution from the predictions of Persinger and Koren (Persinger & Koren, 2007) for the time required for a proton to expand one Planck’s Length according to cosmological concepts derived from the Hubble parameter. There is experimental evidence for this solution (Koren et al., 2014).

When 1 cc cuvettes of this exposed water was measured for fluorescence intensity between 320 and 470 nm, there was an increase of about 150 photon counts per unit wavelength within the 420 to 440 nm range. The peak of the shift (399 nm) between the activated magnetic fields (4.4 to 11. 5 μT) and the weaker (409 nm) magnetic fields (0.1 to 0.6 μT) was about 10 nm. In other words it was the spatial shift (λ) of the classic plasma cell membrane. That narrow increments of energy were essential for the effect was indicated by the measurement for the background exposed water whose peak was 381 nm. The relationship might be considered to be non-linear because the higher intensity

effects were more similar to the background (ambient) power frequencies fields that are encountered within the laboratory environment.

Spectral analysis of the photon emissions from the water that had been exposed to the optimal intensity magnetic fields in the dark for several days before the photon emissions were measured revealed peaks in SPD at functional distances of 10 nm and 5 nm. The shift in wavelength between the photons emissions from the water that had been exposed to the optimal magnetic field intensities and reference group would have been equivalent to about 10^{-20} J. This is the same order of magnitude as the energy quantity associated with the differences between the peak wavelengths that describe the ERK-MAP pathway according to the Cosic' solutions.

These marked similarities which may reflect congruence reiterates that water, often described as "the solvent of Life", at pH levels compatible with living systems may be more than a passive medium. Instead it may contain the "blueprint" or directive structure for the serial activity that traditionally defines signaling pathways. From this context the serial sequence of proteins within a pathway or more appropriately network, such as ERK-MAP, would be the aggregate form of the proton-to-proton displacements in the hydronium ion that have been described by Grotthuss-type mechanisms.

Application of the same patterned magnetic field with the identical point durations (3 ms) has between demonstrated by experiment to produce incremental shifts (toward alkalinity) in pH in spring water during several hours of exposure. Fractional temporal increments of observation indicated that the shifts occurred for about 20 to 25 ms. Although perhaps spurious it may be relevant that the time required to add a nucleotide to a DNA sequence or during the process of transcription has been estimated to be within

this range. Thus the same configuration of magnetic field that produced the shift in the wavelength of the emission of photons can also produce transient shifts in energy that could potentially affect the dynamics of the addition of a nucleotide into a DNA process.

This converge of temporal parameters and energies between the specific features of magnetic fields that affects shifts within pH in spring water only, photon emissions, and the Cosic solutions for the ERK-MAP pathway indicates that the “oscillations of the physical field” that propagate through the water dipoles could be electromagnetic in nature as she predicted. In addition the capacity for this oscillation through these electromagnetic fields is contained within the ionic relationships within the water itself. Appropriately configured and applied magnetic fields access these physical capacities such that energy can be stored within this process and later be released as photons within the visible or near-visible waveband. The wavelengths are shifted or phase-modulated by values that facilitate the occurrence of 10^{-20} J of energetic quantities.

There could be two physical manifestations that interface between traditional matter- based translation of information between the surface of the cell and the nucleus. The first would occur through the more well-known structural changes within causal series of molecules. The second could be measured as resonance electromagnetic patterns (such as photons) that are mediated through the ubiquitous but ephemeral proton of the hydronium ion. Its properties and densities should be reflected quantitatively.

Diffusion velocity of a proton according to the diffusivity term obtained by dividing the proton magnetic moment by the unit charge ($0.88 \cdot 10^{-7}$ $m^2 \cdot s\text{-}1$) for a classic 10 µm (whose energy equivalence is 10^{-20} J) width cells with a surface area of $3.14 \cdot 10^{-10}$ m^2 would require about 3 to 3.5 ms to traverse the volume. If the volume occupied by the

nucleus is considered the time would approach 3 ms, which is the optimal increment of time for the point durations of the applied magnetic fields to produce the diminishment effects upon cell growth. Point durations of 1, 2, 4, or 5 ms are much less effective (Buckner, 2011).

There should be convergence of quantification between well-known features of classical physics and the temporal progress of the information from the resonance components across the molecular sequences for the MAP-ERK pathway. This feature should differentiate the identification of the most likely molecular species and mass concentration that might constitute this “physical” substrate. We considered one of the most likely analogues of candidates for this identification to be drift velocity which is defined as:

$$v = I(n \bullet A \bullet q)^{-1} \qquad \textbf{(2),}$$

where v is the drift velocity of the carrier particle, I is the net current being mediated, n is the number of particles in a mole based upon molar density, A is the area through which the current is mediated, and q is the unit charge.

If one assumes the direct of the information carried as quantities of energy manifested as particles is from the membrane to the nucleus and that energy utilized from glucose-related metabolism per cell is about 10^{-12} J per s, then an estimated number of discrete reactions could be obtained. If the basic energetic unit of these interactions is 10^{-20} J (Persinger, 201), then there would be 10^{8} unit reactions per second (Albert, et al., 2002) with an associated current of $1.6 \cdot 10^{-19}$ A·s or $1.6 \cdot 10^{-11}$ A per second. When

converted to cm^{-2} this would be about ~0.5 μA·cm-2 which is within range of some empirical measurements for cell currents.

If the mediator is the proton from the hydronium ion, then at a typical pH of 7.4, the concentration of H^+ would be $3.98 \cdot 10^{-8}$ M such that the functional density would be [(1 $g \cdot cc^{-1}$) /(18 $g \cdot mol^{-1}$)] ·(3.98·10^{-8} mol for H^+) ·(10^6 $cc \cdot m^{-3}$) ·(6.023·10^{23} $molecules \cdot mol^{-1}$), or $1.33 \cdot 10^{21}$ molecules of H^+ per cubic m. The product of this value with the surface area (A) of the cell ($3.14 \cdot 10^{-10}$ m2) and the unit charge of a proton ($1.6 \cdot 10^{-19}$ A·s) results in a denominator that when divided into the intrinsic current (I) results in a value of $2.4 \cdot 10^{-4}$ m·s-1 as a model drift velocity.

The time required for this “drift” to occur across 0.5 the width of the cell soma width to impinge upon the nucleus would be about 20 ms. The increment is within the order of magnitude of the time required to add a nucleotide to a DNA sequence. Although the precision of this timing would clearly be related to the intrinsic current moving across the cell and its surface area, the role of pH becomes particularly important from this perspective. A shift of only 0.5 of a pH unit around pH 7.4 could be sufficient to affect the drift velocity to values that might precisely overlap with the optimal duration for adding or preventing the addition of nucleotides to a replicating DNA sequence.

THE EMERGENCE OF EXCESS CORRELATION AND ENTANGLEMENT

The occurrence of photon emissions (or absorptions) in molecular pathways as predicted by the results of the present analyses of Cosic’s RRM introduces the possibility that under specific conditions excess correlations could occur at non-traditional distances

between the same pathways in different cells. The cells could be separated at great distance within an organism or potentially at great distance between organisms. The extent of this non-locality remains to be experimentally determined.

However we (Dotta & Persinger, 2012) have shown that two photoluminescent reactions separated by 10 m but sharing the same changing, angular velocity electromagnetic fields behaved as if the loci had been transiently superimposed. The two separate loci displayed the properties of the “same space”. In this condition injection of a single amount of reactant in each of two loci simultaneously resulted in the widening of the duration of the photon emission as if twice the amount had been injected into the same reaction.

A similar effect non-locality was noted for injections of small quantities of protons (a weak acid) into spring water (Dotta et al., 2013). Continuous, simultaneous measurement of shifts in pH in containers separated by 10 m indicated that if the solutions both shared the same, specifically configured magnetic fields with changing angular velocities where the group and phase velocities were not equal, the expected increase in acidity in the injected volume was associated with a net increase in alkalinity in the other volume.

That “excess correlation” can occur with aggregates of cells when they share these similar, rotating magnetic fields, has been demonstrated by Dotta et al (2011) Recently we found that the injections of small amounts of hydrogen peroxide into plates of cancer (mouse melanoma) cells (resulting in partial mortality) exposed to similar rotating magnetic fields was associated with a comparable mortality of these cells split from the same source if they were exposed to a similar magnetic field at the time. In this instance

the distance separating the two plates of cells in each experiment was about 3 km. The results emerged over several days of culturing during which time each pairs of plates were exposed to the specific rotating magnetic field.

The role of signaling pathways for these cells was suggested by the requirement for some proportion of the cell population in the local stimulation (the ones that received the hydrogen peroxide) to remain alive. If there was total mortality in the local cells from the injection of the peroxide there was no change in growth in the non-local cells even if they shared the same magnetic field parameters. For the non-local cells to display the “excess correlation” or “entanglement” at least 30% of the cells in the local population had to survive the hydrogen peroxide treatment.

Cells themselves might generate their own rotating, magnetic fields. Dotta et al 2014 calculated that the lateral diffusion of proteins within the plasma cell membrane had the capacity to interact with magnetic fields to generate photons. A specific intensity, around 1 μT, was predicted to generate the greatest photon emissions. As predicted this intensity elicited the largest radiant flux density when measured by photomultiplier units. Conditions that synchronize the “membrane magnetic moment” of populations of cells could potentially increase their capacity to display quantitative degrees of excess correlation that could affect the signaling pathways of cells and hence their rate of proliferation or diminishment.

CONCLUSIONS

The physical-chemical bases of one of the most well-known signaling pathways in living cells can be described by a resonance pattern based upon de-localized electron potentials. The congruence between the spectral density pattern of the terminal protein (cFOS) in this pathway and the weight average of the spectral density patterns of precursor patterns indicate that wave-functions with electromagnetic characteristics manifested by specific wavelengths of photon emissions may be the energetic bases to serial molecular causality.

The quantitative similarity between the energies associated with differences between the peak photon wavelengths predicted by the Cosic Model and those that exist throughout the universe even when Planck's Length is considered supports their essential function. Multiple molecular pathways that have persisted for billions of years and have been considered to be "conserved" may be present simply because of their prominence and availability rather than their criticality. Quantitative solutions of the drift velocities and diffusivities involving the protons within the hydronium ion of water indicate that water itself may be "progenitor" from which molecular pathways superimpose their properties.

References

Aczel A.D. (2002) Entanglement: the Greatest Mystery in Physics Raincoast Books, Vancouver.

Albert B., Johnson A., Lewis J., Raff M., Roberts K., Walter P. (2002) Molecular Biology of the Cell Garland Science, N.Y.

Buckner C. (2011), Effects of Electromagnetic Fields on Biological Processes are Spatial and Temporal Dependent, Ph.D. Biomolecular Sciences, Laurentian University, Sudbury.

Cosic I. (1994) Macromolecular bioactivity: is it resonant interaction between macromolecules?-theory and applications. IEEE Transactions on Biomedical Engineering. 41: 1101-1114.

Cosic I., Lazar K., Cosic D. IEEE Transaction on NanoBioscience. (2014) DOI: 10.1109/TNB.2014.2365851.

Decoursey T.E. (2002) Voltage-gated proton channels and other proton transfer pathways. Physiological Reivews. 83: 475-579.

Dotta B.T., Buckner C.A., Cameron D., Lafrenie R.M., Persinger M.A. (2011) Biophoton Emissions from Cell Cultures: Biochemical Evidence for the Plasma Membrane as the Primary Source. General Physiology and Biophysics. 30:301-309.

Dotta B.T., Buckner C.A., Lafrenie R.M., Persinger M.A. (2011) Photon emissions from human brain and cell culture exposed to distally rotating magnetic fields shared by separate light-stimulated brains and cells. Brain Research. 388 (2011) 77-88.

Dotta B.T., Lafrenie R.M., Karbowski L.M., Persinger M.A. (2014) Photon Emission from Melanoma Cells during Brief Stimulation by Patterned Magnetic Fields: Is the Source Coupled to Rotational Diffusion within the Membrane? General Physiology and Biophysics. 33:63-73.

Dotta B.T., Murugan N.J., Karbowski L.M, Lafrenie R. M , Persinger M.A. (2014) Shifting wavelengths of ultraweak photon emissions from dying melanoma cells: their chemical enhancement and blocking are predicted by Cosic's theory of resonant recognition model for macromolecules. Naturwissenschaften. 101 87-94.

Dotta B.T., Murugan N.J., Karbowski L.M, Lafrenie R. M , Persinger M.A. (2013) Excessive correlated shifts in pH with distal solutions sharing phase-uncoupled angular accelerating magnetic fields: macro-entanglement and information transfer. International Journal of Physical Sciences. 8 (2013) 1783-1787.

Dotta B.T., Persinger M.A. (2012) Doubling of Local Photon Emissions from Two Simultaneously Separated, Chemiluminescent Reactions Share the Same Magnetic Field Configurations. Journal of Biophysical Chemistry. 3:72-80.

Koren S.A., Dotta B.T., Persinger M.A. (2014) Experimental Photon Doubling as a Possible Local Inference of the Hubble Parameter. The Open Astronomy Journal. 7 (2014) 1-6.

Levin M. (2012) Molecular bioelectricity in developmental biology: New tools and recent discoveries. BioEssays. 34: 205-217.

Murugan, N.J., Karbowski, L.M. and Persinger, M.A. (2014) Serial pH Increments (~20 to 40 Milliseconds) in Water during Exposures to Weak, Physiologically Patterned Magnetic Fields: Implications for Consciousness. Water Journal. 6, 45-60.

Persinger M.A. (2010) 10^{-20} Joules as a Neuromolecular Quantum in Medicinal Chemistry: An Alternative Approach to Myriad Molecular Pathways? Current Medicinal Chemistry. 17: 3094-3098.

Persinger M.A. (2014) Quantitative Convergence between Physical-Chemical Constants of the Proton and the Properties of Water: Implications for Sequestered Magnetic Fields and a Universal Quantity International Letters of Chemistry, Physics and Astronomy. 12: 1-10

Persinger M.A. Lafrenie R.M. (2014) International Letters of Chemistry, Physics and Astronomy. 17 : 67-77.

Persinger M.A., Koren, S. (2007) A theory of neurophysics and quantum neuroscience: Implications for brain function and the limits of consciousness. International Journal of Neuroscience. 117: 157-175.

Persinger M.A., Koren, S., Lafreniere G.F. (2008) A Neuroquantologic Approach to How Human Thought Might Affect the Universe. NeuroQuantology. 6 :262-271.

Persinger M.A., Koren, S.A. (2014) Potential Role of the Entanglement Velocity of 10^{23} $m \cdot s^{-1}$ To Accommodate Recent Measurements of Large Scale Structures of the Universe. International Letters of Chemistry, Physics and Astronomy. 15: 80-86.

Chapter Transition: Filtering Biophotonic Signatures

The previous chapter demonstrated the validity of the RRM model as a predictive system. We linked the periodicities found within linear sequences of pseudopotentials converted from amino acids to wavelengths suggestive of intrinsic features of biomolecules, focusing in on the MAP-ERK pathway. The following chapter employs the same concepts and methods to detect unique photon emission profiles in cancer and non-cancer cells. Photomultiplier tubes, equipped with exclusion filters which selectively allow certain photon wavelengths to pass through, collected photons emitted by cells in vitro. We then used discrimination techniques and other statistical manipulations to model a cancer detector. Our results demonstrate that cancer and non-cancer cells can be discriminated based upon the ratio of ultra-violet (UV) and infrared radiation where non-cancer cells display proportionally greater standardized photon emissions within the infrared (IR) range (>900 nm) relative to cancer cells. We also identified three key wavelengths which could be used to discriminate between cancer and non-cancer cells though our model was most accurate when excluding one cell type: HBL-100. The results are discussed within the framework of a detection method whereby cancer and non-cancer biophoton signatures can be identified and separated statistically to infer the source of the emissions. We hypothesize that the current methods involving exclusion filters can be applied to detect cancer cells on the basis of expected IR-UV ratios.

Chapter 3

Biophotonic Markers of Malignancy: Discriminating Cancers Using Wavelength-Specific Biophotons

(Original Research)

Murugan N.J., Rouleau N, Karbowski L.M., Persinger M.A.

[Submitted to *Biochemistry and Biophysics Reports,* 2017]

Abstract

Early detection is a critically important factor when successfully diagnosing and treating cancer. Whereas contemporary molecular techniques are capable of identifying biomarkers associated with cancer, surgical interventions are required to biopsy tissue. The common imaging alternative, positron-emission tomography (PET), involves the use of nuclear material which poses some risks. Novel, non-invasive techniques to assess the degree to which tissues express malignant properties are now needed. Recent developments in biophoton research have made it possible to discriminate cancerous cells from normal cells both in vitro and in vivo. The current study expands upon a growing body of literature where we classified and characterized malignant and non-malignant cell types according to their biophotonic activity. Using wavelength-exclusion filters, we demonstrate that ratios between infrared and ultraviolet photon emissions differentiate cancer and non-cancer cell types. Further, we identified photon sources associated with three filters (420-nm, 620-nm., and 950-nm) which classified cancer and non-cancer cell types. The temporal increases in biophoton emission within these wavelength bandwidths is shown to be coupled with intrisitic biomolecular events that using Cosic's resonant recognition model. Together, the findings suggest that the use of wavelength-exclusion filters in biophotonic measurement can be used to detect cancer *in vitro*.

Introduction

Malignant growths, left undetected, can become increasingly difficult to treat or remove. It is therefore imperative that technologies are developed which can detect malignancies before cells invade neighboring tissues or metastases are generated elsewhere in the body. Though molecular techniques are currently available which detect biomolecules within specimens obtained by biopsy, recent advances have produced alternative non-invasive detection methods which do not require surgery. Among them, biophotonic techniques represent a novel approach which makes use of light that is derived from cells to differentiate malignant and non-malignant tissues (Giser et al., 1983; Chilton & Rose 1984). Shimizu and colleagues (2014) have not only measured weak biophoton emissions from transplanted tumors but observed differences in these emission profiles amongst different types of tumors. Dotta et al. (2014) have recently demonstrated that, using a serious of wavelength exclusion filters *in vitro*, the temporal emission of these photons can be correlated to precise biomolecular cascades that are associated with cancer processes. Even, elevations in biophoton emissions from serum or urine obtained from cancer patients have shown to display distinctive profiles compared to the bio-fluids obtained from healthy individuals (Amano et al. 1995, Chilton & Rose 1984).

Cell-derived ultra-weak biophoton emissions can be used as a biological marker which could represents an important step toward the establishment of novel detection methods in oncology. Imaging tissues without the use of nuclear materials, as is required in positron-emission tomography (PET), could reduce the time necessary to detect and

diagnosis cancers, however, display several shortcomings such as exclusion of vulnerable population (i.e. patients who are pregnant or breastfeeding) or the cost effectiveness/maintenance of the imaging tool (Hanasono et al. 1999; Gallamini et al. 2014). Even utilizing biophotons as a method for pathological detection possess its own obstacles. The central challenge here is that biophoton markers must be characterized and separated from normal cellular biophotonic activity as well as extraneous sources of noise. The Cosic Resonant Recognition Model (RRM) represents a practical solution in this regard (Cosic et al. 2016; Cosic 1994). This physiciomathemtical model was used to determine the characteristics frequencies of a protein using the energy of the delocalized electrons from its linear amino acid sequence. She developed this model to investigate the significant resemblance between functionally similar proteins using the idea of electromagnetic resonance. She later identified that based on these coherent domains, frequencies can emerge that are founded on the basis of electromagnetics or light. The proteins that drive molecular pathways are highly associated with the peak frequencies within the ultraviolet through the visible to the near infrared range has been shown by Dotta et al. (2014). In the same study they shown the proteins where the dominant frquency was determined it could be manipulated by treating the cells with activators or inhibitors, proving that these frequencies are strongly correlated to specific protein functions.

There are many classes of proteins where over- or under-expression can be predictive of malignancy. Therefore resonant signatures of biophotonic activity which are known to pair reliably with key biomolecular events involved in cancer can be used as biophotonic markers. Whereas temporal patterns of photon emissions can be indicative

of malignancy or human presence (Takeda et al 2004, Vares et al. 2016; Dotta et al. 2016), wavelength should be considered as a critical parameter. The wavelength of a photon is proportional to its energy. Biophoton emissions are known to reliably increase in cells which display increased metabolic activity or energy consumption (Popp 1979, Fels 2009, Dotta et al. 2011, Dotta et al. 2016). Increased metabolism drives chemical reactions which release detectable photonic energy. It is known that tumors consume a lot of energy – as such they'll be brighter and the bright light will have key frequencies embedded. In this present study, we harness these increases in biophoton intensity and energy to discriminate between healthy and malignant cells.

Materials and methods

Cell cultures

Both normal and malignant cell lines used in this study have been derived and obtained from the American Type Culture Collection (ATCC). The source type of each cell line can be seen in Table 2.

Acronym	Derivation
B16-BL6	Murine melanoma
MDA-MB 231	Human mammary adenocarcinoma (derived from metastatic site)
MCF-7	Human mammary adenocarcinoma
AsPC-1	Human pancreatic metastatic
HEK-293	Human embryonic kidney
HBL-100	Normal mammary

Table 2: Complete list of cell lines used in this study and their source.

All cell cultures were maintained in 150 × 20 mm cell culture plates using Dulbecco's Modified Essential Medium supplemented with 10% fetal bovine serum, 100 µg/m streptomycin, and 100 U/ml penicillin. The cell cultures were incubated at 37ºC in 5% CO_2. For experimentation, the cell monolayers were washed with room temperate, neutral pH PBS, cultivated by incubation in a 0.25% trypsin solution, collected by centrifugation and seeded onto 60 × 15 mm culture plates. A final cell density in each culture plate prior to biophoton emission recording was 1.0 x 10^6 cells each containing a total medium volume of 2.5 cm^3.

Detection of wavelength specific photon emission

Immediately after removal from the incubator, a single plate was placed onto the aperture of a Model DM 0090-C digital photon multiplier tube (PMT) (SENS-TECH Sensory Technologies), located in an adjacent room. The wavelength bandwidth or this PMT was between 280-975nm. Depending on the wavelength of emission to be measured, the appropproprite band-pass filter (Chroma Technologies), was placed on top of the aperture before exposure above the culture dish (figure 5). The band-pass filters used in this study were 370nm, 420nm, 500nm, 620nm, 790nm, and 950nm – each rated with a filter error range of +/- 5 nm. These filters were selected based upon the Cosic RRM equivalencies of proteins tied to physiological processes as shown by Dotta et al. (2014). The entire experimental detection system was placed into a darkened wooden box, covered with black material to ensure no environmental light pollution would alter the sensitivity of the PMT. The typical dark counts or background ambient recordings

obtained for this PMT were in the range of 15-25 photon units per second. Measurements were recorded by the DM0101 Counter timer Module with a sampling rate of 2.5 seconds for 22.5 hours. Each cell line was measured in triplicate with the presence of each of the 6 filters and without the presence of any filter to measure the total photon emission from the cell.

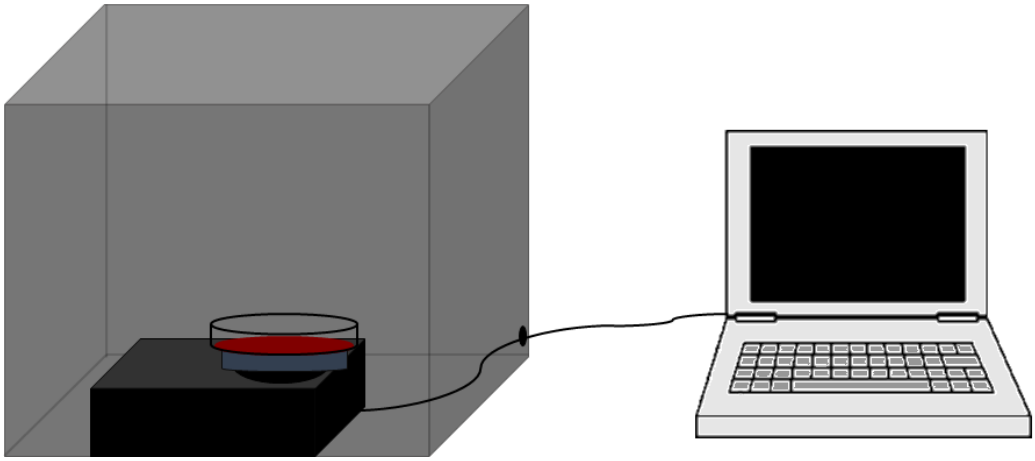

Figure 5: Schematic for wavelength-specific biophoton emission detection within a darkened wooden box. The wavelength specific band-pass filter (blue disc) that only allows the emission of light of either 370nm, 420nm, 500nm, 620nm, 790nm, or 950nm to be detected by the PMT (black box) is placed below a confluent plate of malignant or healthy cells.

Results

Classifying cell types as malignant (cancer) or non-malignant (non-cancer), a two-way analysis of variance (ANOVA) identified a filter by cell type interaction, F(6,102)=

2.69, $p<.005$, $\eta^2=.21$. The source of variance was identified as significantly decreased photon emissions from non-cancerous cells (M= 6752.38, SEM= 66.18) relative to cancerous cells (M= 7958.22, SEM= 262.87) when selecting for the 420-nm wavelength filter applied to the PMT, $t(12)= -2.82$, $p<.05$, $r^2=.40$ (Figure 6). Equality of variances as inferred by Levene's Test were assumed ($p>.05$) and the reliability of the phenomenon was robust in triplicate.

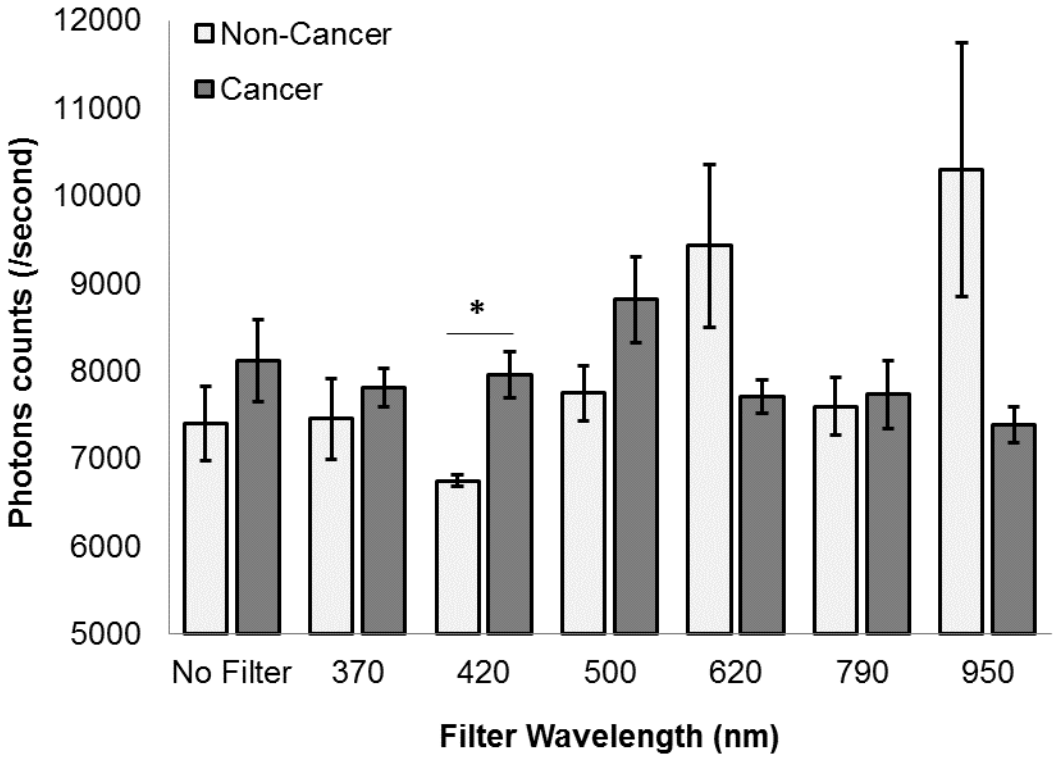

Figure 6. Photon counts per second increment for non-cancer (light) and cancer (dark) cells as a function of the applied PMT filter. A significant difference after accommodating for homogeneity of variance is indicated ($p<.05$).

Employing discriminant analyses to classify photon emissions into nominal categories of “cancerous” and “non-cancerous” cell type aggregates was unsuccessful without the application of appropriate filters to the PMT, Λ =.99, $\chi^2(1) = 1.84$, $p > .05$. However, selecting for photon data which had been filtered before interfacing with the PMT and therefore subject to the exclusion of all light with the exception of a single wavelength could differentiate the two systems. Of the 6 filters, 3 were associated with photon counts which could be used to discriminate cancerous and non-cancerous cell type aggregates: 420-nm (Λ =.66, 78.6% correct classification), 950-nm (Λ =.72, 70.6% correct classification), and 620-nm (Λ =.76, 70.6% correct classification). Selecting for cases associated with a combination of the three significant filter applications (420-nm, 620-nm, and 950-nm) produced results which were comparable to individual applications, Λ =.87, $\chi^2(1) = 6.16$, $p<.05$, classifying 69% of cases. However, when systematically removing cell types from the binary model, the removal of HBL cells increased the classification result to 92%, Λ =.43, $\chi^2(1) = 29.67$, $p > .001$. Whereas the classification of photon emissions from non-cancerous cells was moderate (63%), 100% (n= 30) of cases associated with cancer cell emissions were correctly classified.

A significant, positive linear relationship was identified between standardized photon emissions and the wavelength of the applied PMT filter for non-cancer cells, r= .48, $p<.005$, rho= .41, $p<.05$ (Figure 3). The trend suggested that, for non-cancer cells, greater proportions of emitted photons were within the near-infrared red range which decreased moderately with successively shorter wavelengths. In contrast, a negative linear relationship was identified between the same variables for cancer cells, r= -.27, $p<.05$, rho= -.33, $p<.05$ (Figure 2). From this perspective, cancer cells displayed a reverse

trend – emitting greater proportions of near-UV range photons with decreasing counts as wavelength increased. It was therefore apparent that a ratio of photon counts obtained using the UV (370 nm) and IR (950nm) filters could serve as a measure of malignancy. An examination of the 23 hour period of measurement revealed a discrete time period between the 13th and 15th hours of measurement during which standardized UV-IR ratios for non-cancer cells were elevated relative to cancer cells, $t(18)=3.72$, $p<.005$, $r^2=.44$. UV-IR photon emission ratios displayed by non-cancer and cancer cells during 1 hour periods before and after this discrete window were not significantly different ($p>.05$).

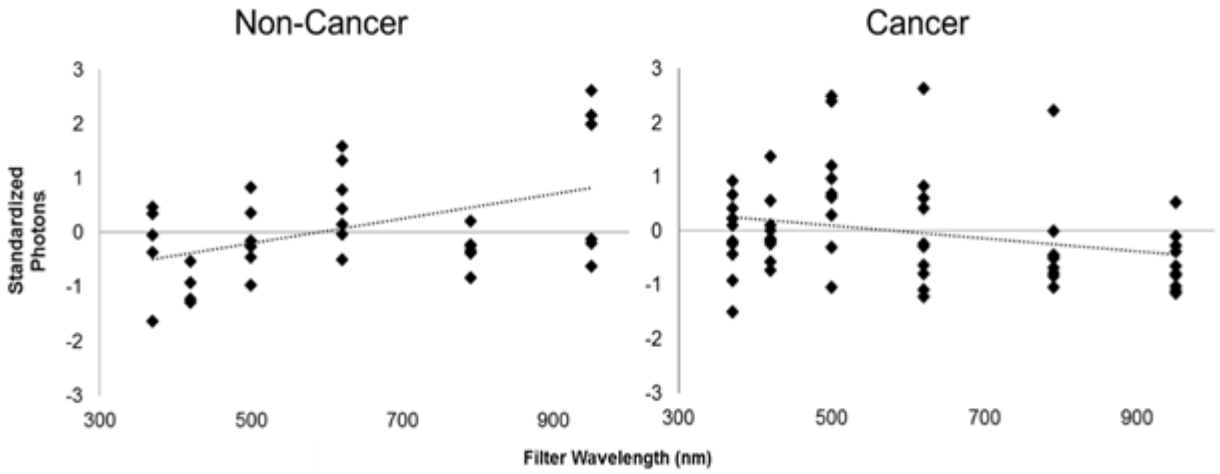

Figure 7. Non-cancer (left) and cancer (right) cells display opposite linear relationships between standardized photon emissions per second increment and the wavelength of the applied PMT filter.

Examining hourly photon counts, an ANOVA identified a 5 hour period during which individual cell types differed significantly ($p<.05$) with a peak effect size of 43% during the 13th hour of measurement, $F(4,28)=4.61$, $p<.01$ (Figure 8). Homogeneous subsets revealed that HBL-100 and HEK-293T cells were reliably different from MDA-

MB-231 cells over the 5 hour period where the non-cancer cells displayed more extreme standardized photon count scores relative to MDA-MB-231 ($p<.05$). This was likely due to the highly-variable and wavelength-independent standardized photon counts displayed by MDA-MB-231 cells which, in Figure 7, are compared to those displayed by HEK-293T cells.

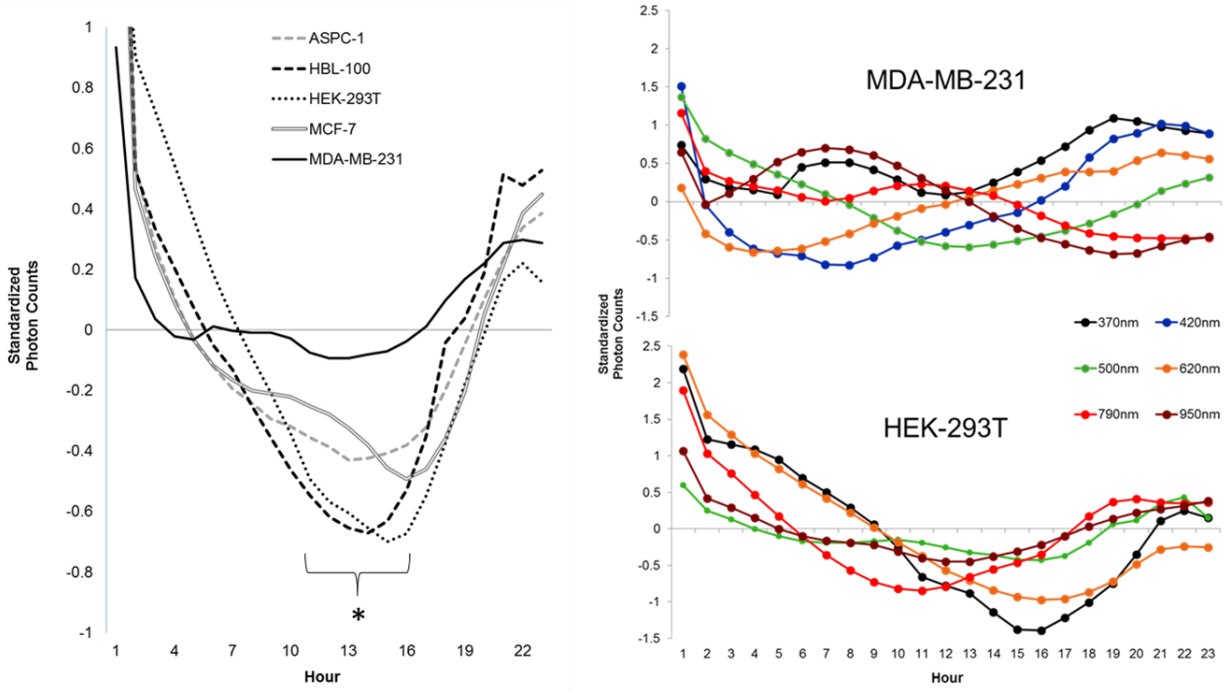

Figure 8. A series of significant differences during a consecutive 5 hour period (*$p<.05$) during which HEK-293T and HBL-100 cells displayed reduced averaged standardized photon counts per 20 ms increment relative to MDA-MB-231 cells (left). Profiles of MDA-MB-231 and HEK-293T cells revealed that the former cell type displayed greater variability over time and between PMT filter conditions relative to the latter cell type (right).

Discussion

Our results demonstrated that malignant (cancer) and non-malignant (non-cancer) cells could be discriminated as a function of raw photon counts if the PMT device was

pre-filtered to exclude all wavelengths of light with the exception of 420-nm, 620-nm, and 950-nm. Whereas moderate classifications were achieved for both independent filters and a combination of filters, our most accurate classification was only achieved when removing HBL100 cells. Further, we identified a clear correlate of cancer and non-cancer cells which were inverse proportions of IR and UV photon sources. Though the correlations were weak, the trend reversal indicated that a ratio of IR to UV sources could be useful in further classifications of malignancy based upon biophoton emissions. Finally, we identified a temporal discriminant factor, standardized photon counts approximately 13 hours into recording, between the non-cancerous cell group (i.e., HBL100 and HEK-293T) and MDA-MB-231 cells. This period of measurement was marked by a separation of the standardized photon count trends where non-cancer cell types displayed decreased values relative to MDA-MB-231 cells.

The exclusion-filters which produced optimal classification (420nm, 620nm, 950nm) could be significant for several reasons. As described by Dotta et al. (2014) these wavelengths are coupled to distinct families of biomolecules that drive signal cascades. Namely, 420nm, using the Cosic RRM, has been correlated to proteins stemming from SOS response proteins, and actin/myosin molecules. The 620nm is associated with lysosomes whilst 950nm is associated with signal proteins. Each of these family of proteins have all been experimentally validated to be directly involved with the formation (Sutton et al., 2000, Edinger & Thompson 2003), proliferation (Maclean et al. 2008) and spread (Glude et al. 2008, Glude et al. 2011) of various malignant systems.

It was observed that the removal of HBL100 cells from the discriminant analysis produced the most accurate classification function. This could suggest that photon

emissions from HBL100 cells are, in fact, not representative of the group in which they were originally classified (i.e. non-cancer). There is evidence to suggest that HBL100 cells are significantly different than HEK293 cells in many respects (Cheng Lin et al., 2014), one of which is that they are not healthy breast-derived cells, but are transformed non-tumorigenic cells, incorrectly classified unknown origins (Lacroix 2008).

The opposed relationships between the wavelengths of the applied exclusion filters and standardized photon counts per unit time indicate that biophotons emitted from cancer and non-cancer sources are fundamentally different in their spectral distributions. Whereas non-cancer cells displayed predominantly IR-centered biophoton emissions with proportional decreases as a function of deviating wavelengths, the reverse was true of cancer cells, displaying predominantly UV-centered biophoton emissions. Similar observations have been reported in the literature, indicating that considerable shifts of wavelength are typical of the transition between malignant and non-malignant cell groups (Tafur et al. 2010, Dotta et al. 2014). It should be noted that the distribution of points for cancer cells (Figure 7) are relatively variable as compared to non-cancer cells. This level of heterogeneity could be indicative of the increased number of cells within the non-cancer cell group aggregate or could be indicative of intrinsic variability characteristic of malignant cells. Distributions of wavelength-specific photon emissions from cancer cells over time as visualized in Figure 8 support the latter possibility.

In general, the results demonstrate that biophoton emissions from cancer and non-cancer cells differ fundamentally as a function of wavelength and temporal patterning. These observations are entirely predicted by Cosic's RRM which would presuppose the pairing of emissions and specific biomolecular events which are known to differ as a

function of malignancy. That there are biophysical correlates tied to cell types which are known to harbor disparate biomolecular signatures is unsurprising given recent discoveries (Dotta et al. 2014, Karbowski et al. 2016). However, as demonstrated here the utility of band-pass or exclusion filters as tools to enhance the classification accuracy of PMT data could provide a basis for new imaging technologies to detect or screen for signatures indicative of malignancy *in vitro* and *in vivo*. Further, the use of IR-UV ratios as crude determinants of malignancy could be a novel and potent method of supplementing said detection. Further studies should aim to expand the spatial resolution of the exclusion filters to accommodate intermediate wavelengths. By identifying key wavelengths which reliably differentiate cancer and non-cancer cells, biophoton classifications of malignancy can become increasingly powerful as a screening tool.

References

Amano, T., Kobayashi, M., Devaraj, B., Usa, M., Inaba, H. (1995) Ultraweak biophoton emission imaging of transplanted bladder cancer. Urological Research. 23 (5), 315-318.

Chilton, C. P., Rose, G. A. (1984) Urinary chemiluminescence – an evaluation of its use in clinical practice. British Journal of Urology. 56, 650-654.

Cosic, I., Cosic, D., Lazer, K. (2016) Analysis of tumor necrosis factor function using the resonant recognition model. Cell Biochem Biophys. 75 (2), 175-180.

Cosic, I. (1994) Macromolecular bioactivity: is it resonant interaction between macromolecules? Theory and applications. IEEE Trans on Biomedical Engineering. 41, 1101-1114.

Dotta, B. T., Murugan, N. J., Karbowski, L. M., Lafrenie., R. M., Persinger, M. A. (2014) Shifting wavelengths of ultraweak photon emissions from dying melanoma cells: their chemical enhancement and blocking are predicted by Cosic's theory of resonant recognition model for macromolecules. Naturwissenschaften. 101 (2), 87-94.

Dotta, B. T., Buckner, C. A., Cameron, D., Lafrenie, R. F., Persinger, M. A. (2011) Biophoton emission from cell cultures: biochemical evidence for the plasma membrane as the primary source. Gen Physiol Biophys. 30 (3), 301-309.

Dotta, B. T., Karbowski, L. M., Murugan, N. J., Vares, D. A. E. Persinger, M. A. (2016) Ultra-weak photon emissions differentiate malignant cells from nonmalignant cells in vitro. Archives in Cancer Research. 4 (2), 1-4.

Edinger, A. L., Thompson, C. B. (2003) Defective autophagy leads to cancer. Cancer Cell. 4 (6), 422-424.

Fels, D. (2009) Cellular communication through light. PLOS One. 4 (4), 1 -8 (e5086).

Gallamini, A., Zwarthoed, C., Borra, A. (2014) Positron emission tomography (pet) oncology. Cancers (Basel). 6 (4), 1821-1889.

Gisler G. C., Diaz, J., Duran, N. (1983) Observation on blood plasma chemiluminescence in normal subjects and cancer patietnts. Arq Biol Technol. 26 (3): 345-352.

Glunde, K., Bhujwalla, Z. M., Ronen, S. M. (2011) Choline metabolism in malignant transformation. Nat Rev Cancer. 11 (12), 835-848.

Glude, K., Jacobs, M. A., Pathak, A.P., Artemov, D., Bhujwalla, Z. M. (2008) Molecular and functional imaging of breast cancer. NMR Biomedicine. 22, 92-103.

Hanasono, M. M., Kunda, L. D., Segall, G. M., Ku, G. H., Terris, D. J. (1999) Uses and limitations of FDG positron emission tomography in patients with head and neck cancer. Laryngoscope. 109 (6), 880-885.

Karbowski, L. M., Murugan, N. J., Persinger, M. A. (2016) Experimental evidence that specific photon energies are “stored” in malignant cells for an hour: the synergism of weak magnetic field-led wavelength pulses. Biology and Medicine. 8 (1), 1-8.

Lacroix, M. (2008) Persistent use of “false” cell lines. Int J Cancer. 122, 1-4.

Lin, Y. C., Boone, M., Meuris, L., Lemmens, I., Roy, N. V., Soete, A., Reumers, J., Moisse, M., Plaisance, S., Dramanac, R., Chen, J., Speleman, F., Lambrechts, D., de Peer, Y. V., Travernier, J., Callewaert, N. (2014) Genome dynamics of the human embryonic kidney 293 lineage in response to cell biology manipulations. Nature Communications 5, 1-12 (4767).

Maclean, K. H., Dorsey, F. C., Cleveland, J. L., & Kastan, M. B. (2008). Targeting lysosomal degradation induces p53-dependent cell death and prevents cancer in mouse models of lymphomagenesis. The Journal of clinical investigation, 118(1), 79-88.

Popp, F. A. (1979) Coherent photon storage of biological systems. In: Electromagnetic bioinformation, Popp F. A., Becker, G., Konig, H. L., Peschka, W. (eds) Urban and Schwarzenbeg: Munich, pp. 123-149.

Shimizu, S., Miyamoto, N., Matsuura, T., Fujii, Y., Umezawa, M., Umegaki, K., Hiramoto, K., Shirato, H. (2014) A proton beam therapy system dedicated to spot-scanning

increases accuracy with moving tumors by real-time imaging and gating and reduces equipment size. 9 (4), e94971.

Sutton, M. D., Smith, B. T., Godoy, V. G., & Walker, G. C. (2000). The SOS response: recent insights into umuDC-dependent mutagenesis and DNA damage tolerance. Annual review of genetics, 34(1), 479-497.

Tafur, J., Van Wijk, E. P. A., Van Wijk, R., Mills, P. J. (2010) Biophoton detection and low-intensity light therapy. a potential clinical partnership. Photomed Laser Surg. 28 (1), 23-30.

Takeda, M., Kobayashi, M., Takayama, M., Suzuki, S., Ishida, T., Ohnuki, K., Moriya, T., Ohuchi, N. (2004) Biphoton detection as a novel technique for cancer imaging. Cancer Sci. 95 (8), 656-661.

Vares, D. A. E., Dotta, B. T., Saroka, K. S., Karbowski, L. M., Murugan, N. J., Persinger, M. A. (2016) Spectral power densities and whole body photon emissions from human subjects sitting in hyper-darkness. Archives in Cancer Research. 4 (2), 1-4.

Chapter Transition: Predicting Viral Lethality

The previous chapter serves as a demonstration that practical applications of RRM are possible. That is, cancer and non-cancer cells can be differentiated on the basis of their wavelength-specific photon emissions wherein infrared (IR) to ultraviolet (UV) ratios are considered the discriminating factor. This reported observation was applied on a greater scale in the following chapter where we attempted to predict the differentiating factor between lethal and non-lethal strains of Ebola on the basis of the RRM method. The following chapter demonstrates, once again, that IR- and UV-range biophoton emissions as predicted by RRM can be used as discriminating factors to statistically infer the lethality of Ebola. We provide lines of evidence which converge upon the conclusion that the periodicities examined within sequences of pseudopotentials converted from amino acid sequences can be predictive of biomolecular and cellular function. On the basis of our findings and the assumption that biomolecules can interact with narrow-band photostimuli, we propose that full body application of the light could interact with virulent processes within an infected human body. We emphasize that pulsed light should be physiologically-patterned – a recommendation which is based upon many years of research involving interactions between electromagnetic fields and physiological processes. In general, both the previous and following chapter substantiate the practical application of RRM as a tool to predict features about biomolecules which assume matter-energy equivalencies.

Chapter 4

Cosic's Resonance Recognition Model for Protein Sequences and Photon Emission Differentiates Lethal and Non-Lethal Ebola Strains: Implications for Treatment

(Original Research)

Murugan N.J., Karbowski L.M., Persinger M.A.

[Published in *Open Journal of Biophysics*]
Vol 5, pp. – 35-43, 2015

Abstract

The Cosic Resonance Recognition Model (RRM) for amino acid sequences was applied to the classes of proteins displayed by four strains (Sudan, Zaire, Reston, Ivory Coast) of Ebola virus that produced either high or minimal numbers of human fatalities. The results clearly differentiated highly lethal and non-lethal strains. Solutions for the two lethal strains exhibited near ultraviolet (~230 nm) photon values while the two asymptomatic forms displayed near infrared (~1000 nm) values. Cross-correlations of spectral densities of the RRM values of the different classes of proteins associated with the genome of the viruses supported this dichotomy. The strongest coefficient occurred only between Sudan-Zaire strains but not for any of the other pairs of strains for sGP, the small glycoprotein that intercalated with the plasma cell membrane to promote insertion of viral contents into cellular space. A surprising, statistically significant cross-spectral correlation occurred between the “spike” glycoprotein component (GP1) of the virus that associated the anchoring of the virus to the mammalian cell plasma membrane and the Schumann resonance of the earth whose intensities were determined by the incidence of equatorial thunderstorms. Previous applications of the RRM to shifting photon wavelengths emitted by melanoma cells adapting to reduced ambient temperature have validated Cosic’s model and have demonstrated very narrow- wave-length (about 10 nm) specificity. One possible ancillary and non-invasive treatment of people within which the fatal Ebola strains are residing would be whole body application of narrow band near-infrared light pulsed as specific physiologically-patterned sequences with sufficient radiant flux density to perfuse the entire body volume.

Introduction

From a biophysical and ecological perspective, the proliferation and density of all life forms, including the human population, are subject to physical constraints determined by the parameters of physical and chemical reactions within the terrestrial environment. The intrinsic processes often described as dynamic equilibrium suggest there are mechanisms that mediate this control. Minute alterations in the genetic expression of opportunistic infections or modified vulnerability to pathogens have been considered as the standard forms of contagion by which populations are controlled or eliminated. However interpretations are subject to change, such as for the case of malaria that was once attributed to “bad air” before the recondite stimuli responsible for this disease was measured, and often require a significant change in perspective from contemporary assumptions. Here, we present an alternative mechanism for the proliferation of Ebola, the possible biophysical mechanism for the marked strain variation in fatality, the potential etiology, and a possible non-invasive treatment.

The current Zaire Ebola virus is a subset of the genus of Ebola viruses for which the most typical symptom is fatal hemorrhagic fever in human beings. The recent (2014) proliferation in Africa is considered similar if not identical to that form first identified in the Democratic Republic of Congo and is considered similar to the Mar- burg virus. Transmission is presumed to involve proximity with fluids originating from an infected person. However, unlike the first known manifestations ~1976, the proliferation has escalated since the spring of 2014 although precise inflections of the growth curves for prevalence and incidence could extend to 2012.

Not all subsets of Ebola are deadly. There are at least four locations where the manifestations occurred (year of onset in parentheses). Two of them, Reston (1995) and Ivory Coast (1994) were associated with minimum or no mortality. The Sudan (1976) and Zaire (1976) varieties were associated with 54% and 88% mortality, respectively.

The Ebola virus contains ~19,000 base pairs and encodes for seven structural proteins whose sequences have been isolated (Lee et al., 2008). The essential structure is a cylinder or tube whose length ranges within the near infrared wavelength (800 to 1000 nm) with a radius of ~40 nm (~251 nm circumference). From the bilayer lipid surface, glycoproteins extend as 10 nm projections with interspaces of ~10 nm (Licata et al., 2004). The latter is effectively the same width as a plasma membrane of a mammalian cell and the equivalence of the phase modulation for visible pho- ton emissions (~10^{-19} J) from cells (Dotta et al., 2012) resulting in energies of ~10^{-20} J. This increment of energy is associated with a plethora of critical biophysical processes that includes the sequestering of ligands to receptors and the resting membrane potential (Persinger, 2010).

The virus itself has four strains with a genome of 19 kB. This genome encodes 8 - 9 proteins that facilitate infection and proliferation within the host organism. From the NIH (National Institute of Health) databank we obtained the genomic sequences for the four strains Sudan (18,875), Zaire (18,839), Reston (18,960) and Ivory Coast (18,930) as well as the associated (34) proteins from the various strains. The acronyms, names and number of amino acids for the major proteins are shown in Table 3.

Acronym	Protein	Amino Acids
NP	Nucleoprotein	738
VP35	Polymerase complex protein	329
VP40	Matrix protein	326
GP1	Spike glycoprotein	676
sGP	Small secreted glycoprotein	372
VP30	Minor nucleoprotein	288
VP24	Membrane-associated protein	251
L	RNA-dependent RNA polymerase	2210

Table 3. Acronyms, name and Amino Acid (AA) lengths of components of Ebola.

Irena Cosic's Resonant Recognition Model (RRM)

The Resonant Recognition Model (RRM) was developed by Irena Cosic (1994) who was attempting to reconcile the unexpected, marked resemblances between functionally dissimilar proteins. She assumed that a type of spectral density of the spatial sequences of the amino acids in different proteins might be more revealing than simply comparing classic chemical "structures". The model is based upon representing the protein's primary structure as numerical series by assigning each amino acid with a physical value. This value was the energy of delocalized electrons for each amino acid. She has obtained characteristic RRM values for different functional groups of proteins and DNA regulatory sequences.

We (Dotta et al., 2014) have experimentally supported the predictions and applications of the Cosic model by measuring the photon emissions from mouse (B16) melanoma cells that had been removed from incubation. The cells emit specific increments of 10 nm wavelengths from the near ultraviolet through the visible to the near infrared range as measured by photomultiplier units. This shift in photon emission wavelengths (as inferred by the results of different filters) changed from primarily near infrared to near ultraviolet over a ten hour period. Specific chemical activators or inhibitors for specific wavelengths based upon the RRM elicited either enhancement or diminishment of photons at the specific wavelength predicted by Cosic. Activators or inhibitors predicted for other wavelengths were not effective or much less effective. The spike in near-infrared energies preceded a spike in near-ultraviolet energies by about 3 hours. The temporal sequence was consistent with the activation of signaling pathways (near-infrared) followed by activation of protein-structural factors (near-ultraviolet).

Wu and Persinger (2011) had shown that the wavelength of infrared photons predicted from Cosic's model for cytochrome c and cytochrome oxidase II, proteins associated with activation in the regenerating blastema within planarian, facilitated the rate of growth of sectioned organisms. The power density of the 880 nm light was ~10^{-3} $W \cdot m^2$. The energy at the level of a symmetrical patch of plasma cell membrane (10^{-16} m^2) would have been ~10^{-19} J. When considered together the potential utility of RRM for pursuing the optimal photon frequencies that could differentially affect viral activity was considered feasible.

Biophotons are emitted by bacteria (Trushin 2004) and cells (Popp et al., 1988) and may be a means by which intercellular communications (Fels, 2009) occur rather

than just a spurious correlate of biochemical activity. Their power (flux) densities are in the order of 10^{-11} to 10^{-13} $W \cdot m^2$. Biologically-relevant reactions such as the addition of hydrogen peroxide to hypochlorite solutions emit copious photons and may be involved with non-local interactions between chemical reactions (Dotta & Persinger 2012) as well as shifts in pH (Dotta et al., 2013) . Photon emissions from microtubule preparations respond to the application of relatively weak (μT) extremely low frequency magnetic fields when they display changing angular velocities around a circular array of solenoids (Dotta et al., 2014) . Comparable magnetic field strengths that match the “mem- brane magnetic moment” of cells facilitate the release of photons and suggest the involvement of very small energies such as the difference between electron spin and orbital magnetic moments (Dptta etl al., 2014) . At a cellular level biophoton emission is induced by heat shock (Kobayashi et al., 2014).

Applying light with specific frequencies can preserve biological function. Exposure of optic nerves after partial injury to about 250 $W \cdot m^{-2}$ of 670 nm for 30 min reduced oxidative stress (Fitzgerald et al., 2010) and attenuated secondary de- generation. Low power laser light (685 nm) exposure for 3 min to 910 $W \cdot m^{-2}$ stimulated stem cell proliferation in planaria (deSouza et al., 2005) . In fact near-infrared photoimmunotherapy that targets specific membrane molecules (Mitsunaga et al., 2011) has been successful in vivo by binding to the cell membrane which has been shown by Dotta et al. (2011) to be a primary source of biophotons in the order of 10^{-20} J per s per reaction. Because visible light penetrates the mammalian brain and body the presence of encephalopsin (extraretinal opsins within for example brain tissue) suggests external photons of specific wavelengths may be more effective than now appreciated. Opsins mediate

transmembrane proteins that act on G-protein-coupled receptors (Nissila et al., 2012). Exposure of the human skull (via the ear canal) to blue (465 nm) LEDs with a luminous flux density of about 10 $W \cdot m^{-2}$ elicits discernable changes throughout the brain as inferred by fMRI activity (Starck et al., 2012).

Cosic Procedure

The genomic and proteomic information for each of the four strains of the Ebola virus were obtained from the National Center for Biotechnology Information data (NCBI). The NCBI reference sequence or identification number for each strain, along with the initial year of outbreak and resulting deaths can be seen in Table 3. The NCBI reference (RefSeq) was: Zaire: http://www.ncbi.nlm.nih.gov/nuccore/10313991. The suffixes for the Su dan, Reston, and Ivory Coast references were: 55770807, 2278922, and 302315369, respectively.

Ebola Virus Strain	NCBI RefSeq	Year	RRM frequency	True Frequency	Deaths
Sudan	NC_00643	1976	0.8745789	1.3E+15	53%
Zaire	NC_00254	1976	0.8759736	1.31E+15	88%
Reston	NC_00416	1995	0.1887494	2.52E+14	0%
Tai Forest	NC_01437	1994	0.1959063	2.92E+14	0%

Table 4. Ebola Virus Strain, the NCBI RefSeq, Cosic's Resonant Recognition Model (RRM), the actual or true frequency, and the percentage of deaths of each strain.

The primary amino acid sequence was transformed into a numerical sequence using the Resonant Recognition Model (RRM). Each of the 20 amino acids in the entire sequence was assigned an electron-ion interaction potential (EIIP) value (Persinger, 2010). This value represents the average energy state of all of the valence electron associated with that amino acid. The numerical sequence was then subjected to a signal analysis to determine a characteristic RRM frequency. The RRM frequency was converted to a true frequency by determining the appropriate wavelength using the function fRRM = 201/λ. This method was also applied to the genomic sequence of each strain, where each nucleotide was represented by an EIIP value, and then subjected to signal analysis.

Results of Cosic's RRM

As shown in Table 3, the results indicated a clear difference between the rarely fatal and very fatal strains of Ebola. The primary resonance frequency fRRM for the two deadliest strains (Sudan and Zaire) were 0.87457 and 0.8759. This would be equivalent to an actual frequency of 1.3044×10^{15} and 1.3065×10^{15} Hz, respectively. Although very similar the difference between the two strains is equivalent to ~0.01 eV (10^{-21} J) which is similar to the average energy required for A-T/C-G base pairing in the human genome.

Assuming the velocity of light in a vacuum, the equivalent wavelengths for the Cosic frequencies for the two stains would be ~230 nm. If we assume the variable velocity of light in water (Lubsandorzhiev et al., 2003), which ranges from 2.147×10^{8} $m \cdot s^{-1}$ for

370 nm to 2.206 × 108 $m \cdot s^{-1}$ at 520 m, the wavelengths would be closer to ~160 to 165 nm depending upon inferences of linearity. In other words the electromagnetic equivalent of the Cosic frequency would involve photons within the near ultraviolet band. Interestingly, the radius of the circular wavelength (230 nm) would be 36.6 nm, that is, within the range of the radius of the Ebola virus.

On the other hand the least fatal Ebola strains, the Reston and Ivory Coast varieties, which after infecting the host are asymptomatic, display Cosic frequencies of 2.51691×10^{14} Hz and 2.92195×10^{14} Hz, respectively. The equivalent wavelength for photons would be 1.19 and 1.03 µm, respectively, that is within the near infrared range. If we assume the adjustment for the velocity of light in water, for example, 2.3×10^{8} $m \cdot s^{-1}$ the effective Cosic solution would be narrow-band wavelengths of 912 and 815 nm. This is within the range of the length (800 to 1000 nm) the virus.

There are major implications for this clear dichotomy in association with photon frequency between the more lethal and non-symptomatic forms of Ebola. Functional wavelengths that encompass near-UV are usually associated with growth and dynamic protein changes. Wavelengths involving near-IR are associated with general activation. The clear discrepancy of wavelengths between the lethal and nonlethal strains could be sufficient to al- low therapeutic intervention by applied, narrow band light spectra. If the viral activities operate similarly to what was measured with melanoma cells, the application of the photon wavelengths must be within 10 nm of the predicted Cosic frequency or there would be no effect (Persinger, 2010).

The most parsimonious intervention would be the whole body application of the 1.02 to 1.19 µm (near IR) wavelength to patients who have contracted Sudan and Zaire

strains. If, as our melanoma and planarian experiments imply (Dotta et al., 2014; Wu & Persinger, 2011) the photon frequencies predicted by the Cosic RRM are the equivalent of the molecular structure or a type of “virtual” structure, the IR should produce a non-lethal representation within the viral proteins. If valid, this could reduce the fatality by directly disrupting the intrinsic proliferative mechanisms. It would be essential to employ LED (Light Emitting Diodes) that were manufactured specifically for those frequencies. “Red” lights from incandescent sources or simply painted light bulbs based upon full (visible) spectrum emission would be less effective.

The optimal power or photon flux density of the near IR LED frequencies for whole body exposure may be less intense than anticipated. For treatment of SAD (Seasonal Affective Depression) white light in excess of 2500 lux or ~1 $W \cdot m^{-2}$ (1 lux = ~1.5 × 10^{-3} $W \cdot m^{-2}$) is required; radiant flux density approximately 10 fold weaker was not effective (Rosenthal et al., 1987). Our direct experiments with white light (10,000 lux) applied to the skull indicate that photon energies move across this impediment through cerebral tissue and are emitted distally (Persinger et al., 2013). The slow latency for photon detection (1.7 s along the rostral-caudal axis; 0.7 s across the width of the skulls) compared to the “instantaneous” detection expected by direct light suggested the role of Grotthuss-like mechanisms involving protons.

Within the darkness of the internal organs and blood occupied by the virus the photon flux density is likely to be in the order of 10^{-12} $W \cdot m^{-2}$ (Kobayashi et al., 1999). This is consistent with the results from multiple studies (Yoon et al., 2005; Vogel & Suessmuth, 1998) that showed that cell-to-cell communication as well as functional electrical correlations involved power densities in this range (Dotta et al., 2012). Our experiments

with specific filters have suggested that picoWatt per meter-squared photon pat- terns, if appropriately patterned, may be the “information” that initiates the much more glucose energy demanding cascade of molecular pathways. We have shown this for preparations of microtubules (Dotta etl a., 2014). In other words the inter-cell photon emissions and correlated information are equivalent to turning the ignition on or off in an automobile and involve minimal energy. The major energy that operates this method of conveyance is contained within the construction of the automobile.

In the balance of probabilities the static application of the optimal LED-emitting photons would not be as effective as the appropriate, physiologically-patterned pulsation of the light. The rationale for this statement is based upon what we have measured for weak, biofrequency magnetic fields. Different temporal patterns of weak (nanoTesla to microTesla) magnetic fields generated by specific point durations (the duration of each computer-generated voltage that generates the field) produce very specific effects (Vogel & Suessmuth, 1998; Martin et al., 2004) Light flashes coupled to magnetic fields applied across the brain enhance physiological effects (DeSano & Persinger, 1987). Our recent unpublished results involving patterns of light flashes from near-ultraviolet and near-infrared LEDs applied to cancer cells have verified the efficacy of specific light wavelength patterns generated from exact point durations.

Spectral Analysis of Cosic’s RRM and Ebola Protein Patterns

We have found that the greatest congruence between applied, physiologically-patterned magnetic fields, photon emissions from cells, and the responses of the

molecular pathways of cells is not the absolute measures of the numbers of or flux density of photons over time, per se, but rather the spectral power densities of these changes. For example (Karbowski et al., 2012) the comparisons of the physiologically patterned (frequency- and phase-modulated) weak magnetic fields that slow the proliferation of cancer cells and the digitized patterns extracted from the quantitative electroencephalographic activity of a person with specific abilities to affect cancer cells showed no obvious visual similarities. However the spectral densities of the two patterns were significantly congruent.

The differences in correlation coefficients for protein sequences' spectral analyses were completed for the frequency patterns generated by the Cosic procedure for the proteins in Table 3. The proteins were sequenced according to their amino acids, analyzed by the Cosic method, and spectral analyzed using SPSS (SPSS-16 PC). The spectral profiles for each protein were compared by correlation between each pair of strains. Because raw spectral densities display an intrinsic decrease in power from the lowest to the highest frequencies, this serial order was co-varied first before the cross-correlations were completed to minimize this possible artifact. However the changes in the strengths of coefficients were relatively minimal.

The results are shown in Table 4. The strongest correlations occurred between the two most lethal strains (Sudan-Zaire) compared to all of the other pairs of strain comparisons. In fact the strength of the averaged correlation coefficient according to one-way analysis of variance as a function of the six pairs was statistically significant [$F_{(5,26)} = 8.85$, $p < 0.001$; $omega^2 = 63\%$ of variance explained]. The post hoc test (Tukey, $p < 0.05$) indicated that the Sudan-Zaire comparison was significantly stronger than the other

pairs that did not differ significantly from each other. One inference is that the Sudan-Zaire pair correlation strengths accommodated two- thirds of the variability in all of the coefficients for the groups (pairs). The most singularly powerful correlation (r = 0.62) occurred between the sGP spectral profiles for the Sudan and Zaire strains. These results suggest that all of these strains have the ability to attach, invade, and replicate inside the host cell. However the Zaire and Sudan strains are enhanced. The sGP component has been attributed to the capacity for the glycoprotein covering (~10 nm) of the virus to fuse (and integrate) into the plasma cell mem- brane. This is followed by the insertion of the viral contents into the cell. At face value this enhanced correlation of spectral densities which only occurred between the two most lethal forms could be consistent with their high rates of successful modification of normal cells. It may be relevant that the associated energy per molecule from the Cosic frequency for the strains that generate the greatest mortality could exceed the born self-energy cost for an ion permeating a pure lipid bilayer for H_3O^+. This threshold is not reached for the energy from the Cosic frequencies for the non-lethal strains.

Protein	Sudan -Zaire	Sudan-Reston	Sudan -Ivory	Zaire - Reston	Zaire-Ivory	Ivory-Reston
NP	0.352	0.231	0.294	0.275	0.267	0.311
VP35	0.407	0.349	0.298	0.216	0.265	0.375
VP40	-	-	-	-	-	-
GP1	0.366	0.315	0.258	0.246	0.23	0.309
SGP	0.624	-	-	-	-	-
VP30	0.373	0.219	0.228	0.301	0.264	0.352
VP24	0.514	0.206	0.196	0.283	0.312	0.344
L	-	-	-	-	-	0.395

Table 5. Correlations between spectral densities of RRM profiles for different proteins for different pairs of Ebola strains

Spectral Analyses Congruence with the Schumann Resonance

During abiogenesis and the early production of amino acids from atmospheric gases through electrical dis- charges or “lightning” (Johnson et al., 2008), the fundamental resonances of the earth were present (Graf et al., 1974). The fundamental frequency which is determined by the ratio between the velocity of light and the earth’s circumference is ~7.8 Hz with harmonics that appear every ~6 Hz (e.g., 14 Hz, 20 Hz, 26

Hz). They are generated by the approximately 40 to 100 lighting discharges per second globally that originate primarily from equatorial regions.

Koenig (1981) noted the conspicuous similarity between the structures of these resonances and human electroencephalographic patterns almost 50 years ago. The intensity of the magnetic field component of the fundamental frequency is about 2 to 4 nT while the electric field component is about 1 $mV \cdot m^{-2}$ (Persinger 2014). These values are within the same order of magnitude and even approach the coefficients for the primary magnetic and electric field components associated with human cerebral activity (Nickolaenko & Hayakawa 2014).

Alterations in the amplitudes of the Schumann resonances reflect the variations in global thunderstorm activity and exhibit a yearly maximum during May and a minimum in October-November. There are intrinsic periodicities of 5, 10 and 20 days. The mild shift in frequency with a peak around 15 hr UT has been attributed to the meridian drift in global lightning activity (Persinger, 2014). Increased amplitudes within the third and fourth harmonic precede some seismic events. What may be particularly relevant for biological processes is that the ~125 ms cycles for completion of the circular waves display phase shifts approaching 20 to 25 ms, which is considered to be one of the latencies required to add a base to a DNA sequence.

That very weak magnetic fields such as those generated normally between the earth surface and the ionosphere due to global lighting can show cross-spectral congruence with electroencephalographic activity within the human brain was recently reported by Saroka and Persinger (2014). Although the intensities may be considered “too weak”, both quantitative calculations and direct comparisons in real time of rates of

change in electroencephalographic power density within Schumann frequencies and actual power directly measured from Saroka's Sudbury station exhibit clear phase coherence.

To discern if there was spectral density congruence between the Cosic solutions for various components of the Ebola protein and the Schumann pattern, the two were correlated. Two random samples of Schumann resonances were obtained from an Italian station and our local (Saroka) station. Results for the Italian station are shown in Table 6. The Schumann spectral density correlation was strongest and statistically significant with the GP1 protein. This protein is associated with the 10 nm "spikes" that protrude from the major mass and allow the virus to anchor to the host's cell membrane. Hence if the most lethal forms whose SGPs are highly correlated were more "cohesive" because of the enhanced properties of the GP1 whose spectrum is correlated with the Schumann resonance, the probability of transcellular infection could be markedly enhanced.

-

Protein	Schumann
NP	-
VP35	-
VP40	-
GP1	0.411
SGP	-
VP30	-
VP24	0.264
L	-

Table 6. Correlation coefficients between spectra densities of RRM Profiles for different proteins from Ebola and Schumann resonance spectral densities. Only statistically significant ($p < 0.05$) values are shown.

For the Saroka (Sudbury) Station the only statistically significant cross-correlation again occurred for the GP1 protein (0.287). The congruence for GP1 was evident for both Schumann patterns separated by two loci (Canada and Italy), indicating although not proving a potential source of shared variance. This suggests that global variables that produce increases in the Schumann intensities which could involve uninvestigated stimuli such as the enhanced lightning (thunderstorm) frequencies associated with global warming or alterations in vertical atmospheric current density (~10^{-12} A·m^{-2}) from specific arrays of human population density could facilitate this activation (Saroka & Persinger, 2014). We cannot exclude the possibility that man-made technical energies penetrating in the earth ionosphere cavity could also modify Schumann factors.

Conclusion

Although current models for viral proliferation and contagion are congruent with accepted mechanisms, there may be parallel perspectives that could facilitate the understanding and treatment, particularly for the very lethal viruses such as Ebola. The transformation of amino acid sequences to spectral densities based upon de-localized electron densities as proposed by Irena Cosic completely differentiated the very lethal and effectively asymptomatic strains of Ebola. The electromagnetic wavelengths within the near ultraviolet for the lethal forms and the near infrared for the non-lethal forms indicate that application of the appropriately patterned “monochromatic” or narrow band, LED generated wavelengths might attenuate the undesirable activities that lead to mortality. The technique would be non-invasive, relatively inexpensive, and if successful would support the alternative model that molecular reactions can be simulated or virtually controlled by the equivalent electromagnetic energy applied as specific quanta of photons.

References

Cosic, I. (1994) Macromolecular Bioactivity: Is It Resonant Interaction between Macromolcules? IEEE Transactions of Biomedical Engineering, 41, 1101-1114. http://dx.doi.org/10.1109/10.335859

De Sano, C.F. and Persinger, M.A. (1987) Geophysical Variables and Behavior: XXXIX. Alterations in Imaginings and Suggestibility during Brief Magnetic Field Exposures. Perceptual and Motor Skills, 64, 968-970. http://dx.doi.org/10.2466/pms.1987.64.3.968

de Souza, S.C., Munin, E., Alves, L.P., Salgado, M.A.C. and Pacheco, M.T.T. (2005) Low Power Laser Radiation at 685 nm Stimulates Stem-Cell Proliferation Rate in Dugesia tigrina during Regeneration. Journal of Photochemistry and Photobiology, 80, 203-207. http://dx.doi.org/10.1016/j.jphotobiol.2005.05.002

Dotta, B.T. and Persinger, M.A. (2012) “Doubling” of Local Photon Emissions When Two Simultaneous, Spatially- Separated, Chemiluminescent Reactions Share the Same Magnetic Field Configurations. Journal of Biophysical Chemistry, 3, 72-80. http://dx.doi.org/10.4236/jbpc.2012.31009

Dotta, B.T., Buckner, C.A., Cameron, D., Lafrenie, R.M. and Persinger, M.A. (2011) Biophoton Emissions from Cell Cultures: Biochemical Evidence for the Plasma Membrane as the Primary Source. General Physiology and Biophysics, 30, 301-309.

Dotta, B.T., Lafrenie, R.M., Karbowski, L.M. and Persinger, M.A. (2014) Photon Emission from Melanoma Cells during Brief Stimulation by Patterned Magnetic Fields: Is It the Source Coupled to Rotational Diffusion within the Mem- brane? General Physiology and Biophysics, 33, 63-73. http://dx.doi.org/10.4149/gpb_2013066

Dotta, B.T., Murugan, N.J., Karbowski, L.M., Lafrenie, R.M. and Persinger, M.A. (2014) Shifting the Wavelengths of Ultraweak Photon Emissions from Dying Melanoma Cells: Their Chemical Enhancement and Blocking Are Predicted by Cosic's Theory of Resonant Recognition Model for Macromolecules. Naturwissenschaften, 101, 87-94. http://dx.doi.org/10.1007/s00114-013-1133-3

Dotta, B.T., Murugan, N.M., Karbowski, L.M. and Persinger, M.A. (2013) Excessive Correlated Shifts in pH within Distal Solutions Sharing Phase-Uncoupled Angular Accelerating Magnetic Fields: Macro-Entanglement and Information Transfer. International Journal of Physical Sciences, 8, 1783-1787.

Dotta, B.T., Saroka, K.S. and Persinger, M.A. (2012) Increased Photon Emission from the Head While Imagining Light in the Dark Is Correlated with Changes in

Electroencephalographic Power: Support for Bokkon's Biophoton Hypothesis. Neuroscience Letters, 513, 151-154. http://dx.doi.org/10.1016/j.neulet.2012.02.021

Dotta, B.T., Vares, D.A.E., Buckner, C.A., Lafrenie, R.M. and Persinger, M.A. (2014) Magnetic Field Configurations Corresponding to Electric Field Patterns that Evoke Long-Term Potentiation Shift Power Spectra of Light Emissions from Microtubules from Non-Neural Cells. Open Journal of Biophysics, 4, 112-118. http://dx.doi.org/10.4236/ojbiphy.2014.44013

Fels, D. (2009) Cellular Communication through Light. PloS ONE, 4. http://dx.doi.org/10.1371/journal.pone.0005086

Fitzgerald, M., Bartlett, C.A., Payne, S.C., Hart, N.S., Rodger, J., Harvey, A.R. and Dunlop, S.A. (2010) Near Infrared Light Reduces Oxidative Stress and Preserves Function in CNS Tissue Vulnerable to Secondary Degeneration Follow- ing Partial Transection of the Optic Nerve. Journal of Neurotrauma, 27, 2107-2119. http://dx.doi.org/10.1089/neu.2010.1426

Graf, F.E. and Cole, E.R. (1974) Precambrian ELF and Abiogenesis. In: Persinger, M.A., Ed., ELF and VLF Electro- magnetic Field Effects, Praeger, New York, 243-275.

Johnson, A.P., Cleaves, H.J., Dworkin, J.P., Glavin, D.P., Lazcano, A. and Bada, J.L. (2008) The Miller Volcanic Spark Discharge Experiment. Science, 322, 404. http://dx.doi.org/10.1126/science.1161527

Karbowski, L.M., Harribance, S.L., Buckner, C.A., Mulligan, B.P., Koren, S.A., Lafrenie, R.M. and Persinger, M.A. (2012) Digitized Quantitative Electroencephalographic Patterns Applied as Magnetic Fields Inhibit Melanoma Cell Proliferation in Culture. Neuroscience Letters, 523, 131-134. http://dx.doi.org/10.1016/j.neulet.2012.06.059

Kobayashi, K., Okabe, H., Kawano, S., Hidaka, Y. and Hara, K. (2014) Biophoton Emission Induced by Heat Shock. PLoS ONE, 9.

Kobayashi, M., Takeda, M., Sato, T., Yamazaki, Y., Kaneko, K., Ito, K.I., Kato, H. and Inaba, H. (1999) In Vivo Im- aging of Spontaneous Ultraweak Photon Emission from a Rat's Brain Correlated with Cerebral Energy Metabolism and Oxidative Stress. Neuroscience Research, 34, 103-113. http://dx.doi.org/10.1016/S0168-0102(99)00040-1

Koenig, H.L., Krueger, A.P., Lang, S. and Sonning, W. (1981) Biological Effects of Environmental Electromagnetism. Springer-Verlag, New York. http://dx.doi.org/10.1007/978-1-4612-5859-9

Lee, J.E., Fusco, M.L., Oswald, W.B., Hessell, A.J., Burton, D.R. and Saphire, E.O. (2008) Structure of the Ebola Virus Glycoprotein Bound to an Antibody from a Human Survivor. Nature, 454, 177-182. http://dx.doi.org/10.1038/nature07082

Licata, J.M., Johnson, R.F., Han, Z. and Harty, R.N. (2004) Contributions of Ebola Virus Glycoprotein, Nucleoprotein and VP24 to Budding of VP40 Virus-Like Particles. Journal of Virology, 78, 7344-7351. http://dx.doi.org/10.1128/JVI.78.14.7344-7351.2004

Lubsandorzhiev, B.K., Pokhil, P.G., Vasilev, R.V. and Vyatchin, Y.E. (2003) Measurements of Group Velocity of Light in the Lake Baikai Water. Nuclear Instruments and Methods in Physics Research Section A, 502, 168-171. http://dx.doi.org/10.1016/S0168-9002(03)00269-9

Mach, Q.H. and Persinger, M.A. (2009) Behavioral Changes with Brief Exposures to Weak Magnetic Fields Patterned to Simulate Long-Term Potentiation. Brain Research, 1261, 45-53. http://dx.doi.org/10.1016/j.brainres.2009.01.002

Martin, L.J., Koren, S.A. and Persinger, M.A. (2004) Thermal Analgesic Effects from Weak, Complex Magnetic Fields and Pharmacological Interactions. Pharmacology Biochemistry and Behavior, 78, 217-227. http://dx.doi.org/10.1016/j.pbb.2004.03.016

Mitsunaga, M., Ogawa, M., Kosaka, N., Rosenblum, L.T., Choyke, P.L. and Kobayashi, H. (2011) Cancer Cell-Selective in Vivo near Infrared Photoimmunotherapy Targeting Specific Membrane Molecules. Nature Medicine, 17, 1685-1691. http://dx.doi.org/10.1038/nm.2554

Nickolaenko, A. and Hayakawa, M. (2014) Schumann Resonance for Tyros. Springer, Tokyo. http://dx.doi.org/10.1007/978-4-431-54358-9

Nissila, J., Manttari, S., Sarkija, T., Tuominen, H., Takala, T., Timonen, M. and Saarela, S. (2012) Encephalopsin (OPN3) Protein Abundance in the Adult Mouse Brain. Journal of Comparative Physiology A, 198, 833-839.

Persinger, M.A. (2010) 10^{-20} Joules as a Neuromolecular Quantum in Medicinal Chemistry: An Alternative Approach to Myriad Molecular Pathways. Current Medicinal Chemistry, 17, 3094-3098. http://dx.doi.org/10.2174/092986710791959701

Persinger, M.A. (2014) Schumann Resonance Frequencies Found within Quantitative Electroencephalographic Activity: Implications for Earth-Brain Interactions. International Letters of Chemistry, Physics and Astronomy, 11, 24-32.

Persinger, M.A., Dotta, B.T. and Saroka, K.S. (2013) Bright Light Transmits through the Brain: Measurement of Pho- ton Emissions and Frequency-Dependent Modulation

of Spectral Electroencephalographic Power. World Journal of Neuroscience, 3, 10-16. http://dx.doi.org/10.4236/wjns.2013.31002

Popp, F.-A., Li, K.H., Mei, W.P., Galle, M. and Neuohr, R. (1988) Physical Aspects of Biophotons. Experientia, 44, 576-585. http://dx.doi.org/10.1007/BF01953305

Rosenthal, N.E., Sack, D.A. and Wehr, T.A. (1987) Light, Seasonal Effects on Mood. In: Adelman, G., Ed., Encyclopedia of Neuroscience, Birkhauser, Boston, 586-588.

Saroka, K.S. and Persinger, M.A. (2014) Quantitative Evidence for Direct Effects between Earth-Ionosphere Schumann Resonances and Human Cerebral Cortical Activity. International Letters of Chemistry, Physics and Astronomy, 20, 166-194.

Starck, T., Nisslia, J., Aunio, A., Abou-Elseoud, A., Remes, J., Nikkinen, J., Timonen, M., Takala, T., Tervonen, O. and Kiviniemi, V. (2012) Stimulating brain tissue with bright light alters functional connectivity in brain at resting state. World Journal of Neuroscience, 2, 81-90.

Trushin, M.V. (2004) Light-Mediated “Conversation” among Microorganisms. Microbiological Research, 159, 1-10. http://dx.doi.org/10.1016/j.micres.2003.11.001

Vogel, R. and Suessmuth, R. (1998) Interaction of Bacterial Cells with Weak Light Emission from Cell Media. Bio- electrochemistry and Bioenergetics, 45, 93-101. http://dx.doi.org/10.1016/S0302-4598(98)00067-1

Wu, H.-P.P. and Persinger, M.A. (2011) Increased Mobility and Stem-Cell Proliferation Rate in Dugesia tigrina Induced by 880 nm Light Emitting Diode. Journal of Photochemistry and Photobiology B: Biology, 102, 156-160. http://dx.doi.org/10.1016/j.jphotobiol.2010.11.003

Yoon, Y.Z., Kim, J., Lee, B.C., Kim, Y.U., Lee, S.K. and Soh, K.S. (2005) Changes in Ultraweak Photon Emission and Heart Rate Variability of Epinephrine-Injected Rats. General Physiology and Biophysics, 24, 147-159.

Chapter Transition: From Ebola to Zika

Our ability to predict when and where an event will occur is dependent upon the relationship between the variables we use in our statistical models and the system under observation – the subject of the prediction. The two previous chapters demonstrated that biophoton emissions, particularly those which were subject to exclusion filtration, were tied to biomolecular events and were predicted by the periodicities intrinsic to the linear sequences of pseudopotentials which result from the RRM conversion of amino acid sequences in a protein to electronic form (charge-based). In the following chapter, we use a combination of previous methods as well as public data which describe the topographical distribution of UV radiation over time and space to predict the spatial and temporal coordinates which are most likely to be associated with enhanced prevalence of Zika virus. A peak wavelength within the ultraviolet subset of the electromagnetic spectrum (235 nm) was inferred based upon the RRM. Consequently, we reinterpreted the classic assumptions surrounding the historical epidemiological spread of Zika, pointing to transient monthly increases of UV as an “activator” of the virus. Our interpretation is based upon the assumption that natural light sources can interact with biomolecules and that the optimal wavelengths of interactions are related to intrinsic spatial features of proteins which translate to unique charge distributions emphasized in RRM.

Chapter 5

Cosic's Molecular Resonance Recognition and the Zika Virus: Predicting Local Enhancements of Prevalence

(Original Research)

Murugan, N.J., Rouleau N., Karbowski L.M., Persinger M.A.

[Submitted to *Open Journal of Biophysics,* 2016]

Abstract

The quantitative relationship between the electromagnetic resonance of energy within the visible range for sequences of amino acids and nucleotides and their chemical properties may reflect a duality that has direct relevance to some of the enigmatic features of contagion. Cosic analyses were completed for the Zika Virus sequence. We found that A) spectral power density analyses of the linear sequences of its components revealed a peak wavelength around 235 nm with several minor peaks within the visible range, B) discrete regions of diminished density of the ozone layer that filters this band of UV energy predict areas where proliferations of the Zika Virus have been recorded over distances not easily accommodated by a single mosquito vectors, C) the models of serial contagion classically correlated with contact may be a misperception of a third factor that activates the virus which is pervasively present but exists in a dormant state until activated by appropriate wavelengths, and D) -the calculated energies involved with the peak wavelengths that match the Resonant Recognition model for Zika Virus occur are associated with phase modulations in the order of 10^{-20} J, the same increments associated with hydrogen bonds and sequestering to receptor proteins. These results suggest that facilitation or blocking of specific combinations of wavelengths might be employed to attenuate the proliferation and “contagion” of the Zika Virus and there may be initiators of epidemics other than only mosquitoes

Introduction

The concept of contagion assumes implicitly the presence of a medium through which particulate matter is diffused or propagated through space over time. The apposition between two surfaces, one containing the contagion and the other pathogen free, can vary from maximum proximity such as touch to indirect proximity due to diffusion through the medium, e.g., air. Irena Cosic's development of the Molecular Resonance Recognition principle (Cosic, 1994) has significantly changed the potential mechanisms and explanations for "contagion" of diseases as well as their origins. The essence of Cosic's principle is that when each amino acid in a protein or base nucleotide in a ribonucleic sequence is assigned a pseudopotential an electromagnetic equivalent within the visible light range emerges. Spectral analyses are performed on these linear spatial sequences of pseudopotentials to produce a profile of power densities (PD). When the width of the spatial unit, such as the amino acid, is accommodated any protein or ribonucleic sequence displays a configuration that primarily occurs within the visible or para-visible wavelength. If there are equivalences between protein or ribonucleic matter and electromagnetic energy whose etiology begins with the Sun (Popp, 1979), then there is the possibility (Persinger, 2016) that the emergence of particular viral or bacterial forms could be enhanced by Cosic profiles from peak ambient wavelengths of light. Here we present evidence for this possibility for the Zika virus (ZV).

Cosic's original formulation (Cosic, 1994) reflects an imaginative and perspicacious understanding of the extraordinary amount of information contained in Spectral Power Densities (SPD) that do not necessarily require a shift in intensity or

amplitude of the phenomenon. One metaphor would involve speech. The intensity of the voice in milliPascals may not change during a conversation. It is the complexity of the spectral power density of the sounds associated with different words within the narrative that mediates the information that affects the outcome of the interaction. The concept has been validated for cell dynamics. Whereas the application of weak, physiologically-patterned magnetic fields to preparations of microtubules does not significantly alter the total output of the photons as measured by photomultiplier units, there are clear shifts in the SPD of the profile (Dotta et al., 2015). One of the persistent shifts that occur when cells are exposed to conditions that facilitate a homogeneous, shared environment (such as the same patterned magnetic field) is an enhancement of SPD within a narrow band within the 7-8 Hz range. This is the same band as the fundamental frequency of the Schumann Resonance (Cherry et al., 2002) that is generated within the earth-ionospheric wave guide or cavity by global lighting strikes which average about 44±4 Hz (Saroka 2014). Most lightning occurs within tropical regions along the equatorial belt. All living systems are immersed within this fundamental frequency as well as its harmonics that average as increasing multiples of 6 Hz.

The validity of Cosic's concept was demonstrated experimentally with photomultiplier units by Dotta et al (2014) who measured the photon emissions from cultures of melanoma cells after they were removed from incubation and were maintained at room temperature. They had measured, by employing a series of different 10 nm filters applied over the aperture of the PMT, a shift in the peak wavelength from the infrared to ultraviolet boundaries. Cosic patterns for different components of the biomolecular pathways that were activated during this period were calculated. When either antagonists

or agonists were applied to those cells for specific protein sequences, only the amplitude (flux power density) of the wavelengths predicted for specific protein sequences by the Cosic formula were either inhibited or enhanced.

The traditional dichotomy between spatial patterns that determine the functions of particulate matter such as chemical structures and temporal patterns that determine the functions energy such as of electromagnetic fields is reflected in the properties of the photon. It can exhibit the properties of a particle or a wave depending upon measurement and context. While examining the potential sources for thixotropy (Verdel et al., 2011), which involves the slowly increasing viscosity of water and enlargement of coherent domains when left undisturbed in a dark environment, Persinger (2015) calculated the interaction between Casimir and magnetic energies. One quantitative derivation was that with each orbit of an electron one-half of the cycle behaves as a classic particle while the other behaves as a wave. During the latter transience virtual particles that define the vacuum oscillations of zero point potentials could become actual particles. This sets the condition for non-locality and excess correlations. Persinger concluded that there is equivalence between spatial patterns of matter and temporal patterns of energy. Cosic's RRM is one application of this practical concept.

Zika Virus Application and Results

The Zika Virus (ZV) has been attributed to the etiology of symptoms that include mild fever, conjunctivitis, and cluster headaches (Gatherer & Kohl, 2016). Its presence has been identified in at least 21 countries in North and South America. It has been linked

or correlated with Guillain-Barre Syndrome in adults. No treatment or vaccine is available at this time. The “pandemic in progress” profile is markedly similar to the outbreak of Ebola in Northern Africa in 2015. Application of the Cosic formulation to the four strains of the Ebola virus (2 lethal, 2 relatively asymptotic) had shown a marked different in peak photon profiles that differentiated the two types (Murugan et al., 2015).

ZV, another model organism used to link the biophysics to virulence using Cosic’s RRM, is an RNA virus containing 10,794 nucleotides that encode for 3,419 amino acids. The entire proteomic sequence of the “BeH815744” strain whose host was a Homo sapiens, was obtained from the NCBI Databank (GenBank: AMA 12087.1) and transformed into a numerical sequence of pseudopotentials as described by Cosic (1997) in order to obtain a characteristic RRM frequency. This relative value was then transformed to a true frequency by determining the wavelength using the function $f_{RRM}=210/\lambda$. The peak wavelength of the polyprotein for this virus was calculated to be 237.83 nm. This peak wavelength is striking similar to the two (of four) virulent strains of Ebola which had peak wavelengths of 230.61 nm (Sudan, 53% of deaths) and 228.85 nm (Zaire, 88% of deaths). On the other hand the two non-lethal forms displayed peak wavelengths of 11,897 nm (Reston, 0% death) and 10,267 nm (Cote d’Ivoire, 0% deaths).

As shown by Dotta et al (2014) agonists of a specific molecular sequence in a signaling pathway specifically enhanced the spectral power density of the Cosic wavelength for that sequence. Further exploring the applications of the Cosic RRM in biological systems, Karbowski et al. (2015) demonstrated, employing spectroflourometry, the specific and conspicuous peak (a factor of 7 greater compared to background) of 380 nm which was the Cosic value for the 607 amino acid sequence that defines bovine

albumin. Later Karbowski et al (2015) showed that application of a temporal pattern of 470 nm (blue) light flashes with 1 ms point durations concurrently with 1 ms point durations of weak magnetic fields through melanoma cells resulted in representation of the photonic energies for at least an hour after the termination of the exposure. During the subsequent hour after the termination of the magnetic field and light pulse presentations there was marked increased in photon emissions which peaked at 470 nm (the same wavelength to which the cells had been exposed during the previous hour). These results suggest that very specific wavelengths of light can be maintained and released from living organisms.

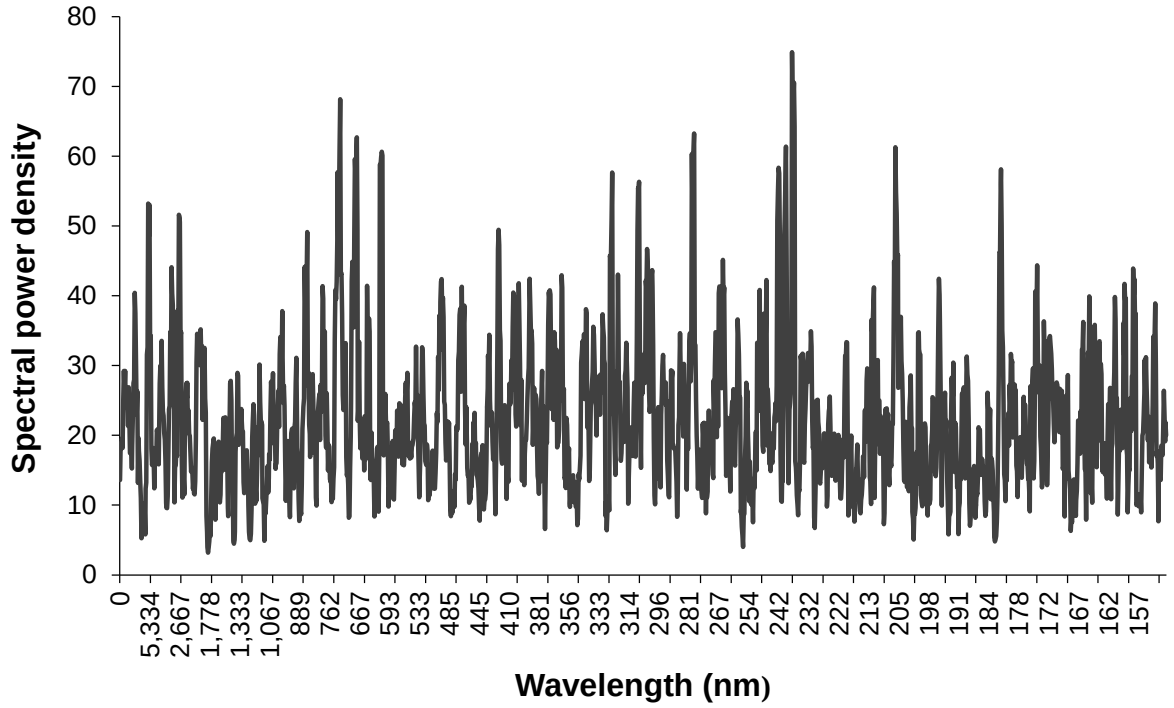

Figure 9. Relative spectral power density reflected in the sequences of nucleotides for the Zika Virus as a function of the wavelength of light derived from Cosic's RRM procedures. Note the concentrated peak around 240 nm.

The actual profile for the Cosic solution for the ZV virus is shown in Figure 9. Although the greatest power peaks were about the 240 nm region, there were other peaks with narrower bands whose significance is not clear. If shifting of the SPD of the visible wavelengths from the sun occurred such that a peak was enhanced around 238 nm (UV-C band), which is the RRM for the ZV, our experimental results in the laboratory and the Cosic function predicts there would be an enhancement of ZV potency and proliferation. Even if the ZV was distributed more or less randomly across habitation the enhancement of the wavelength in specific geographical areas would increase the probability of manifestation in those regions.

Figure 10: The temporal and geographical progression of the Zika virus. Adapted from WHO: Countries and territories showing historical time-line of Zika virus spread (1947 - 2016).

The temporal progression of the appearance of the Zika virus after it was first measured in Uganda in 1947 is shown in Figure 2 (Kindhauser et al., 2016) . During the years 1977-1978 it appeared in Malaysia and Indonesia and about a decade later (2007) there was evidence for its presence in Yap, Micronesia. French Polynesia reported indicators six years later in 2013 and during the following year (2014) an “epidemic” occurred in Brazil. As shown in Figure 10, the movement was primarily along the equatorial band in an easterly direction, that is, in the direction of the earth rotation on its axis. The greatest concentration of ozone which is known to filter in general a wide band of wavelengths occurs above the regions that are spatially most associated with the occurrence of ZV.

The spatial distributions of the outbreaks of ZV for November and December of 2015 and January and February of 2016 are shown in Figure 11. For comparison the global ozone thickness (densities) in Dobson Units (DU, 1 DU=0.01 mm) is also shown. The medium grey areas indicate the lowest total ozone densities, i.e., about 250 DU compared to the more typical 300 DU. It is quite evident that during November 2015 and January 2016, the two months when the ZV outbreaks involved the greatest numbers of countries, the lowest values of ozone densities were noted over these regions. During January of 2016 16 countries locally reported the ZV infection. These countries included the regions within South America which was covered extensively by the press. What is less known is that ZV manifestation and the corresponding decrease in ozone density

was also measured in the Maldives (Indian Ocean) and Samoa (Pacific Ocean). It would be seem highly unlikely that the mosquito would be the only mode of transmission.

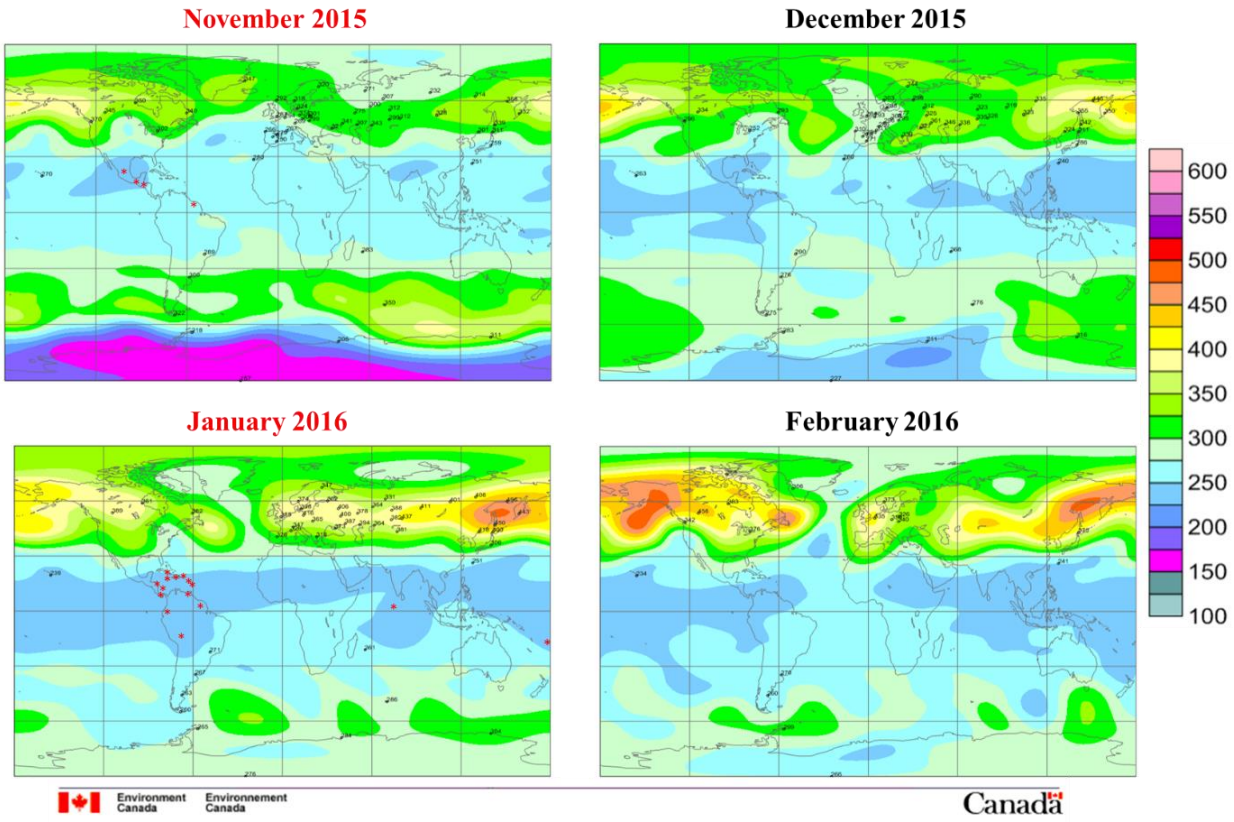

Figure 11. Global distribution of for November and December 2015 and January and February 2016 of the Zika Virus outbreaks (indicated by red dots). The corresponding concentrations of ozone density (measured in Dobson Units) is shown in color. Grey indicates the lowest ozone densities which included the Zika Virus outbreak regions around South America, the Pacific Ocean and the Indian Ocean. (reproduced with permission)

To discern the quantity of UV-light that might be transmitted based upon the diminishment of 50 DU, the Beer-Lambert equation of absorbance (A) = ε•b•c where ε is the molar absorptivity (3000), b=path length (0.3 cm to 0.25 cm) and c=concentration (0.012) in moles, i.e., 12 mM was applied. It can be employed to calculate transmittance as $A=2-\log_{10} \%T$. Assuming the concentration remained relatively stable during the month and was distributed more or less equally over ZV outbreak areas, this value would represent a 1.85% increase in transmittance of UV-C (100 to 280 nm). This can affect the oxidation of many charged molecules.

A first order estimate of the equivalence of a diminishment of ozone density (and hence increase in UV and potentially UV-C) was obtained by employing $E=hc\lambda^{-1}$ where h is Planck's constant, c is the velocity of light and λ is the wavelength (250 nm). This results in $7.5 \cdot 10^{-19}$ Joules. When divided by the square of the wavelength, the resultant flux density is $3 \cdot 10^{-12}$ $W \cdot m^{-2}$. This is within the range of the photon flux densities involved with intercellular interactions (Dotta et al., 2015; Dotta et al, 2014; Murugan et al., 2015).

Discussion

The distributions of diseases as a function of latitude, temperature, and season have been well documented. These variations are often synchronized with the myriad of chemical and physiological changes that occur in a variety of body measurements that are employed to infer medical status (Tromp, 1963). For several decades there was enthusiastic pursuit of disease patterns as a function of constituents within soils that either reduced essential elements or contributed potential toxins (Persinger, 1987). The

recognition of the subtle factors that accommodated and identified those factors that had been previously unexplained in epidemiological patterns has encouraged different approaches and perspectives.

The more conspicuous disorders such as rickets or skin melanomas are largely related to scalar values, i.e., the amount of total sunlight. The potential contributions of enhanced power within discrete bands of ambient sunlight have not been pursued systematically. The results of Van der Mei et al (2001) demonstrated the utility of this approach. They found regional variations in the prevalence of multiple sclerosis as a function of the specific UV band. Presumably the energies from these specific wavelengths would differentially intercalate with the actual physical bases of this demyelization disorder rather than actually produce the disorder.

Our analyses indicate that the same regions in which outbreaks of Zika Virus were recorded were also the regions where the diminishment density within the ozone layer was occurring. In the balance of probabilities UV-C, the same band that over laps with the Cosic solution for the Zika sequence would have been markedly enhanced. Our estimates of the equivalence of increased absorbance due to diminishment of 50 DU indicate an increase in photon flux density ~10^{-12} $W \cdot m^{-2}$. This is within the range of photon flux densities that have been associated with communications between cells and bacteria during periods of proliferation (Trushin 2003; Fels, 2009;, Persinger et al., 2015). *The possibility that the enhanced UV-C that overlaps with the Cosic frequency for the Zika Virus would encourage its replication might be considered.*

If the temporal configuration of the RRM for a molecule is the analogue of its molecular structure then the more complex the structure the more specific the function

and the more precise the mechanisms by which it interacts with other related structures. Karbowski et al (2015) who examined the JAK-STAT signaling pathway and Persinger et al (2015) who examined the ERK-MAP- signaling pathway in cells showed that the signature for a “system” of interaction was more complicated than a single peak wavelength which is found with simpler molecules such as bovine albumin. As noted in Figure 1, there were also elevations of SPD around 208 nm and 300 nm and within the 600 to 800 nm range. Knowing such profiles would be essential for simulating a combination of experimentally generated fields. They could involve a combination of light emitting diodes (LEDs) that emit competitive wavelengths and filters that attenuate the key Cosic wavelengths might be employed to attenuate the proliferation of the virus.

For the JAK-STAT pathway the difference in energies between the peaks of 441, 430 and 416 nm was within the range of 10^{-20} J. This is not only within the range associated with hydrogen bonds (0.04 to 0.3 eV or 0.7 to $2.2 \cdot 10^{-20}$ J) but also reflect the energy required to add one base-nucleotide to a RNA sequence. As described and calculated by Persinger (2010) $\sim 2 \cdot 10^{-20}$ J is the quantum of energy associated with a single action potential from neurons as well as the energy involved with the sequestering of many agonists to receptors. It is also within the range of the second shell electrons of the proton associated with its movement through water to form the hydronium ion, the major correlate of cellular pH.

Conditions that produce 10^{-20} J within a closed volume of biological tissue could have the capacity to contribute to the phase modulation component of a Cosic configuration. Saroka and Persinger (2016) and Persinger and Saroka (2015) have emphasized the similarity of the magnetic field intensity, electric field intensity, and

harmonics of the electrodynamic properties of the human brain and the Schumann Resonances. Saroka and Persinger demonstrated quantitatively the presence of these resonances within the normal quantitative electroencephalographic profile of human subjects (2016).

In addition real-time analyses indicated reliable enhanced coherence between the power values within the Schumann Resonance (as measured by local and distal stations) and human brain activity. The interface occurred for about 0.5 s once every approximately 30 min. The energy available within the human cerebral volume ($\sim 10^{-3}$ m^3) from a magnetic field strength within the 2 to 5 picoTesla range (the amplitude fluctuations for both the fundamental Schumann frequency and human cerebral cortical activity) would be $\sim 10^{-20}$ J. This would have the potential to influence specific functions within the cerebral volume.

The involvement of UV in biological systems has been implicated since the likely beginning of life-related molecules. As indicated by Black and Schwartz (1989), UV and electric discharge within aliquots of carbon dioxide, water vapor and nitrogen-methane mixtures result in ubiquitous distributions of formaldehyde and hydrogen cyanide from which adenine and other purines can form. The Raman spectrum is primarily a UV resonance phenomenon that can be a marker for DNA and protein constituents of viruses. Wen and Thomas (1998) found that excitation (by laser) of 257 nm, 244 nm, 238 nm, and 229 nm reveal ultraviolet resonance Raman spectra of nucleosides and aromatic amino acids (Tyr, Trp, Phe), which are also power photon generators. They constitute DNA viruses. Although the ZV is a RNA based virus, equivalent concepts might apply.

From the perspective of epidemiology and public health the results of this study indicate that mosquitoes may not be the only vector that is associated with the spread of the Zika Virus. The association between the epidemics of ZV and mosquitoes infected with this virus is a correlation. If all living systems contained small sub-detectable concentrations of this virus that are typically dormant and the appropriate UV-C values are achieved secondary to diminishment of the ozone level, then proliferation of the virus could occur within both humans and mosquitoes. Because only the latter two variables are apparent to the observer one variable might considered the cause of the other. If amplification of the Cosic profile for the ZV due to the local, changing diminishment of ozone density contributes to these epidemics, then a different approach might be considered. It may not be spurious that portions of ozone levels are partially replenished by lightning and its proportion is influenced by the densities of plants and conditions that maintain the equatorial climate.

References

Cherry, N. Schumann resonances, a plausible biophysical mechanism for human health effects of solar/geomagnetic activity. Nat Hazards 2002, 26: 279–331.

Cosic, I. Macromolecular Bioactivity: Is It Resonant Interaction between Macromolcules? IEEE Trans. of Biomed. Eng. 1994, 41: 1101-14.

Cosic, I. The Resonant Recognition Model of Macromolecular Bioactivity: Theory and Applications. 1997. 8. Birkhauser, Basel.

Dotta, B.T.; Murugan, N.J.; Karbowski, L.M.; Lafrenie, R.M.; Persinger, M.A. Shifting the Wavelengths of Ultraweak Photon Emissions from Dying Melanoma Cells: Their Chemical Enhancement and Blocking Are Predicted by Cosic's Theory of Resonant Recognition Model for Macromolecules. Naturwissenschaften. 2014, 101: 87-94.

Dotta, B.T.; Vares, D.A.E.; Persinger, M.A. Spectral Power Densities of the Fundamental Schumann Resonance Are Enhanced in Microtubule Preparations Exposed to Temporally Patterned Weak Magnetic Fields. JCER 2015, 6 (9): 716-27.

Fels, D. Cellular communication through light. PLOS One, 2009, 4: e5086.

Gatherer, D.; Kohl, A. Zika virus: a previously slow pandemic spreads rapidly through the Americas. J. Gen. Virol. 2016, 97: 269–73.

Karbowski, L.M.; Murugan, N.J.; Persinger, M.A. Novel Cosic resonance (standing wave) solutions for components of the JAK-STAT cellular signaling pathway: A convergence of spectral density profiles. FEBS Open Bio. 2015, 5: 245-50.

Kindhauser, M.K.; Allen, T.; Frank. V.; Santhana, R.S.; Dye, C. Zika: the origin and spread of a mosquito-borne virus [Submitted]. Bull World Health Organ E-pub: 2016. doi: http://dx.doi.org/10.2471/BLT.16.171082

Murugan, N.J.; Karbowski, L.M.; Persinger, M.A. Cosic's Resonance Recognition Model for Protein Sequences and Photon Emission Differentiates Lethal and Non-Lethal Ebola Strains: Implications for Treatment. OJBIPHY. 2015, 5: 35-43.

Persinger M.A. Experimental Evidence That Specific Photon Energies Are "Stored" in Malignant Cells for an Hour: The Synergism of Weak Magnetic Field-LED Wavelength Pulses. BLM. 2016, 8(1): 162-16.

Persinger, M. A. Geopsychology and Geopsychopathology: mental processes and disorders associated with geochemical and geophysical factors. Experientia. 1987, 43, 92-104.

Persinger, M. A. Spontaneous photon emissions in photoreceptors: potential convergence of Arrhenius reactions and the latency for rest mass photons to accelerate to Planck unit energies. Journal of Advances in Physics 2016, 11. 3529-3534.

Persinger, M.A. 10^{-20} Joules as a neuromolecular quantum in medicinal chemistry: an alternative approach to myriad molecular pathways? Curr Med Chem. 2010; 17(27):3094-8.

Persinger, M.A. Thixotropic Phenomena in Water: Quantitative Indicators of Casimir-Magnetic Transformations from Vacuum Oscillations (Virtual Particles). Entropy. 2015, 17: 6200-12.

Persinger, M.A.; Murugan, N.J.; Karbowski, L.M. Combined Spectral Resonances of Signaling Proteins' Amino Acids in the ERK-MAP Pathway Reflect Unique Patterns That Predict Peak Photon Emissions and Universal Energies. Int. Let. of Chem., Phys, & Astrmy 2015, 43, 10-25

Persinger, M.A.; Saroka K.S. Human Quantitative Electroencephalographic and Schumann Resonance Exhibit Real-Time Coherence of Spectral Power Densities: Implications for Interactive Information Processing. J. of Sig. & Inf. Proc. 2015, 6(2): 153-164

Popp, F. A. Coherent protein storage of biological systems. In Popp, F. A., Becker, G., Konig, H. L. and Pescha, W (eds). Electromagnetic Bio-information, 1979, Urban and Schwarzenberg, Munchen-Wien-Baltimore, pp. 123-149.

Saroka, K. S. and Persinger, M. A. Similar spectral power densities within the Schumann Resonance and a large population of quantitative electroencephalographic profiles: supportive evidence for Koenig and Pobachenko. PLOS One 2016, DOI: 10.1371/journal.pone.0146595.

Saroka, K.S.; Persinger M.A. Quantitative Evidence for Direct Effects Between Earth-Ionosphere Schumann Resonances and Human Cerebral Cortical Activity. ILCPA, 2014, 20(2): 166-94.

Schwartz, AW.; Bakker, CG. Was adenine the first purine? Science 1989, 245: 1102-4.

Tromp, S. W. Medical Biometeorology. 1963, Elsevier, Amsterdam.

Trushin, M. V. Culture-to-culture physical interactions causes the alteration in red and infrared stimulation of Escherichia coli growth rates. Journal of Microbiology and Immunological Infections. 2003, 36, 149-152.

Van Der Mei, I.A.; Ponsonby, A.L.; Blizzard, L.; Dwyer, T. Regional variation in multiple sclerosis prevalence in Australia and its association with ambient ultraviolet radiation. Neuroepid. 2001, 20(3): 168-74

Verdel, N., Jerman, I. and Bukovec, P. The “autothixotropic” phenomena of water and its role in proton transfer. International Journal of Molecular Science 2011, 12, 7481-7491.

Wen, Z.Q.; Thomas, G.J. UV resonance Raman spectroscopy of DNA and protein constituents of viruses: assignments and cross sections for excitations at 257, 244, 238, and 229 nm. Biopolymers. 1998, 45(3): 247-56.

Chapter Transition: Applying Electromagnetic Energies

We have hitherto assumed that biomolecules can interact with wavelengths of light which are predicted by RRM-type conversions of amino acid sequences into charge-based, electronic sequences. The previous chapters demonstrated results which support the validity of the RRM and suggested therapeutic interventions wherein light could be applied to biological substrata to elicit specific effects. The following chapter tests the hypothesized biomolecular-photon interactions experimentally. We applied blue, green, and red (visible spectrum) light to planaria and melanoma cells to observe interactions. We combined our photostimuli with electromagnetic field applications as the bulk of our previous work involved the latter stimulus. Our results indicated that an interaction between electromagnetic fields and certain wavelengths of light optimally enhanced physiological processes. Specifically, we found that 2 – 5 microT electromagnetic fields paired to red (680 nm) and blue (470 nm) light facilitated planarian regeneration. However, we noted that electromagnetic fields were more effective than light in diminishing the growth of melanoma cells. These differential effects highlight the selective-enhancements which can be achieved by exposing biological systems to sources of light. The chapter supports the claim that biological systems can be influenced by applications of light – an property which can potentially be exploited in other ways.

Chapter 6

Synergistic interactions between temporal coupling of complex light and magnetic pulses upon melanoma cell proliferation and planarian regeneration

(Original Research)

Murugan N.J., Karbowski L.M., Persinger M.A.

[Published in *Electromagnetic Biology and Medicine*]
Vol.36 (2), pp. 141-148, 2016

Abstract

Synergisms between a physiologically-patterned magnetic field that is known to enhance planarian growth and suppress proliferation of malignant cells in culture and three LED generated visible wavelengths (blue, green, red) upon planarian regeneration and melanoma cell numbers were discerned. Five days of hourly exposures to either a physiologically patterned (2.5-5.0 μT) magnetic field, one of three wavelengths (3kLux) or both treatments simultaneously indicated that red light (680 nm), blue light (470 nm) or the magnetic field significantly facilitated regeneration of planarian compared to sham field exposed planarian. Presentation of both light and magnetic field conditions enhanced the effect. Whereas the blue and red light diminished growth of malignant (melanoma) cells the effect was not as large as that produced by the magnetic field. Only the paired presentation of the blue light and magnetic field enhanced the suppression. On the other hand the changes following green light (540 nm) exposure did not differ from the control condition and green light presented with the magnetic field eliminated its effects for both the planarian and melanoma cells. These results indicate specific colors affect positive adaptation that is similar to weak, physiologically patterned frequency modulated (8 Hz to 24 Hz) magnetic fields and that the two forms of energy can synergistically summate or cancel.

Introduction

Light from the sun has been considered the singular contribution to the formation of the chemistry that contributed to the formation of living systems (Persinger, 2016; Oparin, 1965). According to Wein's law that relates the temperature of a star to its peak wavelength the Sun's central electromagnetic frequency is about 550 nm with a range distributed over what is considered the visible band (400 to 800 nm). The boundaries are not exact. Although the intensity of light has been known for centuries to affect the behaviour of biological systems and is coupled to season and latitude, the influence of specific wavelengths upon biological responses has been pursued only recently following the development of light emitting diodes (LEDs). On the other hand physiologically-patterned, weak magnetic fields with much less absolute energy can also affect biological systems. Interaction and synergism between light and weak biofrequency-relevant magnetic fields was shown decades ago by Olcese and Reuss (1986) for rats during a discriminatory task. The presence of a weak (1 lux) red light enhanced the animals' capacities to discern the presence or absence of an extremely low frequency magnetic field. In the present experiments we examined the single and interactive effects of a known bioeffective, physiologically-patterned magnetic field and three specific visible wavelengths either separately or simultaneously upon the growth of planarian and malignant cell cultures.

The brilliant work of Popp (1979) rejuvenated the importance of photons and virtual photons from solar origin as central to living systems. The regulatory aspects of low photon emission for cell-to-cell communication and influence have been considered by

Trushin (2004), Fels (2009), and Van Wijk and Schamhart (1988). The potency of the effects generated a compelling question. If cells employ endogenous photon transmissions for regulating signaling pathways across the visible spectra as measured by Dotta and colleagues (2014) then application of specific wavelengths should be able to facilitate or inhibit similar pathways. The process would be analogous to employing pharmacological agents to simulate, enhance, or inhibit endogenous ligands for receptor substrates. There is multiple evidence of the validity of this approach. Eells and colleagues (2004) showed that signal transduction was accelerated retinal and wound healing when 670 nm light was applied. Masoumipoor and colleagues (2013) demonstrated that low level 660 nm laser therapy attenuated neuropathic pain. Wu and Persinger (2011) showed that only 1 $mW \cdot m^{-2}$ of 880 nm wavelength LED light increased mobility and stem cell proliferation rates in amputated planarian. Post-ischemic neurite growth with brief 710 nm LED treatment was shown by Choi and colleagues (2012) to be associated with enhancement of the MAPK pathways.

Most if not all of the changes in cells and organisms that have been reported for specific wavelengths of light have also been elicited by physiologically-patterned, weak magnetic fields. Physiologically-patterned refers to temporal configurations of magnetic fields that are similar to those generated by living systems. Martin and colleagues (2004) showed that analgesic effects from whole body 30 min exposures of rats to two specific patterns within intensities between 1 and 5 μT were equivalent to the effects of 4 mg per kg of morphine. The transphyla effectiveness of the analgesia was shown for planaria (Murugan and Persinger, 2014), snails (Kavaliers and Ossenkopp, 1991) and human beings (Baker-Price and Persinger, 2003). That the specific magnetic fields were affecting

specific receptor subtypes were indicated by the abolishment of the patterned magnetic field-induced analgesia when mu (morphine) receptor blockers were pre-applied for both rats (Fleming et al., 1994) and planaria (Murugan and Persinger, 2014). Recent experiments by Buckner and colleagues (2015) indicated that one particular type of physiologically patterned field that is frequency modulated between 6 and 30 Hz involved T-type calcium channels.

Tessaro and Persinger (2013) showed that following mid-body section exposure to the same frequency-modulated patterned magnetic field that produced analgesia facilitated regeneration. The same pattern, when applied to mouse melanoma cells as well as other types of human and non-human malignant cells inhibited growth in culture (Karbowski et al., 2015). The growth of non-malignant or normal cells was not affected by these fields. Considering that this pattern induces both analgesia and suppression of growth of malignant cell lines, the possibility for a third alternative to classic treatments of cancers that would not produce iatrogenic illness and not affect normal cells became apparent. That the simultaneous pulsing of appropriately patterned magnetic fields and LED, specific wavelength light could produce unique phenomena that could exert profound effects upon biologically-relevant chemical pathways was shown by Karbowski and colleagues (2016). They showed that the simultaneous application of a blue wavelength and pulsed magnetic field with 1 ms point durations resulted in the maintenance of energy within melanoma cells that were re-released as photons 30 to 100 min after the cessation of the exposures. Considering these effects we designed the following experiments to discern the specifics by which different wavelengths (blue,

green, red) could synergistically enhance the facilitative adaptive effects of physiologically-patterned magnetic fields.

Methods

Planarian Exposures

Dugesia tigrina planarian were removed from their housing populations, cut in half above the pharynx employing our standard procedure (Murugan et al., 2015) and placed in 1.5 mL Eppendorf tubes filled with 1 mL of fresh spring water. The planarian had been selected from the source to be visibly the same length so any discernable variations as a function of treatment could be readily observed as well as measured. For the treatment sequence planaria (4 per dish) were transferred to a 60 mm plastic culture dish. The plates were placed within a darkened box. The magnetic field-LED device was placed directly upon the top of the covered dish by suspending it from the top of the box. The distance between the exposure device and the top of the plate was 3cm. The application of the light or EMF was controlled using a switch mechanism which is a part of the hardware.

The physiologically-patterned stimulus sequence was generated by transforming a series of numbers from 0 through 256 to voltages between -5 and +5 V through a digital to analogue converter (DAC) where 127=0 V. The software allowed any series of numbers that could be theoretically derived or recorded from physiological conditions and transformed to this number range. The pattern selected for this experiment was a

frequency-modulated configuration that has been called the “Thomas pattern” because of it potent effects in many settings across levels of discourse. The pattern is shown in Figure 1.

The software also allows the point duration of each of the series of integers from 0 to 256 to be to be programmable. We selected 3 ms because this point duration has produced the most significant effects upon a variety of biological and behavioural systems over the years (Fleming et al., 1994, Martin et al., 2004, Murugan and Persinger, 2014). The pattern was generated through the original Complex software created by Professor Stanley Koren. It was contained with a Lenovo computer that was connected to a DAC and then to the application unit where either the magnetic field only, the LEDs (either 470 nm, 540 nm or 680 nm) only, or both the magnetic field component and the LED could be activated over the exposed planarian. As a result there were 8 treatments with 12 planarian per treatment (n=96) completed in 3 separate experiments.

The duration of the exposures to the various treatments (magnetic field, LED only or field plus LED) was 1 hr per day for 5 consecutive days. Daily images in order to discern length were recorded by a digital camera for each planarian. Each worm was placed in a glass Pyrex dish that was positioned over 1 cm x 1 cm grid paper. Image J was employed to quantify the daily lengths.

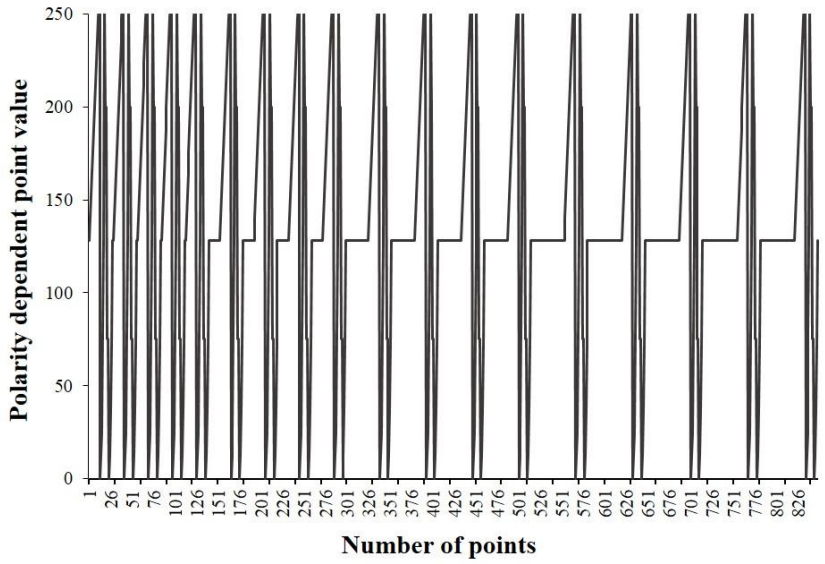

Figure 12. Shape of the frequency-modulated ("Thomas") pattern through which either the magnetic field, the colored light (either blue, green or red), or both the magnetic field and each of the colored lights were presented. The point durations for each of the 859 components (x-axis) between -5 and +5 V (y-axis) generated by the computer were all 3 ms.

Cells

B16-B6 melanoma cells were cultured onto 60 mm plates according to our standard procedures (Karbowski et al. 2012). The plates were exposed individually daily to light only, magnetic field only, or combination of light and magnetic fields for 1 hr per day for 5 days under standard incubation conditions. Similar to the planarian exposures, the exposure device was suspended 3cm from the top of the culture dish. A schematic of the exposure conditions can be seen in figure 2. For sham conditions, cultured plates of

B16-Bl6 cells were placed in the same position underneath the magnetic field-LED device, however, no light or magnetic field were turned on. Using 1.5 mL of PBS the cells were counted from a haemocytometer using our typical procedures. For each of the 8 treatment conditions there were 5 plates exposed on different days.

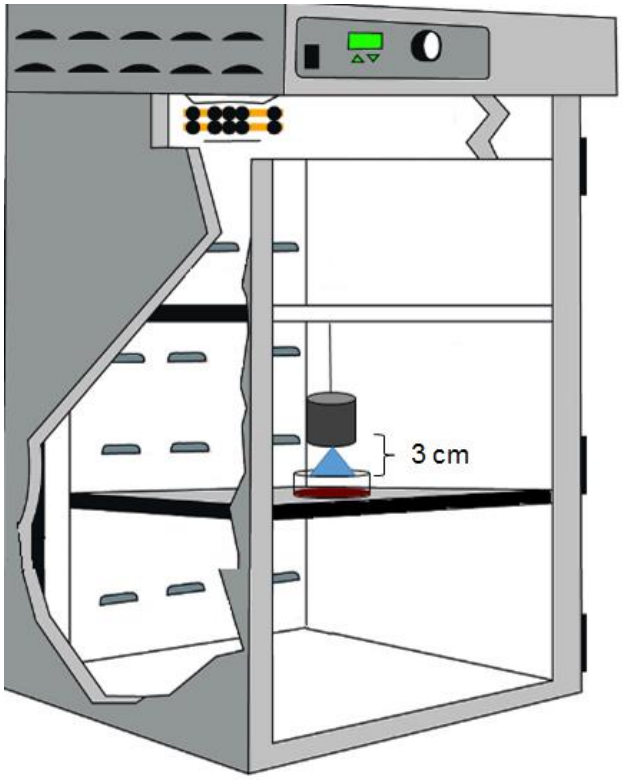

Figure 13. Schematic of light or magnetic field exposure setup for B16-Bl6 cell exposures.

Equipment

A picture of one of the devices is shown in Figure 3. They were composed of 8 LEDs (of the same wavelength) arranged in a circle as described by Karbowski and colleagues (2016). The two nails in the center of the array were extensions of a pair of solenoids that were modified reed relays (RadioShack 275-0232 SPST 5VDC, rated at 0.5 A at 125 VAC, with 20 mA nominal current) from which the magnetic field was generated.

According to a lux meter the flux density over the dish of cells or the planarian within the tissue plates containing either the cells or the planaria averaged 3000 Lux (range 2700 Lux to 3300 Lux) Magnetic field intensities as measured by power meters were between 26 and 40 mG (2.6 to 4.0 μT). We selected this intensity because it is the threshold for the value that converges with the Nernst component (about 26 mV) of the resting membrane potential that is independent of cation or anion gradients [25]. When both the field and the light were activated there was no appreciable reduction in the flux densities of either the light or the magnetic field.

Figure 14. An example of one of the arrays of 8 LEDs (separate device for the blue, green, and red wavelengths) surrounding the two poles from which the patterned magnetic field was generated. The software was designed such that either the magnetic field only, the LEDs only, or both magnetic field and LEDs could be pulsed at the same time.

Statistical Analyses

Means and standard deviations were obtained by SPSS-16 software for PCs. Because statistical significance between groups has been traditionally inferred by the absence of overlap between standard errors of the mean (SEMs) which is the standard deviation divided by the square root of the sample size we concluded that no overlap between standard deviation ranges would be sufficient criteria for statistical significance.

In addition we were interested in robust effects rather than marginal statistical fluctuations. For estimated effect sizes (estimated Ω^2) separation of the means by more than two standard deviations was equivalent to explaining about 40% of the variance.

Results

Planarian

The means and *standard deviations* for lengths of the dissected worms after 5 days of treatments are shown in Figure 15. Compared to the sham field exposed planarian the magnetic field produced a significant increase in planarian length, as displayed by one-way analysis of variance analyses ($p<0.01$). Either exposures to only the blue light or the red light elicited a significant increase in planarian length compared to the sham controls ($p<0.01$) but did not differ from the magnetic field conditions ($p=0.994$ and $p=0.577$, respectively). However, the blue light plus the magnetic field pattern ($p<0.01$) and the red light plus the magnetic field pattern ($p<0.01$) produced an additional increase in growth of the planarian. In contrast the planarian exposed to the green light or the green light plus the magnetic field did not differ from the control group ($p=1.00$). In fact the group exposed to the magnetic field plus the green light displayed less growth than the group exposed to the magnetic field only. In other words the green light exposures cancelled the effect of the exposure to this physiologically-patterned (Thomas pulse) magnetic field.

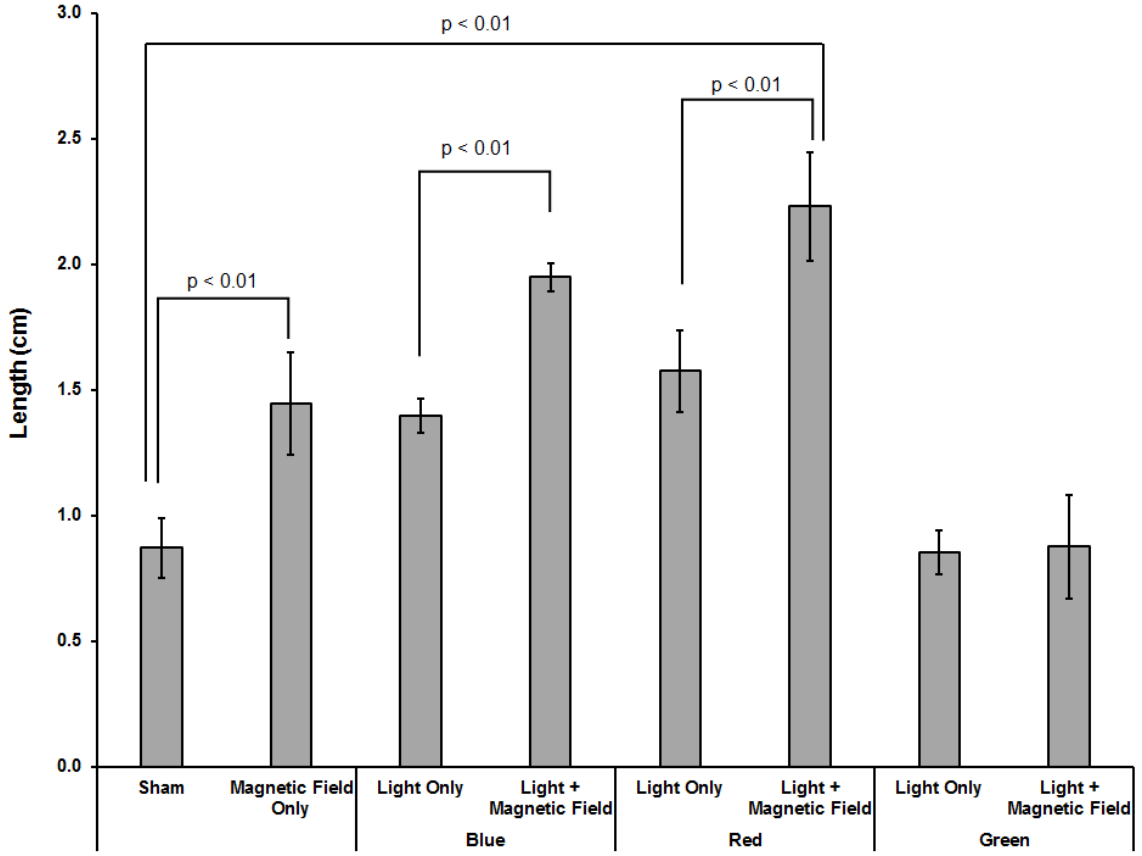

Figure 15. Length of planarian after 5 days of treatments that included exposure to no field or light, the physiologically-patterned magnetic field intensity only, the different LED wavelengths (blue, red, green) or to both the magnetic field pattern and each of the different colors. Vertical bars indicate *standard deviations*.

These effects are more clearly demonstrated in Figure 16 which shows the relative changes in length compared to sham field reference groups. The green light and magnetic field plus green light did not differ from the reference group. The group exposed to the Thomas pattern magnetic field only displayed a 40% increase in growth rate that was

comparable to exposures to blue or red light only but not green light. The combination of the red light or blue light with the synchronized magnetic field was associated with an increase in growth length of 60%.

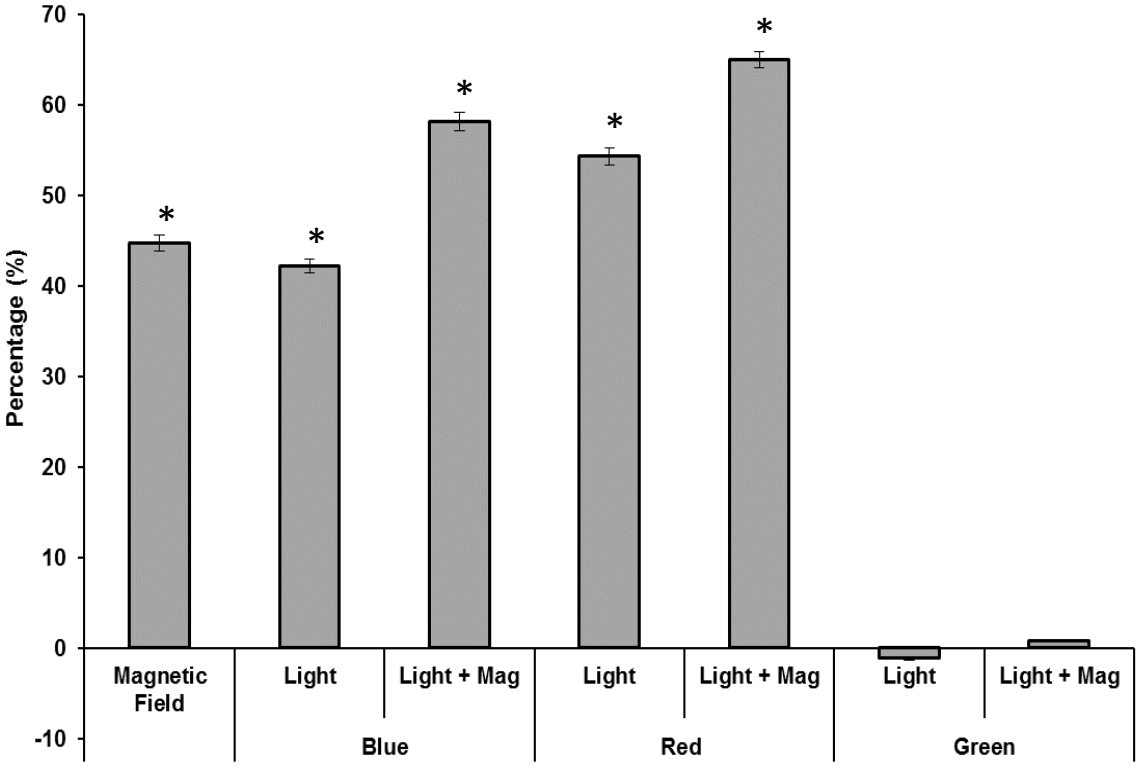

Figure 16. Percentage of increased length (growth) after 5 days of treatment compared to the reference group (sham field controls) after exposures to the physiologically-patterned magnetic field intensity only, the different LED wavelengths (blue, red, green) or to both the magnetic field pattern and each of the different colors. An asterisk indicates significant differences with a p value < 0.05.

Cells

The results of the treatments upon the growth of the malignant mouse melanoma cells in culture are shown in Figure 17 which shows the means and standard deviations for numbers of cells per unit measurement volume. Cells exposed to this particular frequency-modulated magnetic field only displayed less growth. This was called the suppression rate. For example if there 83 cells in the treated dish and 127 in the reference dish, then 1- (83/127) would be 35% suppression.

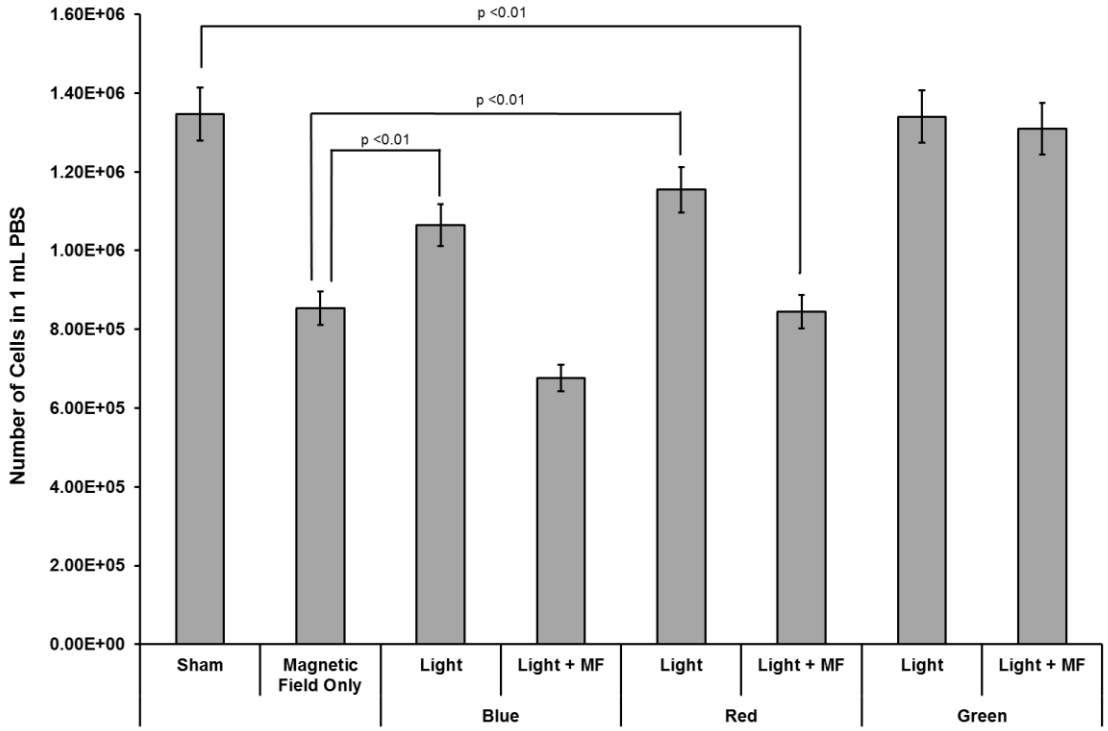

Figure 17. Number of melanoma cells in culture per unit volume after 5 days of treatment compared to the reference group (sham field controls) after exposures to the physiologically-patterned magnetic field intensity only, the different LED wavelengths

(blue, red, green) or to both the magnetic field pattern and each of the different colors. Vertical bars indicated *standard deviations.*

The proportion was similar to that found in other studies for magnetic field only treatments with the Thomas pattern. One-way analysis of various showed that exposures only to blue light reduced the effect whereas the combination of blue light and the magnetic field enhanced the growth diminishment significantly more than exposure to red light only. In other words the blue and red light only conditions diminished cell growth compared to no treatment ($p<0.01$ and $p<0.01$, respectively) but were not as effective as the magnetic field only condition ($p<0.01$) . The magnetic field plus red light condition did not differ appreciably from the magnetic field only condition ($p=1.00$).

The cells exposed to green light only did not differ significantly from cells that were exposed to nothing (the controls). Combination of the magnetic field and the green light produced cell numbers that was comparable to the controls. In other words the combination of the green light and the magnetic field eliminated the suppressing effects of this patterned magnetic field.

Discussion

Photons, particularly within the visible range, have been considered the functional source of living systems. Popp, (1979) has argued that the photons from the sun have been represented or stored as virtual photons within the intricate structure of living matter since initial abiogenesis. They are intricately connected to the processes that define life. White light or “natural” light that is composed of various proportions of all of the increments of wavelengths within the visible spectrum might be expected to exhibit “averaging effects” in manner similar to the simultaneous stimulation of all of the receptor subtypes for any chemical system such as opiates, dopamine, or serotonin when simultaneously exposed to their common ligand. Only when one particular receptor subtype is activated or blocked compared to all others do very specific behaviors emerge or states emerge.

The employment of LEDs with very specific wavelengths can be considered the analogue of targeting receptor subtypes. Our experimental results clearly indicated that the same frequency-modulated magnetic field that promotes analgesia in rats (Martin et al., 2004) or simulates this condition in planarian (Murugan and Persinger, 2014) facilitated the growth in regenerating planarian. This effect has been reported previously (Tessaro and Persinger, 2013). However in addition the exposure of only red or blue light simulated this growth effect. The combination of the red or the blue light and the magnetic field pattern increased this effect even more. From a pharmacological perspective the combination of the ultrahigh frequency (TeraHz) light and extremely low frequency frequency-modulated magnetic field could be considered a summation effect.

Such a “summation” effect would suggest that the two types of electromagnetic fields exhibited similar magnitude effects upon the biochemical processes that contribute to regeneration in planarian. According to the classic inference of magnetic energy where $E=[B^2 \cdot 2\mu^{-1}] \cdot m^3$ where the latter is volume the energy from the 5 μT magnetic field within the volume of a planarian ($10^{-9}\ m^3$) would be ~10^{-14} J. On the other hand 3,000 Lux would have projected about 10 $W \cdot m^{-2}$ upon the surface of the planarian. Assuming a flat worm of $3 \cdot 10^{-6}\ m^2$ the energy would be about 10^{-5} J per s.

For the energy values for the incident photons at specific wavelengths to converge with the energy within the volume of the planarian, the photon effectiveness must occur in an area of $10^{-15}\ m^2$. This would be equivalent to a linear distance of ~$3 \cdot 10^{-8}$ m or about 30 nm which is well within the range of the plasma cell membrane. The role of the plasma cell membrane in the generation of photons has been demonstrated experimentally by Dotta and colleagues (2011a) and calculated theoretically by Bokkon and his colleagues (2010). Several other authors have indicated the importance of the membrane source for biophotons.

Applied photons can interact with membranes. In addition to the well-known rhodopsin relationship for photon energy transformations to signaling pathways, cephalopsins have been identified in brain tissue (Blackshav et al., 1999). That proteins embedded in membranes experimentally can enhance the photon-initiating features of pathways and ion channel conditions has been shown by many authors and is the bases of the new research area of optogenetics (Deisseroth, 2015). Mitsunaga et al., (2011) showed that selective *in vivo* infrared photoimmunotherapy could target specific membrane molecules. The effect was sufficient to induce shrinkage of tumors.

Whereas the red and blue wavelengths produced increases in planarian length there were comparable to that from exposure to the physiologically-patterned magnetic field, the melanoma cells showed less suppression of growth relative to the magnetic field treatment. Only the blue light in conjunction with the magnetic field presentation facilitated the suppression of this particular malignant cells growth. The red light plus magnetic field exposures were not more effective than the magnetic field only. This differential pattern for melanoma cell proliferation compared to planarian regeneration suggests that different mechanisms may be involved.

The most challenging and intriguing result from the present study is the ineffectiveness of the green wavelength. In fact exposure of either the planarian or the melanoma cells to the green light or the green light at the same time as the magnetic field exposure *eliminated* the strong effects of the magnetic field exposure. According to Horne and colleagues, (1991) human beings, for example, are particularly sensitive to green light. Nocturnal circulating melatonin levels are readily suppressed by this hue. The effect is not likely due to non-specific energies because the blue light and the red light which exhibit more and less energy photons were effective for the planarian. Other researchers have shown the efficacy of red and blue lights. For example Figueiro and Rea (2010) showed that both narrow band blue (470 nm) and red (625 nm) lights diminished the lower cortisol levels typically measured in the dark condition from human subjects. They did not employ green light.

There is another possibility. Green is a color that is ubiquitous in Nature. Some theorists argue that animal cells were derived from plant cells early in evolutionary history. Chlorophyll displays almost no absorption of green wavelengths. As a result the primary

reflection is perceived as green. The trough of the curve is about 575 nm which is proximal to the green wavelength employed in our studies. On the other hand 470 nm is highly absorbed by chlorophyll B while 680 nm is the range of highest absorption for chlorophyll A. If some recondite and quintessential process involving the 575 nm range was the antecedent for the evolutionary developments of biochemical pathways in living systems then interference with it by any exogenous wavelength may have been excluded from these pathways.

One possibility would involve one of the states of iron valence states, some of which are associated with green spectra. If the absorption of green wavelengths had not been controlled by exclusion, sensitive pathways such as the Fenton reaction would have allowed substantial variability of reactive oxygen species (ROS) substrates within cellular pathways. Another possibility is that because the green portion of the solar output contains the peak flux within the band, the consistent presence of this wavelength with little variability would have produced habituation very early in abiogenesis. From the results of the present experiments, this wavelength can even suppress the facilitative effects of physiologically-patterned magnetic fields.

Conclusion

The results of the present experiments demonstrated that both appropriately patterned magnetic fields and blue or red LED-generated wavelengths can comparably facilitate normal regeneration of planarian. The light was less effective than the magnetic field for suppression of malignant cell's abnormal proliferation. When the field and red or blue lights are pulsed together coherently the beneficial effects are enhanced. On the other hand the effects of exposure to green light did not differ from reference groups for cells or planarian. The simultaneous presentation of the magnetic field and the green light totally eliminated the facilitative effect of the magnetic field on planarian regeneration and the inhibitory effect of melanoma cell proliferation.

References

Baker-Price L., Persinger M.A. (2003) Intermittent burst-firing weak (1 microTesla) magnetic fields reduce psychometric depression in patients who sustained closed head injuries: a replication and electroencephalographic validation. Perception and Motor Skills 96: 965-974

Bokkon, I., Salari, V., Tuszynski, J.A. and Antal, I. (2010) Estimated numbers of biophotons involved in the visual perception of a single-object image: Biophoton intensity can be considerably higher inside cells than outside. Journal of Photochemistry and Photobiology B, 100, 160-166

Blackshaw, S., Snyder, S.,H. (1999) Encephalopsin: A Novel Mammalian Extraretinal Opsin Discretely Localized in the Brain. The Journal of Neuroscience, 19(10):3681–3690

Buckner, C.A., Buckner, A.L., Koren, S.A., Persinger, M.A., Lafrenie, R.M. (2015) Inhibition of cancer cell growth by exposure to a specific time-varying electromagnetic field involves T-type calcium channels. PLoS One. 10(4):e0124136.

Choi, D.H, Lee, K.H., Moon, J.J., Kim, Y., Lim, J.H., Lee, J. (2012) Effect of 710 nm visible light irradiation on neurite outgrowth in primary rat cortical neurons following

ischemic insult. Biochemical and Biophysical Research Communications. 422; 274-279.

Deisseroth, K. (2015) Optogenetics: 10 years of microbial opsins in neuroscience. Nature Neuroscience 18, 1213–1225.

Dotta, B. T., Buckner, C. A., Cameron, D., Lafrenie, R. M., Persinger, M. A. (2011a) Biophoton emissions from cell cultures: biochemical evidence for the plasma membrane as the primary source, General Physiology and Biophysics. 30, 301-309.

Dotta, B.T., Murugan, N.J., Karbowski, L.M., Lafrenie, R.M. and Persinger, M.A. (2014) Shifting the Wavelengths of Ultraweak Photon Emissions from Dying Melanoma Cells: Their Chemical Enhancement and Blocking Are Predicted by Cosic's Theory of Resonant Recognition Model for Macromolecules. Naturwissenschaften, 101, 87-94.

Eells, J.T., Wong-Riley, M.T.T., VerHoeve, J., Henry Salzman, M.M., Buchamn, E.V., Kane, M.P. (2004) Mitochondrial signal transduction in accelerated wound and retinal healing by near-infrared light therapy. Mitochondrion. 4(5-6):559-67

Fels, D. (2009) Cellular Communication through Light. PloS ONE, 4

Figueiro M.G., Rea M.S. (2010) The effects of red and blue lights on circadian variations in cortisol, alpha amylase, and melatonin. International Journal of Endocrinology. 2010:829351

Fleming, J.L., Persinger, M.A., &Koren, S.A. (1994) One second per four second magnetic pulses elevates nociceptive thresholds: comparisons with opiate receptor compounds in normal and seizure-induced brain damaged rats. Electro- and Magnetobiology. 13, 67-75.

Horne, J.A., Donlon, J., Arendt, J.. (1991) Green light attenuates melatonin output and sleepiness during sleep deprivation. Sleep. 14(3):233-40

Karbowski, L.M., Harribance, S.L., Buckner, C.A., Mulligan, B.P., Koren, S.A., Lafrenie, R.M., Persinger, M.A. (2012) “Digitized quantitative electroencephalographic patterns applied as magnetic fields inhibit melanoma cell proliferation in culture”. Neuroscience Letters 523.2 : 131-134.

Karbowski, L.M.; Murugan, N.J.; Koren, S.A.; Persinger, M.A. (2015) Seeking the Source of Transience for a Unique Magnetic Field Pattern That Completely Dissolves Cancer Cells in Vitro . Journal of Biomedical Science and Engineering. 08, 531.

Karbowski, L.M., Murugan, N.J., Persinger, M.A. Karbowski. (2016) Experimental Evidence That Specific Photon Energies Are “Stored” In Malignant Cells For an

Hour: The Synergism of Weak Magnetic Field-LED Wavelength Pulses. Biology and Medicine. (8):1.

Kavaliers, M., Ossenkopp, K-P. (1991) Opioid systems and magnetic field effects in the land snail, *Cepaeanemoralis*. The Biological Bulletin. 180: 301-309

Martin, L.J., Koren, S.A., Persinger, M.A. (2004) Thermal analgesic effects from weak, complex magnetic fields and pharmacological interactions. Pharmacology Biochemistry & Behavior. 78, 217-227.

Masoumipoor, M., Behnam Jameie, S., Janzadeh, A., Nasirinezhad, F., Kerdari, M., Soleimani, M. (2013) Effects of 660 nm Low Level Laser Therapy on Neuropathic Pain Relief Following Chronic Constriction Injury in Rat Sciatic Nerve. Archives in Neuroscience. 1(2): 76-81

Mitsunaga, M., Ogawa, M., Kosaka, N., Rosenblum, L. T., Choyke, P. L., & Kobayashi, H. (2011). Cancer Cell-Selective In Vivo Near Infrared Photoimmunotherapy Targeting Specific Membrane Molecules. Nature Medicine, 17(12), 1685–1691.

Murugan, N.J., Persinger, M.A. (2014) Comparisons of responses by planarian to micromolar to attomolar dosages of morphine or naloxone and/or weak pulsed magnetic fields: revealing receptor subtype affinities and non-specific effects. International Journal of Radiation Biology. 90(10):833-40

Murugan, N.J., Karbowski, L.M., Mekers, W.F.T., Persinger, M.A (2015) Group planarian sudden mortality: Is the threshold around global geomagnetic activity ≥K6? Communicative & Integrative Biology. 8(6)

Olcese J., and Reuss, S. (1986) Magnetic field effects on pineal gland melatonin synthesis: comparative studies on albino and pigmented rodents. Brain Research, 369, 365-368

Oparin, A. I (1965) The Origins of Life. New York, Dover Publications.

Persinger, M.A., Lafrenie, R.M. (2014) The cancer cell plasma membrane potentials as energetic equivalents to astrophysical properties. International Letters of Chemistry, Physics and Astronomy. 17(1):66–77.

Persinger, M. A. (2016) The biomass of the earth as the direct energy-mass equivalence from ≈3.5 billions of years of solar flux (in submission).

Popp, F.-A. (1979). “Photon storage in biological systems,” in Electromagnetic Bioinformation, eds Popp F. A., Becker G., Konig H. L., Pescha W., editors. (Munich: Urban and Schwarzenberg), 123–149

Tessaro, L. & Persinger, M. A. (2013) Optimal durations for single exposures to a frequency-modulated magnetic field immediately after bisection in planarian predict final growth values. Bioelectromagnetics. (8):613-7

Trushin, M.V. (2004) Light-Mediated “Conversation” among Microorganisms. Microbiological Research, 159, 1-10

Van Wijk, R. and Schamhart, D.H.J. (1988). Regulatory effects of low intensity photon emission. Experientia; 44: 586- 593.

Wu, H-P., Persinger, M.A. (2011) Increased mobility and stem-cell proliferation rate in Dugesia tigrina induced by 880nm light emitting diode. Journal of Photochemistry Photobiololgy B., 102(2), 156-160.

Chapter Transition: Patterned Light and Learning

Chapters 2 – 5 represent a collective validation of the RRM from a theoretical perspective. That is, the model has predictive validity and can be observed to track empirical measurements, converging upon the data. Chapter 6 represents a preliminary investigation into the potency of light as a physiological modulator in planarian worms and melanoma cells. The following chapter, however, demonstrates that the memory capacities of planarian worms can be enhanced by physiologically-patterned, wavelength-specific applications of photostimuli. Further, we demonstrate that the RRM predicts that certain biomolecules (tPA, BDNF, and cAMP) underlie the events which lead to modulated responses in the organisms. The pulse pattern which elicited optimal effects was used in previous studies, modelled originally after the electrophysiological activity coupled to long-term potentiation (LTP). The results demonstrate that particular wavelengths of light applied as pulse patterns can affect biological systems in ways predicted by RRM. We suggest that the same technology could be applied to target other systems, enhancing or suppressing normal physiological events via photostimulation.

Chapter 7

Patterned LED Pulsation Enhances Learning in Planarian Worms

(Original research)

Murugan N.J., Rouleau N., Persinger M.A.

[Submitted to *Journal of Experimental Biology*, 2017]

Abstract

The capacity to achieve a task by repeated exposure, learning, and to retain the information sufficiently to continue to display the optimal behavioral output, memory, are highly adaptive. While the physiological mechanisms of learning and memory remain to be fully elucidated, long-term potentiation (LTP) has been identified as an important electrochemical correlate in many organisms. Studies have shown that in rats, chemical analogues or external application of physical forces such as magnetic fields can interfere with or enhance LTP, altering an organism's capacity to retain information. In our study, freshwater flatworms (*Dugesia tigrina*) were used as the model organism in the investigation of light-mediated manipulation of molecular events normally associated with LTP, as their photoreceptive capacities and well-defined nervous systems are fundamentally similar to our own. Photostimuli were applied as biomimetic LTP waves at various wavelengths (475-nm, 660-nm, or 880-nm) where control groups received no light or a sine-patterned light pulse. Wavelengths were selected based on the physicochemical property of the proteins involved with the various stages of LTP within the post-synaptic neurons, namely tissue plasminogen activator (tPA), Brain-derived neurotrophic factor (BDNF) and cAMP response element-binding protein (CREB). Results showed that planaria that were exposed to LTP-patterned light displayed increased performance relative to sine wave exposed group and that wavelengths of 475-nm and 880-nm produced optimal performance. We have shown that using the appropriate wavelength, intensity and information within the light packet, or pattern, light can be used as a tool to enhance learning.

Introduction

A neuron's capacity to alter its output based upon a history of inputs is reliant upon an electrochemical process known as long-term potentiation (LTP). LTP consists of repeated stimulation sufficient to increase the strength of synaptic connections. LTP gives synapses their plastic properties, a capacity to re-shape connections with the potential to alter behavior. Its early phase which occurs immediately after an LTP-inducing stimulus is associated with activations of protein kinases such as, protein kinase C (PKC) and $Ca^{2+/}$calmodulin dependent kinases (CaMKII) (Huang 1998). Phosphorylation of AMPA receptors increases their activity, reducing their thresholds of excitation. In combination with the up-regulation of excitatory receptors within the post-synaptic membrane, reduction of excitation thresholds ensure that a history of repeated exposures prime neural networks to increase signalling efficiency. During late-phase LTP, which begins hours after the inducing stimulus and sustained for up to 8 hours after, gene transcription and protein synthesis within the post-synaptic cell are up-regulated. At this point, axonal boutons, dendritic spines, and other morphological features of the post-synaptic cell are molded, restructuring the way in which connections are formed. (Frey et al., 1993) Without LTP, changes to neural hardware sufficient to sustain learned behavior would be energetically unfavorable. Therefore techniques which enhance or suppress LTP or analogous processes are of great consequence.

Photostimulation is a technique by which light is applied directly to an organism with the aim to modulate physiological processes including those associated with behavior (Mester, et al., 1967; Song, et al., 2012). In particular, cells which display highly

regulated membrane potential differences such as neurons and the cells of the myocardium, can be observed to change their polarity upon photostimulation (Fork, 1971; Vinzenz, 1979). Transient reductions of cerebrocortical excitability by photostimulation have been attributed to intrinsic biochemical changes proportional to light exposure conditions (Balaban et al, 1992). Recent reports of transcranial photostimulation of mice (Barrett & Gonzalez-Lima, 2013) as well as human subjects (Karbowski et al., 2015), demonstrates that practical applications of photostimulation are developing rapidly.

The mechanism by which photostimulation exerts effects upon biological organisms is contested. Theories of photoexcitation (Karu, 1999) suggest that molecules become excited as they absorb electromagnetic energy, increasing their reactivity. Consequently, molecular cascades which are dependent upon energetically unfavourable chemical reactions become more likely, precipitating physiological consequences. Examples of such molecules include photo-sensitive, wavelength-specific rhodopsin proteins (Palczewski, 2006) as well as non-specific photoacceptors (i.e., they absorb light) including the common molecule cytochrome c oxidase (Karu, 2008). The ubiquitous energy source of the cell, adenosine triphosphate (ATP), is a synthetic product of increased cytochrome c oxidase activity by way of electron transport, which has been experimentally promoted by photostimulation (Passarella et al., 1984). However, the presence or absence of light might not be the sole determinant of whether biomolecules interact with radiative energy.

The novel bioinformatics tool that might offer a critical link between the biophysical and biomolecular interactions is the Cosic's Resonant Recognition Model (RRM). The method offers a way by which the side-chains of linear amino acid sequences of particular

proteins can be converted to equivalent charges and, assuming an electromagnetic basis, a discrete wavelength in nanometers (Cosic, 1994). The resulting unit length describes the peak-to-peak wavelength associated with the intrinsic resonant frequency of the biomolecule. Recent experiments have confirmed the relevancy of this conversion method by empirical observation of nano-scale wavelengths shifts in photon emissions (Karbowski et al., 2015). Insofar as photostimulation is partially contingent upon the wavelength of the applied light, the RRM could be used to target protein candidates which facilitate the desired response. Here we demonstrate that a combination of RRM and photostimulation techniques can optimize task performance in planarian worms by reducing task completion time after a brief, wavelength- and pattern-specific photostimulation exposure.

Methods & Materials

Planarian Colony Care

One hundred and twenty (n= 120) *Dugesia tigrina* worms obtained from Carolina Biological Supply (Burlington, NC, USA), were removed from their housing colony and housed individually in 2.0 mL clear, aerated, conical tubes containing 1.5 mL of spring water. The worms were given with bovine liver as a nutrient source during the 3 month feeding cycle before being starved for 1 week immediately preceding experimental exposure. The temperature of the testing and housing area were regulated and maintained at approximately 23 °C.

Overall Paradigm

The basic procedure involved exposing planaria to pulsed LED light 30 minute before observing task acquisition using a T-maze paradigm. Planarian worms were first randomly assigned to one of two pulse pattern groups. The first pulse pattern consisted of a simple 7Hz sine wave whereas the second pulse pattern involved a complex series of pulses which were previously configured (Mach et al., 2009) to simulate electrophysiological spike potentials recorded from neurons expressing long-term potentiation (LTP). Worms were then further divided into one of three LED wavelength groups: 475-nm, 665-nm, or 880-nm.

Light Sources and Application Patterns.

Custom photostimulation devices, which were first tested by Karbowski et al. (2016) were constructed by embedding 8 LEDS arranged into a circle of either 475-nm, 665-nm, or 880-nm into a plastic casing containing electronics paired to a power switch which could toggled manually. The illuminance value for the LEDs was measured at 1mW/m^2 respectively at 5 cm, which is similar to the irradiation distance for the planaria worms. The appropriate signals were generated and controlled by The Complex software developed by Koren and Persinger (U.S. Patent 6,312,376 B1: November 6, 2001; Canadian Patent No. 2214296) using a Lenovo computer. This software is a custom-constructed digital-to-analogue converter (DAC) software, where a series of numbers

(1through 256) which represent a signal are converted to voltage between -5 and +5 V, where 0V is denoted by 127 in the series of numbers. The complex LTP sequence employed in this study comprised of 225 points (Figure 18) and applied through the DAC at the appropriate wavelength. The point duration, or the time in which each serial value was activated was 3 msec and the time delay between each activation was 3 msec. A 7Hz sinusoidal signal pulsed at the appropriate wavelength with the same point durations was also employed in the study.

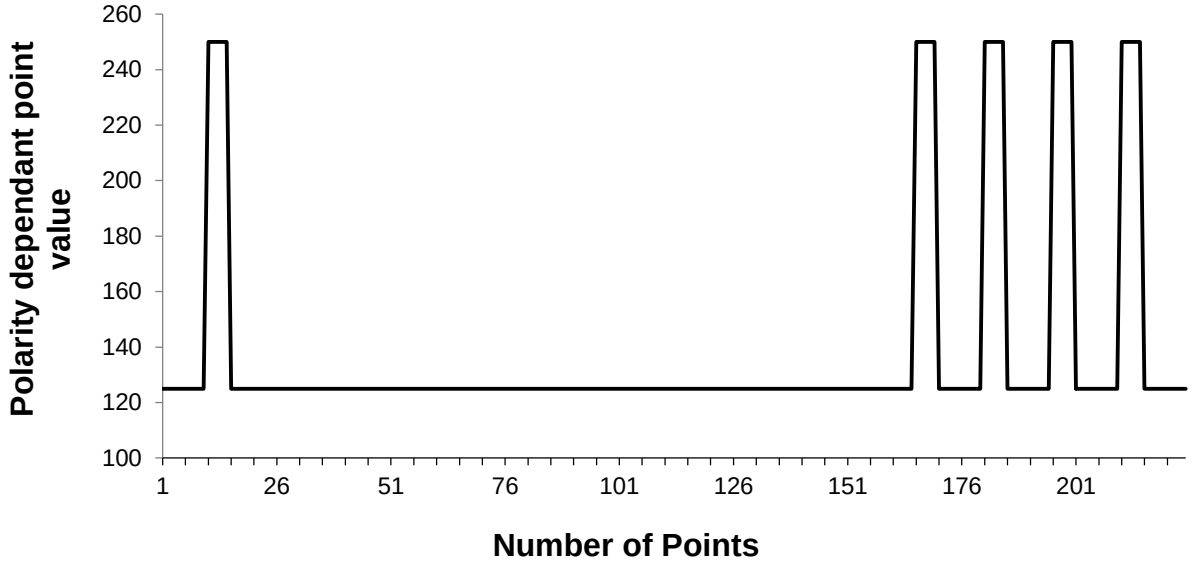

Figure 18: A two-dimensional representation of the frequency-modulated LTP pattern.

Behavioural Measures

T-Maze

A custom 8 cm by 1 cm T-maze was constructed using plastic and filled with paraffin wax (Figure 19). A 1 cm trough which spanned the length and width of the maze

was created in the shape of a cross, where a single planarian could freely move along each arm. To ensure planarian movement, each arm (3 cm in length) was filled with 7 mL of the same type of spring water used for planarian housing.

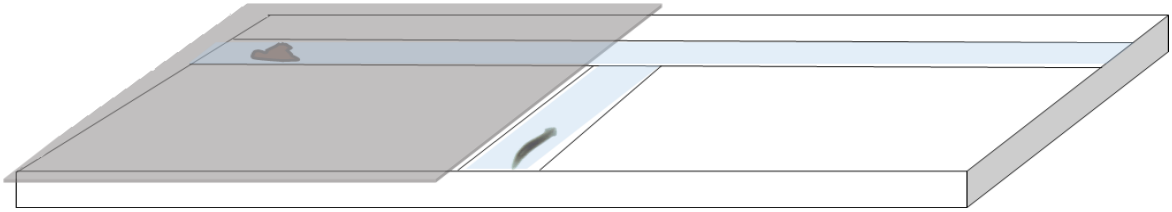

Figure 19: Experimental T-Maze. The darkened arm is baited with bovine liver to increase planarian locomotion to desired arm.

Mobility Assay

The effect on total locomotion as a function of applied wavelength of light was measured using an open field assessment of the planarian following light treatment. Data collection during these trials was limited to mobility and other observable behaviours such as head bops, twists or swaying were not recorded. The mobility of the planarian worms which is measured as locomotor velocity was determined through observation of gridlines crossed on grid paper of known spatial dimensions. During the open field experiments all worms were recorded individually within the same 10 cm diameter petri dish. This

measure was added to see if the applied light influenced the planarian locomotion or strictly their task acquisition, thus reducing their reward time.

Experimental Procedure

Planarian worms were exposed to pulsed sine or LTP patterned light emitted by 475-nm, 665-nm, or 880-nm LEDs for 30 minutes prior to testing. Immediately following photostimulation, planaria were placed within a T-maze in a darkened environment where one of the short arms was focally illuminated by a 970 lux white light lamp. The locus of the darkened short arm (i.e., left or right) was counterbalanced to control for sources of directional bias. The other arm remained darkened and was therefore favoured by the generally photophobic planaria though a 1 cc sample of bovine liver was also added to the darkened arm to ensure reliable responses. (Figure 19) As we endeavoured to measure task acquisition, worms remained paradigm-naïve until testing commenced.

Each trial began by depositing a single worm into the long arm of the T-maze. Planaria were allowed to freely move across the maze for a maximum duration of 5 minutes. The elapsed time from the moment the worm was placed within the long arm until its tail segment had passed into the darkened short arm was recorded for each trial. The procedure was conducted 3 times per individual planarian with a 60 minute inter-trial delay. Immediately after T-maze testing, planaria were placed in an open field, and the number of gridlines crossed were counted for 5 minutes. After all behavioural testing, planaria were returned to their housing conditions.

Statistical analyses

Behavioural data were collected manually and imported to SPSS v20. Data were coded by condition and checked across experimental groups for indications of homogeneity of variance. Analyses consisted of simple tests of differences including analyses of variance (ANOVAs) and t-tests.

Results

The results from the mobility assay were entered into a one-way ANOVA where it displayed a statistically significant effect for wavelength of applied light $F_{(3, 76)} = 10.39$, $p<.05$, where worms exposed to 475nm of light displayed increased mobility, and 880nm displayed decreased mobility compared to control conditions, and no significant differences in mobility was observed with those worms exposed to 665nm light ($p < .01$, $\eta^2 = 0.29$). These results independently confirm a study conducted by Paskin et al. (2014) who show that planaria experience increase photophobic behaviour in response to direct applied of UV-blue light compared to infrared. No significant differences in the pattern of mobility as function of applied wavelength of light was observed between the two LTP and sine wave patterns.

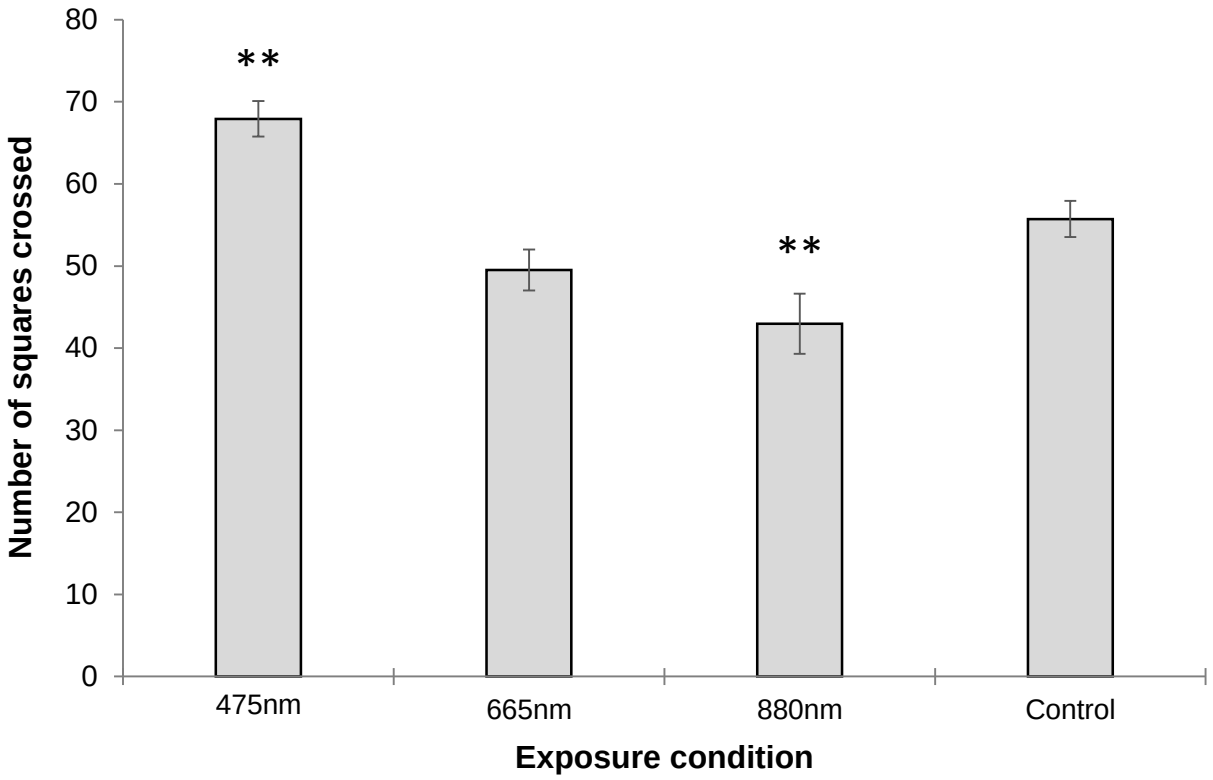

Figure 20: Mean number of squares crossed (locomotor velocity) over a 5 minute observation period for planaria exposed to 30 minutes of sham or LTP-patterned wavelength of light. Vertical bars indicate standard error of the mean (SEM). Significant differences are noted (**, p<.05).

An ANOVA revealed an interaction of pattern and wavelength for the final testing period only, $F_{(3,29)}$= 4.236, p<.05, η^2=.12. Earlier testing periods did not display similar effects (p>.05). In general, planaria exposed to LTP patterned light displayed decreased task acquisition time relative to the sine-exposed group, t(1.217)=,p<.05, r^2=10.5%. However, two wavelengths of LTP-patterned light emerged as statistically significant from control (no exposure): 475-nm and 665-nm (Figure 21). In both cases, reduced elapsed

time to the darkened arm was observed relative to controls with effect sizes of 45.3% and 46.1% respectively. The interaction suggests that the wavelength of exposure light was not sufficient to alter task acquisition relative to control. Rather, a relatively complex pulse pattern was required as a delivery, which was effective at relatively shorter (greater energy) wavelengths.

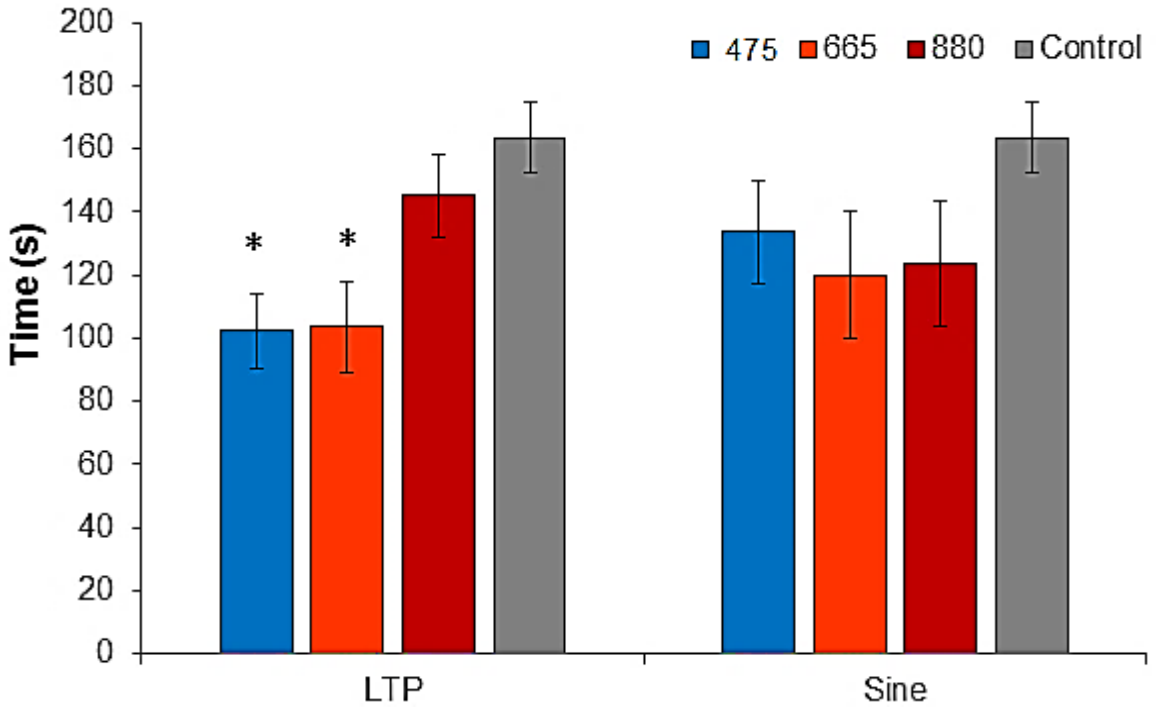

Figure 21: The total time spent within the darkened arm after a 30 minute exposure to sine or LTP- patterned light. Vertical bars indicate standard error of the mean, and the asterisk denote a significant difference from respective sham conditions.

Discussion

Our experiment demonstrated that within the late phases of testing, an interaction between the pattern (LTP) and wavelength (475-nm or 665-nm) of the applied light produced a reduction in T-maze task completion relative to unexposed worms. Stated otherwise, planaria completed the maze more rapidly if pre-exposed to LTP-pulsed light with shorter wavelengths approximately ~3 hours after the initial 30 minute exposure. The relevance of the pattern, the wavelength, and the temporal onset of the effect should be relevant to the biomolecular pathways inherent to the processes of memory formation – more specifically, LTP.

Long-term potentiation (LTP) can be divided into temporal phases. An early phases, characterized by sustained electrical activity can last up to 2 hours (Huang 1998) and is not dependent on *de novo* protein synthesis. As effects reported here occurred approximately 3 hours post-photostimulation, late-phase LTP should have been operating, involving trafficking of proteins and mRNAs from the soma and proximal dendritic sites to the newly-forming synaptic interfaces (Frey et al. 1993). As was stated previously, resonant frequencies which are related to wavelengths of light can be obtained for individual proteins from their linear protein sequence using Cosic's resonant recognition model (RRM). Converting four proteins typical of late phase LTP (PKC-Zeta, tPA, BDNF, and CREB) into their resonant wavelength equivalents yielded the following wavelengths: 1204.73-nm (PKC-Zeta), 200.70-nm (BDNF), 479.02-nm (tPA), and 766.02-nm (CREB).

The resonant frequency associated with the tissue plasminogen activator (tPA) is within range to the applied exposure light that produced the significant increase in learning, ~3hr after exposure (475-nm). These blue, near-ultraviolet sources could potentially overlap when accommodating shifts within the medium (water) and the +/- 5-nm range of the bulb. Close examination of the molecular cascade, shows that in response to theta-burst stimulation, tissue plasminogen activator (tPA) is secreted into the synaptic cleft, where it downstream leads to the cleaving of BDNF, and subsequent signalling into the nucleus for transcription and translation of other proteins to maintain LTP. In other words, tPA is the “key” that can start the process. A possible mechanism is then, that the applied light, effects the structure and activity of tPA to enhance the whole signal transduction, thus increasing spine formation or learning or memory.

These results demonstrate that complex patterned light, rather than simple sinusoidal light, may be able to modulate behaviour. These modulations could be intimately tied to conserved biomolecular pathways, interacting by way of photoexcitation of molecules with intrinsic resonant frequencies which overlap with the applied stimuli. Proteins, typically activated by endogenous molecules, could be induced to exert their effects upon their target sites by resonant mechanisms involving light. That the LTP pattern, designed to emulate electrophysiological activity associated with long-term potentiation, produced the optimal effects was notable. Perhaps by mimicking the resonant functions of proteins and the electrophysiological activity which accompany them, we are now able to non-invasively alter the behavior of organisms without the requirement of photosensitive proteins coupled to viral vectors as has been repeated demonstrated using optogenetics (Yizhar et al. 2011).

References

Balaban, P., Esenaliev, R., Karu, T., Kutomkina, E., Letokhov, V., Oraevsky, A., & Ovcharenko, N. (1992). He-Ne laser irradiation of single identified neurons. Lasers in Surgery and Medicine, 329-337.

Barrett, D., & Gonzalez-Lima, F. (2013). Transcranial infrared laser stimulation produces beneficial cognitive and emotional effects in humans. Neuroscience, 13-23.

Fork, R. (1971). Laser stimulation of nerve cells in Aplysia. Science. 3974, 907-908.

Cosic, I. (1994) Macromolecular Bioactivity: Is It Resonant Interaction between Macromolcules? IEEE Transactions of Biomedical Engineering, 41, 1101-1114. http://dx.doi.org/10.1109/10.335859

Frey U., Huang Y.Y., Kandel E.R. (1993). Effects of cAMP simulate a late stage of LTP in hippocampal CA1 neurons. Science, 260:1661-1664.

Huang, E.P (1998) Synaptic plasticity: Going through phases with LTP. Current Biology 1998, 8:R350–R352

Karbowski LM, Murugan NJ, Persinger MA (2016) Experimental Evidence That Specific Photon Energies Are “Stored” in Malignant Cells for an Hour: The Synergism of Weak Magnetic Field-LED Wavelength Pulses. Biol Med (Aligarh) 8(1): BM-162-16

Karbowski LM, Murugan NJ, Persinger MA (2015). Novel Cosic resonance (standing wave) solutions for components of the JAK–STAT cellular signaling pathway: A convergence of spectral density profiles. FEBS Open Bio. 5, 245-250.

Karbowski LM, Saroka KS, Murugan NJ, Persinger MA (2015) LORETA indicates frequency-specific suppressions of current sources within the cerebrums of blindfolded subjects from patterns of blue light flashes applied over the skull. Epilepsy Behav. ;51:127-32. doi: 10.1016/j.yebeh.2015.06.039

Karu, T. (1999). Primary and secondary mechanisms of action of visible to near-IR radiation on cells. J. Photochemistry and Photobiology, 49, 1-17.

Karu, T. (2008). Mitochondrial Signaling in Mammalian Cells Activated by Red and Near-IR Radiation. Photochemistry and Photobiology, 1091-1099.

Mester E, Szende B, & Tota J.G.(1967). Effect of laser on hair growth of mice. Kiserl Orvostud, 19, 628–631.

Palczewski K (2006). G Protein–Coupled Receptor Rhodopsin. Annu Rev Biochem. 75: 743–767.

Paskin T.R., Jellies J., Bacher J., Beane W.S. (2014) Planarian Phototactic Assay Reveals Differential Behavioral Responses Based on Wavelength. PLOS ONE, 9(12): e114708.

Passarella, S., Casamassima, F., Molinari, S., Pastore, D., Quagliariello, E., Catalano, I., & Cingolani, A. (1984). Increase of proton electrochemical potential and ATP synthesis in rat liver mitochondria irradiated in vitro by He-Ne laser. FEBS Letters, 175, 95-99.

Song, S., Zhou, F., & Chen, W. (2012). Low-level laser therapy regulates microglial function through Src-mediated signaling pathways: Implications for neurodegenerative diseases. Journal of Neuroinflammation, 219-219.

Yizhar O., Fenno L.E., Davidson T.J., Mogri M., Deisseroth K. (2011) Optogenetics in Neural Systems. 71(1): 9-34.

Chapter Transition: Application of Light onto Tissues

The influence of light upon the building blocks of living systems is demonstrative of how applications of electromagnetic energy can substitute events which initiate molecular cascades. Specific wavelengths of light, applied with targeted precision, serve as physiological place-holders – activating structures such as proteins even in the absence of molecules which would otherwise be necessary to initiate cascades. In the previous chapter, planaria were exposed to wavelength-specific, patterned light applications which were found to modulate learning processes. Our interpretation, based upon the RRM, suggested activations of select molecules which would normally be associated with learning – promoting task acquisition and enhancing the performance of the exposed worms. The study was demonstrative of light-mediated effects which can be observed *in vivo*. The following chapter serves to compare the differential effects associated with applications of light to *in vivo* and *ex vivo* brain specimens. In particular, we used quantitative electroencephalography (QEEG) to measure electric potentials (voltage) over the scalps of participants as well as over the cortices of full, unsectioned brain specimens which were preserved in ethanol-formalin-acetic acid. We applied light to both the living and post-mortem brain specimen and monitored voltage to observe frequency-dependent changes in amplitude of the signal contingent upon light applications. We reported several key findings which suggest that the living and post-mortem brain respond differentially to the applied light. We hypothesize that a technology which combines light exposures and electroencephalography could be developed to discriminate between conscious states, coma, and death – a task which can be difficult to assess, particularly in the absence of motor movement.

Chapter 8

Electroencephalographic Measures of Spectral Power and Current Source Densities during Circumcerebral Light Exposure of Living and Fixed Post-Mortem Brains

(Original Research)

Murugan, N.J., Rouleau N., Persinger M.A.

[Submitted to *Brain Research,* 2017]

Abstract

Measurements of microvolt potentials over the human scalp contain a multitude of signals, many of which cannot be directly attributed to activated, coherent neural subpopulations. The intrinsic electrical properties of brain material and their effects upon quantitative electroencephalography (QEEG), independent of metabolically-driven neural activity, should be considered. Combining paradigms involving circumcerebral light applications to living human participants and fixed, post-mortem human brain specimens, we attempted to parse signal sources, separating neural activations from intrinsic brain noise. Our results demonstrate that, in general, QEEG profiles from living human participants display increased amplitude within the theta frequency band (4 Hz – 7.5 Hz) relative to the post-mortem comparator at baseline. Focal white light applications to the right anterior temporal lobe (T4 site) exacerbated these effects. Standardized low-resolution electromagnetic tomography (sLORETA) revealed that focal white light applications to the right anterior temporal lobe generated increased 10 Hz – 13 Hz activity within left frontal lobes of living participants relative to the post-mortem comparator. The post-mortem brain displayed wavelength-specific effects of light exposure and generalized left hemispheric receptivity to photostimulation. In combination, the results demonstrate that post-mortem brain specimen comparators can useful when parsing signals from noise. The technique could be used in clinical settings to classify weak electroencephalographic signals associated with coma or near-death states.

Introduction

The discovery that frequency-dependent electric potential differences between positions over the human scalp relative to the ears could be reliably induced to change by eliciting behaviours as simple as closing one's eyes provided the initial bases for electroencephalography (EEG) (Berger, 1931). Quantitative electroencephalography (QEEG), the modern digital variant of analog EEG, can be used to infer simple cognitive states of arousal (Gugino et al., 2001) or sleep (Paul et al., 2003) as well as guide novel interfaces between humans and machines (Lotte et al., 2007). Whereas QEEG signals are often filtered to eliminate extrinsic sources of noise such as electrical artefacts (i.e., 60 Hz and its harmonics), components of the record will always include data from unaccounted sources, not attributable to sources of variance associated with experimentally manipulated variables.

Little attention has been allocated to concepts of intrinsic brain noise. The human brain consists of a discrete mass of conductive material which may express intrinsic resonant frequencies (Tsang et al., 2004) as well as other properties which are inseparable from the wetware itself. Structurally resonant or otherwise intrinsic signals would be present in all electroencephalographic profiles but not necessarily paired to any particular cognitive state or set of states. Rather, the signal's signature would be characteristic of the brain as an electrical object occupying a discrete section of the broader electromagnetic environment, independent of the default-mode network (Greicius et al., 2003) or any other neural process no matter how conserved. Rather, their origins would be fundamental to the physical shapes and chemical constituents of brain

material itself (Nunez, 1995). Intrinsic brain noise is inherent to brain tissue and unlike the default-mode network should, in principle, be detectable in metabolically inactive, deceased human brains provided that their micro-structures are preserved.

Several experiments have demonstrated that post-mortem human brains preserved in ethanol-formalin-acetic acid express regional and hemispheric asymmetries (Rouleau, et al., 2016) which are selectively responsive to inputs of electrical current (Rouleau & Persinger, 2016a). A systematic comparison of signals obtained from Living and post-mortem, non-living human brains was conducted by Rouleau and Persinger (2016b) who found that the living brain generally expressed greater power under the classic QEEG bands (delta-gamma) compared to its non-living counterpart, though spatial independence of signals within the non-living brain was entirely dependent upon signal frequency. In other words, high-frequency (> 14 Hz) spectral power within the post-mortem, non-living brain tended to be represented non-homogeneously across the cortical manifold, where gyri operated as if functionally independent – just like the Living brain (Rouleau and Persinger, 2016b). This was not the case for low-frequency (< 14 Hz) signals where living and non-living brains differed substantially in their expression of spatial signal independence. Whereas the comparison was conducted with reference to the 10-20 International System of Electrode Placement, the equipment used to measure the Living human participant and the post-mortem brain were different. In the case of the former, the classic QEEG sensor cap was used whereas in the case of the post-mortem brain, needle electrodes were inserted directly into gyri which partly coincide with the cap's electrode array.

Rouleau, Costa, and Persinger (2016) demonstrated that simple 60 Hz flashes of white light (10 lux) induced increased right occipital alpha (7.5 Hz – 14 Hz) spectral power densities in a fixed, post-mortem human brain. The results were unsurprising given experimental results presented by Karbowski, Saroka, Murugan, and Persinger (2015) which indicated that current source densities as computed by low-resolution electromagnetic tomography (LORETA) could be suppressed by pulsed applications of light applied over the skull of human participants. Together, these results indicate that light, if directly applied, can potentially affect microvolt potentials represented over the surface of and within the human brain. In search of intrinsic noise signatures common to both the living and non-living variants of the brain as an organ, we endeavored to apply a combination of these paradigms to assess differential responses of the living and non-living brain to the same photostimuli. If the living and non-living human brains could be observed to express identical patterns of activation or de-activation as inferred by modulated spectral power, said observations would provide a foundation for the study of post-mortem brain tissue signals as they apply to human QEEG and paired cognitive-behavioural states.

Methods and Materials

Participants

A total of 3 adult males and 1 female between the ages of 20 and 26 were recruited for this study. After receiving informed consent, each participant was seated in a comfortable chair within a well-lit room, which was maintained at ambient temperature

(25ºC). This was to ensure that all conditions of living and non-living measurements would remain equivalent.

Post-Mortem Brain Specimen

A full human brain (n=1) fixed in ethanol-formalin-acetic acid was employed as the Non-living reference specimen through the course of the study. It displayed all of the major neuroanatomical structures of the superficial telencephalon as described by Crosby, Humphrey, and Lauer (1962) and as otherwise unremarkable from a gross structural level. The brainstem was intact with fully preserved cerebellar hemispheres, a pons, medulla, and rostral spinal cord. The brain contained all of its original cranial nerves as well as residual vasculature including the middle cerebral artery, anterior cerebral artery, posterior cerebral artery, basilar artery, and partially attached cerebellar components.

Quantitative Electroencephalography

A Mitsar 201 QEEG amplifier was equipped with a 19-sensor cap (10-20 International System of Electrode Placement) which was applied to the head of participants (living) or the brain specimens (non-living). In the case of the living brain, the electrical reference point consisted of an average of 4 signals obtained over the surface of the ear lobes obtained with the use of disc AgCl sensors. In the case of the non-living brain, the reference point was relegated to the ears of the human participants sitting

quietly in front of the brain. The same participants were employed as references and living participants to reduce variability due to individual differences of skin conduction. A sodium-based electroconductive gel served as a conduit for signals between the scalp or surface of the brain specimen and the sensors of the cap. Data were streamed to an HP Envy laptop computer operating Windows 8. WinEEG version 2.93.59 (07.2013) software was employed with a 250 Hz sampling rate. Low- and high-cut filters of 1.6 Hz and 50 Hz respectively were applied throughout testing to exclude extraneous sources of electrical interference. An additional notch filter removed signal sources between 50 Hz and 70 Hz as well as between 110 Hz and 130 Hz to further reduce noise within the record. The gain of the device was set to 5 μV in order to observe electric potentials within the Non-living brain, which is greater than a factor of 10 below that required to observe those associated with the Living brain (150 μV). Data transformations, discussed in detail elsewhere, were performed in order to compare the living and non-living signals which, as expected, differed as a function of amplitude. Raw microvolt potentials were extracted from the WinEEG files and later converted to spectral power density ($\mu V^2 \cdot Hz^{-1}$) profiles to infer frequency-dependent signal sources and their relative amplitudes. For within-subject comparisons of the Non-living brain, spectral power densities were extracted directly from WinEEG.

Once extracted, data were imported to SPSS v.20, z-transformed, and spectral analyzed. A z-transformation was necessary in order to effectively compare the Non-living and living signals due to intrinsic differences of amplitude. Though spectral analyses produced a series of spectral power densities within frequency bins ranging between 0.1 Hz and 125 Hz, aggregated bins were selected based upon typical methodological

practice. Classical EEG bandwidths were selected for the analysis: delta (1.5 Hz – 4 Hz), theta (4 Hz − 7.5 Hz), alpha (7.5 Hz − 14 Hz), beta1 (14 Hz − 20 Hz), beta2 (20 Hz − 30 Hz), and gamma (30 Hz − 40 Hz). Data were then subjected to a series of analyses, investigating interactions as a function of the experimental conditions. These primarily involved analyses of variance as well as independent and paired t-tests.

Light Exposure Devices

A light exposure device, identical to that which was employed by Karbowski et al. (2015), was constructed. The device consisted of 4 pairs of 880 nm or 395 nm LEDs (8 LEDs per device). A HP Envy laptop computer with a Windows 8 operating system controlled the output to the devices via the soundcard. A 20 kHz tone was generated in Audacity 2.0.5 where amplitudes were set between 0.8 and -0.8. The soundcard output was set to maximum (100% capacity), which streamed signals to the LED devices. Termination and initiation of light exposure was controlled by a switch located on the LED device. The light exposure devices were elevated by 2 cm from the surface of the testing area and directed toward the 4 focal regions involved in the study: left frontal pole, right frontal pole, left temporal pole, right temporal pole, left occipital pole, right occipital pole. The devices were separated from the tissue or surface of the scalp by 5 cm. As an alternative to the custom devices, we employed a commercially available, 3V (DC) battery powered flashlight with 5 wide-spectrum (white) LEDs (35 lumens). The circular aperture containing the 5 LEDs had a diameter of 2.5 cm. The device was always elevated by 2

cm from the surface of the testing area and positioned 5 cm from the tissue. The intensity of applied light was similar to those employed by Saroka et al. (2016).

Procedure

In all cases, brains or the heads of human participants were exposed to serially presented, counterbalanced light exposures which were directed to specific target points. QEEG baselines were obtained at the beginning of each experiment for 2 minutes, after which the first exposure was initiated. Light was directed toward either the left or right frontal, temporal, or occipital pole for 2 minutes. The six target points (3 left hemispheric and 3 right hemispheric) were exposed for 2 minutes with 2 minutes of baseline data collected between exposures. The entire procedure lasted 24 minutes. In the case of the Living brains, the human participants were instructed to close their eyes throughout the entire procedure while remaining still and calm.

Results

Non-living Brain: Effects of Wavelength

Exposing the Non-living brain to different wavelengths of light applied focally to the left occipital lobe generated wavelength-dependent differences of unstandardized delta (η^2=.33) and theta (η^2=.25) spectral power densities within the right frontal lobe (Fp2, F4, and F8). In both cases, increased spectral power was observed during white light exposures relative to exposures of 880 nm (Figure 22A). There was no significant difference between 395 nm light and other conditions ($p>.05$). A high-frequency spectral

power effect as a function of wavelength was noted when isolating the left frontal lobe exposure condition, $F(2,17)=4.77$, $p<.05$, $\eta^2=.33$. Exposing the left frontal lobe to white light produced increased unstandardized beta1 spectral power densities within the left temporal lobe (T3 and T5) relative to 880 nm wavelength light exposures, $t(10)=2.71$, $p<.05$, $r^2=.42$ (Figure 22B). There was no significant difference between 395 nm light and white light or between 395 nm and 880 nm light exposures ($p>.05$).

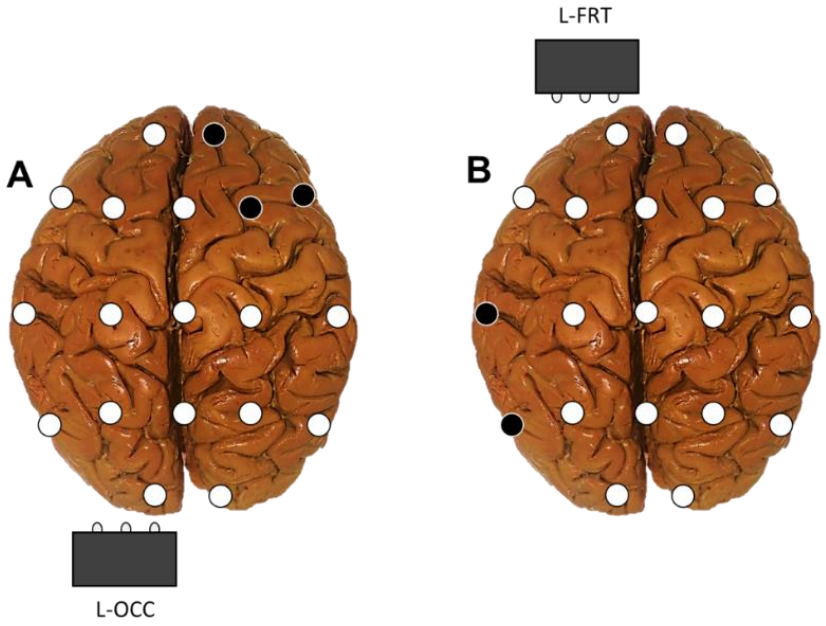

Figure 22. White light directed toward the left occipital (A) and left frontal (B) poles of the cerebrum generated increased right frontal lobe (1.5 Hz – 7.5 Hz) and left temporal lobe (14 Hz – 20 Hz) unstandardized spectral power increases relative to the 880 nm light condition. Black circles indicate significant differences ($p<.05$). The black box represents where the light unit was placed.

Regardless of where light was applied to the Non-living brain, the left frontal lobe expressed different unstandardized spectral power densities for an average of alpha-beta1 (7.5 Hz – 20 Hz) as a function of the wavelength, $F(2, 160)= 4.86$, $p<.01$, $\eta^2=.05$ (Figure 23). The right frontal lobe did not display a similar effect ($p>.05$). The primary source of variance was an increase in alpha-beta1 power when exposed to near-infrared (880 nm) light relative to both white and near-ultraviolet (395 nm) light with effect sizes of 4% and 5% respectively. To summarize, white light produced effects specific to the where the exposure was oriented whereas the 880 nm wavelength produced a generalized effect upon the left frontal lobe irrespective of where the light was applied.

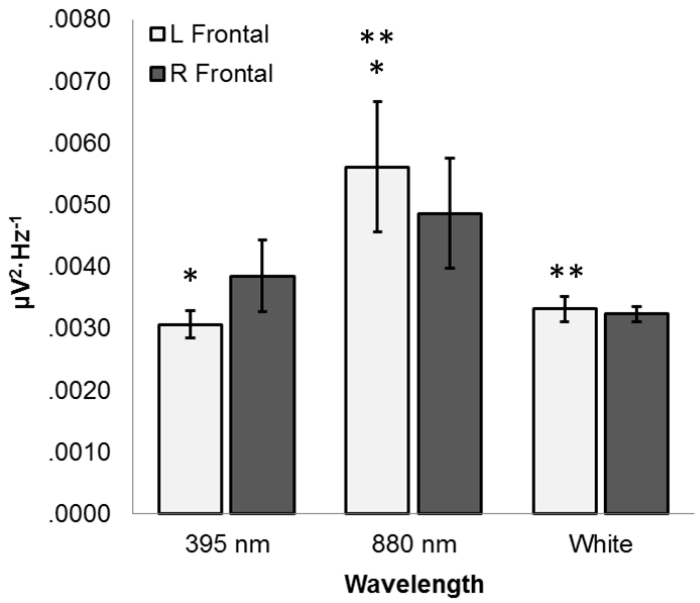

Figure 23. Left (light) and right (dark) frontal lobe unstandardized spectral power densities within the alpha-beta1 range (7.5 Hz – 20 Hz) as a function of wavelength of the applied light. Significant differences between 395 nm and 880 nm (*) as well as between 880 nm and white light (**) conditions are presented.

Living and Non-living White Light Exposures

Figures 23A and 23B illustrate the primary differences between the standardized spectral profiles of the Living and Non-living brains. The profiles consist of an average of spectral densities over the 19 sensor array or a spatially global measure of spectral power. The most conspicuous difference is the clear (z-score > 1.96) 10 Hz peak (Figure 24A) associated with the Living brain which is typical of a human QEEG spectral profile during baseline conditions with the participant's eyes closed. Figure 24B demonstrates that Living brains express greater proportions of global theta (4 Hz – 7.5 Hz) power relative to the Non-living brain whereas the reverse is true for higher frequencies (14 Hz – 40Hz). General applications of white light did not change these basic profiles ($p>.05$). Rather, focal applications of white light to specific regions of the cerebrum were associated with alternative relative power when comparing the Living and non-living brains.

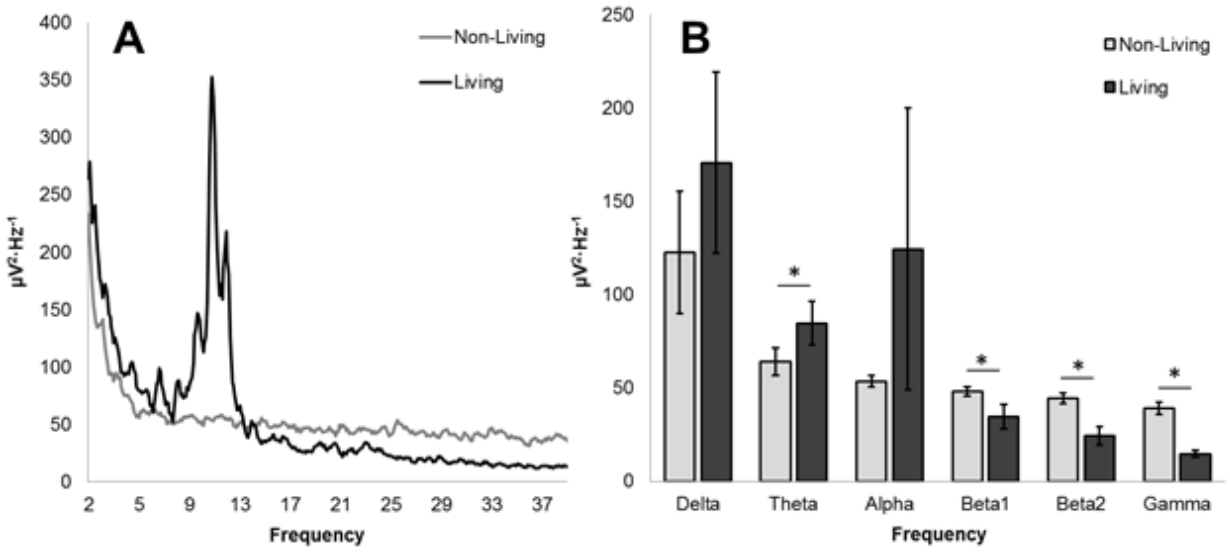

Figure 24. Global (all sensors) baseline spectral density profile of the non-living (light) and Living brain (dark) as inferred by quantitative electroencephalographic data (A). A clear ~10 Hz peak typical of eyes closed baseline recordings is visualized for the Living brain but not for the Non-living brain. Low frequencies dominate the Living brain whereas power is less variable across frequency bands for the non-living brain (B). Standard deviations (SD) are given.

Investigating the major differences between the Living and non-living brain from the perspective of subcortical sources of oscillatory power, sLORETA was employed to infer punctate regions of interest expressing different current source densities. Decreased low beta (13Hz – 20Hz) current source densities within the right post-central gyrus (BA2) were observed within the non-living brain relative to the Living brain during baseline conditions (Figure 25). Though surface potentials revealed increased standardized high-frequency spectral power within the non-living brain relative to the Living brain (Figure

27B), current source densities within the same range were incongruent with these measurements.

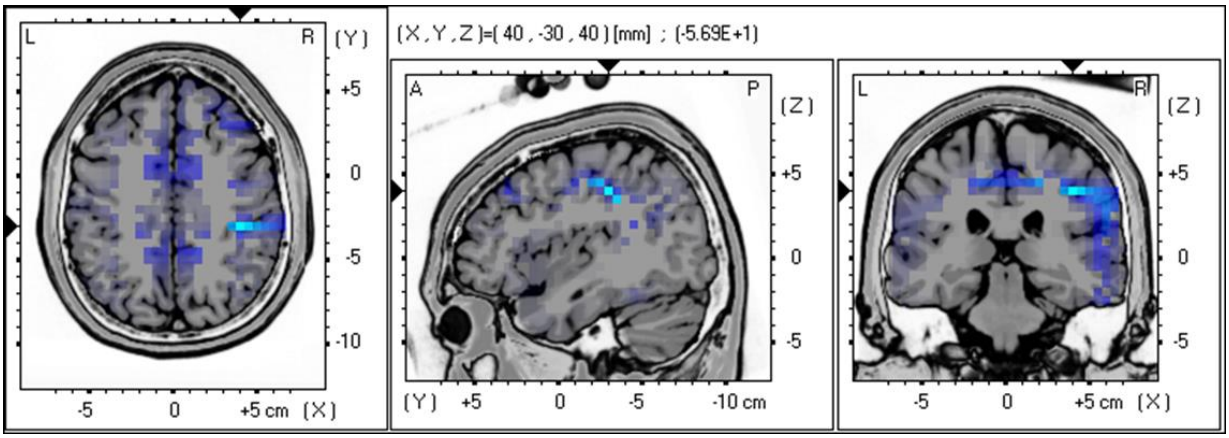

Figure 25. Decreased low beta (13 Hz - 20 Hz) current source densities within the right post-central gyrus (BA2) of the non-living brain relative to the Living brain during baseline conditions (no applied stimulus) viewed in horizontal (left), sagittal (middle), and coronal (right) sections. Light blue indicates significant differences ($p<.05$).

The sensors which were reliably associated with significantly different theta spectral power between the living and non-living brains during applications of white light were Cz (medial longitudinal fissure, central region) and T4 (right anterior temporal lobe). Effects associated with Cz were, however, marginal. Within all white light application conditions, T4 theta was greater in the living brain relative to the non-living brain despite statistical overlap during baseline (no light) conditions (Figure 26). Further, right temporal (R-TMP) applications of white light resulted in a universal theta increase across all sensors within the living brain relative to the non-living brain ($p<.002$). sLORETA revealed

decreased alpha (10Hz – 13 Hz) current source densities within the left middle frontal gyrus of the non-living brain relative to the living brains during right temporal (R-TMP) white light exposures (Figure 27).

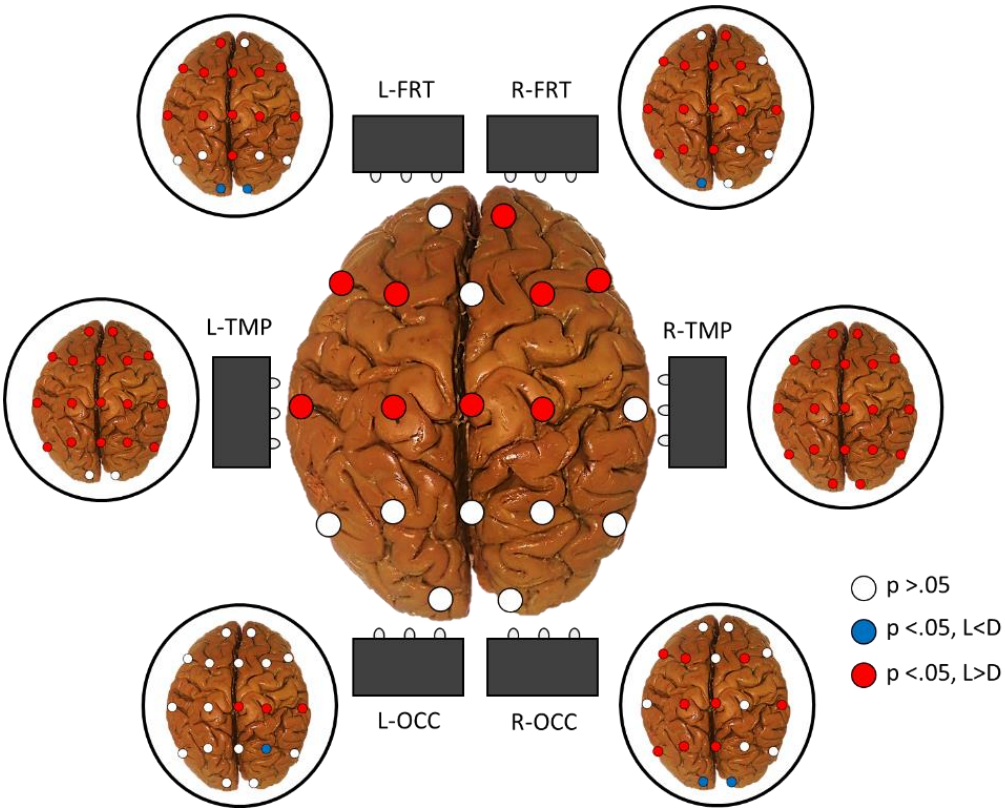

Figure 26. Significantly different theta-band (4Hz – 7.5Hz) spectral power densities between the Living and non-living human brains during baseline condition (center image) as well as left frontal (L-FRT), right frontal (R-FRT), left temporal (L-TMP), right temporal (R-TMP), left occipital (L-OCC), and right occipital (R-OCC) white light exposures. White indicates no significant differences (p>.05), blue indicates less power within the Living brain relative to the Non-living brain (p<.002), and red indicates more power within the Living brain relative to the Non-living brain (p<.002). The black box represents the placement of the light device.

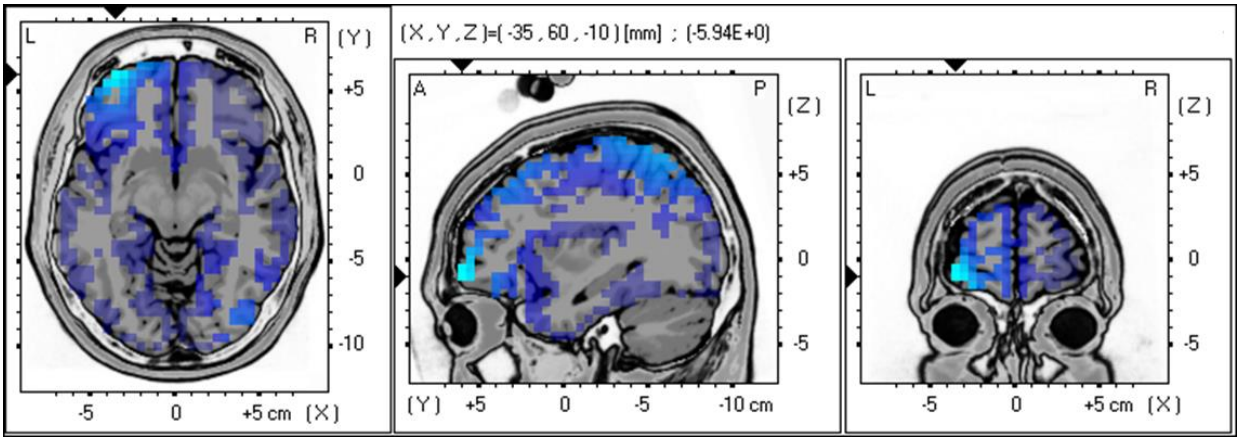

Figure 27. Decreased high alpha (10 Hz -13 Hz) current source densities within the left middle frontal gyrus (BA11) within the non-living brain relative to the Living brains during applications of white light to the right temporal lobe viewed in horizontal (left), sagittal (middle), and coronal (right) sections. Light blue indicates significant differences ($p<.05$). Figure 31 demonstrates the relative inefficacy of white light applications to produce differences in gamma between the living and non-living brains. The one exception consisted of spatially diffuse modulations of select sensors (F3, T3, O1, and T4) when exposed to left frontal (L-FRT) white light. All other conditions failed to alter the baseline configuration. These results demonstrate that the light effects are frequency-dependent rather than general or otherwise spurious.

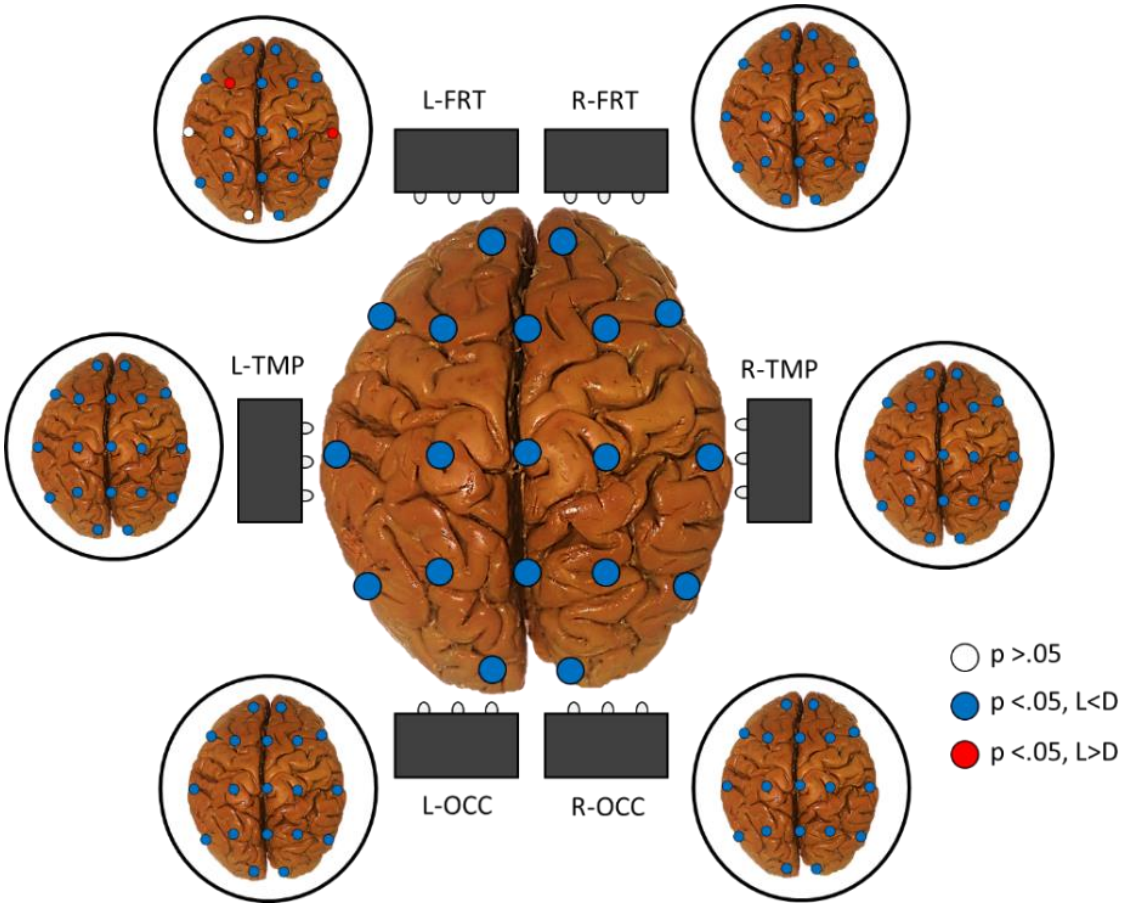

Figure 28. Significantly different gamma-band (30Hz – 40Hz) spectral power densities between the living and non-living human brains during baseline condition (center) as well as left frontal (L-FRT), right frontal (R-FRT), left temporal (L-TMP), right temporal (R-TMP), left occipital (L-OCC), and right occipital (R-OCC) white light exposures. White indicates no significant differences, blue indicates less power within the living brain relative to the non-living brain ($p<.002$), and red indicates more power within the living brain relative to the non-living brain ($p<.002$).

Discussion

Our results indicated that the non-living brain displayed generalized (7.5 Hz – 20 Hz) left frontal activations when exposed to near-infrared, 880 nm light relative to other conditions. When exposed to white light directed toward the left frontal region, the brain displayed increased left temporal spectral power within a subset of the same frequency range (14 Hz – 20 Hz) relative to the 880 nm condition. Similarly, the left occipital white light exposure generated increased low-frequency (1.5 Hz – 7.5 Hz) right frontal spectral power relative to the 880 nm condition. Other focal applications of light did not produce spectral power differences across conditions ($p>.05$). Together, the results show that focal applications of white light along the longitudinal axis within the left cerebral hemisphere generated spatially non-adjacent increases of spectral power elsewhere within the brain. As a general rule, however, 880 nm light generated increased power relative to other conditions. These wavelength-specific effects warranted further experimentation. As we were able to generate reliable spectral responses contingent upon focal applications of white light within the non-living brain, we attempted to apply the same protocol in the case of the living brain to compare the two systems.

Baseline QEEG measurements of the living and non-living brain unsurprisingly indicated that the Living brain displayed increased power relative to its counterpart, primarily within lower frequency bands. The most notable difference between the spectral profiles was the expected ~10 Hz peak characteristic of human QEEG records. It was surprising, however, that upon examination of high-frequency (low beta, 13 Hz – 20 Hz) current source densities, the right somatosensory cortex displayed relative decreases

within the v brain. The corollary is that the living brain displayed relative increases – which is sensible from a physiological perspective though it remains unclear why this particular region and frequency band emerged as statistically significant within the baseline state. Rouleau et al., (2016) demonstrated that the post-mortem brain fixed in ethanol-formalin-acetic acid displays intrinsic spectral differences between the poles and relative center of the brain as well as between structures and across hemispheres. These types of intrinsic differences, independent of incoming stimuli, could have contributed to the differences observed in the present study between the living and non-living brains at baseline.

A sensor-matched comparison of living and non-living brain spectral power during applications of white light revealed that proportions of theta (4 Hz – 7.5 Hz) oscillations were particularly disparate. The baseline condition was marked by a rostro-caudal split where Living theta power was increased primarily within rostral sensors relative to the non-living brain. This was not the case for caudal sensors ($p>.05$). Focal applications of white light reliably induced greater theta power over the T4 (right anterior temporal lobe) site in the Living brain relative to the non-living brain regardless of where the light source was placed around the head of cerebrum ($p<.05$) despite no significant differences over T4 between brains at baseline. Applications of white light over the T4 and other right temporal regions generated increased theta activations across all Living brain sensors relative to the non-living brain. Also of note were the conspicuous sLORETA tomograms presented in Figure 6 which revealed left middle frontal current source densities (10 Hz – 13 Hz) were decreased in the non-living brain relative to the living brain during right temporal lobe white light exposures ($p<.05$). In contrast, gamma-band spectral power remained relatively unaffected by applications of white light (Figure 7). The standard

interpretation would suggest that differences between the living and non-living brain are due to physiological responses typical of the living brain superimposed upon and differing from sources of noise typical of the human brain as an electroconductive object.

That there were observed differences between the living and non-living brains was expected, some of which can likely be attributed to the fundamental differences in referencing procedures. Transforming the data (z-scores) eliminated simple differences associated with microvolt potential amplitude disparity between the two systems. However, it is still possible that the point of reference could have influenced oscillatory activity (i.e., signal frequency and spectral density). That is, sensors placed over the scalp of the living participants referenced to the ears of those same participants might have produced signals that were fundamentally different than those acquired from sensors placed over the surface of the post-mortem brain referenced to the ears of a nearby human participant by dint of physical continuity of the electroconductive medium (i.e., the skin connecting the scalp and the ear) alone.

Comparing spectral power obtained from needle electrodes inserted into gyri across a non-living brain referenced to attached vasculature (the basilar artery) as presented by Rouleau & Persinger (2016b) indicated that spectral power was comparatively amplified across all bands in the present study involving references placed on the ears of living human participants. Rouleau et al., (2016), who also inserted needle electrodes into cerebral gyri though employed the same method of non-living brain referencing as reported in the present study, demonstrated that no differences of spectral power could be discerned when comparing signals obtained from post-mortem brains referenced to the ear lobes of two different human participants over many trials. Likewise,

we did not discern any differences as a function of the reference point (i.e., the ears of particular human participants). They also reported spectral power densities which were much more in line with those presented by Rouleau & Persinger (2016b), suggesting that needle electrodes inserted into the brain tissue produced decreased spectral power relative to cup sensors. Since our measurements of both Non-living and Living brains involved the use of cup sensors rather than needle electrodes, we consider this study to be a better approximation of a true comparison between the two systems. The intrinsic limitation with regard to referencing is that the Non-living brain is not electrically continuous with meninges, bone, muscle, and skin as well as ears. Therefore reference points are necessarily going to be different when comparing living and non-living brains.

What was unexpected was the degree to which signal overlap could be identified between the two systems. For instance, sensor-matched theta power over the entirety of the caudal cerebrum was identical when comparing the living and non-living brains. Stated alternatively, only rostral sensors differentiated the living brain from its Non-living counterpart when examining the theta band. Applications of white light to the frontal regions produced overlapped theta spectral power whereas occipital and right temporal applications were paired with marked differences between living and non-living brains. The primary difference between living and non-living white light exposures was the living brain's relative sensitivity to applications over T4. Theta spectral power (4 HZ – 7.5 Hz) over the right anterior temporal lobe during general and focal white light stimulation was the primary differentiating phenomenon which separated the living and non-living brains.

Practical applications of the work presented here might include circumcerebral photostimulation of patients displaying varying degrees of coma or otherwise

unresponsive states. Classifying the state of brains along a spectrum with respect to normative databases which record responses to stimuli applied directly to living and non-living brains would allow clinicians to plot brain degeneration and track genuine brain healing without recourse to motor-heavy tasks such as physiotherapy. Scales of responsiveness are typically contingent upon motor output, which neglects the majority of the brain's functional capacity. By implementing strategic tests which probe the brain directly and reference responses with respect to large databases, clinicians may be able to assist a subset of unresponsive individuals in ways previously neglected.

References

Berger, H. (1931). Über das Elektrenkephalogramm des Menschen. European Archives of Psychiatry and Clinical Neuroscience, 94(1), 16-60.

Crosby, EC, Humphrey, T, Lauer, EW. Correlative anatomy of the nervous system. Chapter 7: Telencephalon, Part I – Gross structure of the Telencephalon, New York; 1962, p. 343-55.

Greicius, M. D., Krasnow, B., Reiss, A. L., & Menon, V. (2003). Functional connectivity in the resting brain: a network analysis of the default mode hypothesis. Proceedings of the National Academy of Sciences, 100(1), 253-258.

Gugino, L. D., Chabot, R. J., Prichep, L. S., John, E. R., Formanek, V., & Aglio, L. S. (2001). Quantitative EEG changes associated with loss and return of consciousness in healthy adult volunteers anaesthetized with propofol or sevoflurane. British Journal of Anaesthesia, 87(3), 421-428.

Karbowski, L. M., Saroka, K. S., Murugan, N. J., & Persinger, M. A. (2015). LORETA indicates frequency-specific suppressions of current sources within the cerebrums of blindfolded subjects from patterns of blue light flashes applied over the skull. Epilepsy & Behavior, 51, 127-132.

Lotte, F., Congedo, M., Lécuyer, A., Lamarche, F., & Arnaldi, B. (2007). A review of classification algorithms for EEG-based brain–computer interfaces. Journal of neural engineering, 4(2), R1.

Nunez, P. L. (1995). Toward a physics of the neocortex. In P. L. Nunez (Ed.), Neocortical dynamics and human FEG rhythms (pp. 68–132). New York: Oxford University Press.

Paul, K., Krajča, V., Roth, Z., Melichar, J., & Petránek, S. (2003). Comparison of quantitative EEG characteristics of quiet and active sleep in newborns. Sleep Medicine, 4(6), 543-552.

Rouleau, N. & Persinger, M.A. (2016a). Differential Responsiveness of the Right Parahippocampal Region to Electrical Stimulation in Fixed Human Brains: Implications for Historical Surgical Stimulation Studies?. Epilepsy & Behaviour. 60, 181-186.

Rouleau, N. & Persinger, M.A. (2016b). Spatial-Temporal Quantitative Global Energy Differences Between the Living and Dead Human Brain. Journal of Behavioural and Brain Sciences. 6, 475-484.

Rouleau, N., Costa, J.N., & Persinger, M.A. (2017). Evaluating the Signal Processing Capacities of Post-Mortem Cerebral Cortical Tissue by Artificial Phototransduction of Dynamic Visual Stimuli. Open Journal of Biophysics. 7, 1-13.

Rouleau, N., Lehman, B., & Persinger, M.A. (2016). Focal Attenuation of Specific Electroencephalographic Power Over the Right Parahippocampal Region During Transcerebral Copper Screening in Living Subjects and Hemispheric Asymmetric Voltages in Fixed Coronal Sections. Brain Research. 1644, 267-277.

Tsang, E. W., Koren, S. A., & Persinger, M. A. (2004). Power increases within the gamma range over the frontal and occipital regions during acute exposures to cerebrally counterclockwise rotating magnetic fields with specific derivatives of change. International Journal of Neuroscience, 114(9), 1183-1193.

Chapter Transition: Regulating Electromagnetic Effects

Previous chapters have discussed the relevancy of RRM and patterned applications of electromagnetic energy to alter biological systems, whether they be functioning or chemically preserved. Together, they constitute a body of evidence demonstrative of biomolecular-photon interactions. Not only can bioinformatics tools be used to predict biophoton emission profiles, but electromagnetic field and light exposures which aim to influence biological systems can be tuned according to wavelengths predicted by RRM. In the final chapter, we discuss the relevance of complex, temporally patterned weak electromagnetic fields as an effective method by which cancer can be inhibited. Our findings indicated that both the conditions of the application (e.g. the complexity of the pattern or intensity of the stimulus) as well as environmental factors such as limitations imposed upon the system by the incubator within which the cells reside contribute to the net effects. The discussed parameters which optimally produce inhibition of cancer are related to quantum optics where dipole and resonance interactions are considered in the cell. The paper serves as a general overview of our work concerning cancer and electromagnetic fields – emphasizing the role of pattern and precision.

Chapter 9

The Third Option for Stopping Cancer: Complex, Temporally Patterned Weak Magnetic Fields- Critical Factors That Influence Their Efficacy and Potential Mechanisms

(Original Research)

Murugan N.J., Rouleau N., Persinger M.A.

[Published in *World Scientific News*]
Vol. 54 pp. 267-288, 2016

Abstract

One of the most promising technologies for suppressing the growth of malignant (cancer) cells without adversely affecting normal cells involves the application of physiologically-patterned and bioquantum compatible magnetic fields with specific temporal increments generated by optocoupler circuits through each of the three spatial planes. However, experimentally generated magnetic field patterns designed to target cancer cells are also immersed within the magnetic environment of the incubators. We measured anomalous alterations in the horizontal (primarily “east-west”) component of the geomagnetic static field intensity within cell incubators when the most effective experimental field was being generated between three sets of solenoids. The eccentric response was a function of the six solenoids being wrapped or not wrapped with copper foil. In addition, activating or deactivating the experimental field for fixed increments was associated with discrete and obvious DC shifts in the horizontal component as well as emergent patterns that were not a component of either the experimental field or the background incubator 60 Hz source. If the temporal pattern that defines the effects induced by these magnetic fields is analogous to the spatial patterns that define chemical functions, failure to accommodate these anisotropic transients could be a source of the frequent contradictions and inter-laboratory failures to replicate these phenomena. We suggest that the emergent phenomena from these interactions with quantum-like features may be the causal variables responsible for many of the promising effects for cancer suppression. A modified Dicke model derived from quantum optics where cells

cooperatively interact with a single mode of the field and their dipole fields interact coherently may accommodate the observed effects.

Introduction

The central concept that manifested in late 19th and early 20th century chemistry was that molecular structure determined function. The complexity of the functions and the efficacy of any combinations of compounds upon biological systems were further complicated by the precise nature of the microenvironment in which the reaction occurred. The interface between molecules and the external surface of the living cell was realized to be a multivariable configuration. The specific consequences of introducing multiple chemical components within this microenvironment were a function of the molecular structure of the proteins that constituted the receptors, the competition between the many chemical species that were proximal to the reactions, and some measure of compatible resonance that influenced the likelihood of the dose-dependent interaction between the external field of the chemical structures and those expressed upon the cell membrane's surface.

Within the domain of magnetobiology and magnetochemistry, the appreciation for the precision required to produce powerful biological and chemical effects has been minimal. The term "magnetic field effects" is applied homogeneously as if all magnetic field applications are similar. This is analogous to applying a large number of structurally different molecular compounds that would produce different and even contradictory effects but still considering them the same or simply, "chemical effects". These

inconsistencies reflect the precision of the geometries required to produce reliable results. Several theorists and experimenters (Adair, 1991; Berg, 1999; Murugan et al., 2015; Rouleau et al., 2016) have shown that the orientation of the static magnetic field, the local geomagnetic field configuration and the temporal, spatial, and intensity characteristics of the applied electromagnetic fields can affect and even determine the magnitude of effects. Our working hypothesis is that all components and origins of magnetic fields within the region where the exposures and measurements of biological systems occur must be measured and identified in order to discern which synergism is actually producing the significant effects.

Multiple examples of interactions between magnetic fields applied within the same space and time were elegantly described by Burke (1986). Intrinsic features include the Larmor frequency of a proton (proton resonance) which is within the range of cerebral and cell functions (40 Hz) when the applied field is within the μT range and of the electron which is within a similar frequency band (30 Hz) when the applied field is within the nT range. With multiple superimposition of magnetic fields a myriad of phenomena can emerge synergistically such as photomagnetic effects, inductive reactance (the characteristic of a coil to oppose current depending upon its rate of change and inductance), eddy currents, thermoelectric effects, intrinsic thermal gradients, and magnetoacoustics phenomena. Although the traditional proclivity is to simplify the exposure system this reduction in complexity also indicates fewer degrees of freedom for which specific interactions are required. Simplifying the geometry of magnetic field exposures for biomagnetic interactions might be considered analogous to attempting to ascertain the specificity of large molecular compounds by ignoring their complex

configurations and using a “simple” substance such as water. The subsequent modelling may be palatable and conceptually parsimonious but the effects would be both trivial and limited.

The importance of understanding synergisms between experimental and natural magnetic fields is not trivial. The contemporary treatment of most cancers and malignant cell growth is confined to either intense radiation or toxic chemotherapies. These procedures, although effective, frequently eliminate normal cells as well as malignant cells. In addition they result in significant cognitive compromise and untoward side effects that reduce the quality of life. We (Buckner, 2012; Karbowski et al., 2012) have found that applications of physiologically patterned, weak magnetic fields to dozens of different human and animal malignant cell lines reduce their proliferation by approximately 50% without influencing normal cells. In addition, the temporal patterns of these magnetic fields provide beneficial analgesic effects (Martin et al, 2004) without activating the molecular pathways through which morphine operates and metastases occurs (Afsharimani et al., 2011). Other researchers have found that complex-patterned magnetic fields with spectral power densities within the 8 to 25 Hz range retard or eliminate the growth of malignant cells in vitro. This optimal range had been discovered decades ago by Adey (1981) while studying calcium efflux across membranes. If physiologically-patterned magnetic fields are a third option to treat one of the most challenging conditions in the history of medicine and science, then understanding all of the nuances that can diminish their efficacy must be explored.

For example the presence of copper as shielding or shelving within cell culture incubator systems is remarkably common. However, sheets of this metal produce

anomalous effects for which the total physical mechanism is not clear. Murugan et al (2015) exposed spring water (to simulate cell physiological conditions) to frequency-modulated, weak (1 microTesla) magnetic fields generated between two coils. One coil was activated and the other was not activated. The intention was to produce the potential conditions for a Bohm- Aharanov effect as well as a magnetic vector A. These researchers then measured the photon emissions from aliquots of that water once removed from the field. The glass containers that had been wrapped with aluminum, plastic or no material all showed markedly enhanced fluorescence photon emissions between 275 and 305 nm. The flux was a factor of 25 greater than photon emissions below or above this band. The containers of water wrapped with copper during the magnetic field exposure displayed complete abolishment of this emission band.

Karbowski et al (2016a) expanded the investigation of this phenomenon by exposing mouse melanoma (skin cancer) cells in plates between three pairs of solenoids (one pair in each spatial plane). They reiterated the descriptions of Tonomura et al (1986) who had nicely articulated the Aharanov-Bohm effects involving electron beams and copper shielding. Karbowski et al (2016a) predicted that a phase shift might occur between the opposite solenoids in a plane independent of the magnetic flux. They assumed an essential energy unit of 10^{-20} J (2010), the involvement of the Compton wavelength, and the time within the voltage field to be a unit electron orbit. The phase modulation required for this increment of energy with these parameters was about $1.5 \cdot 10^{-12}$ m per phase. When voltage was reconfigured, the optimal value to produce the Aharanov-Bohm effect was about 4.3 V.

This discrete voltage was within the range of the ± 5 V systems (Koren et al, 2015) employed to produce the effective suppression rates in the growth of cancer cells. Multiple experiments demonstrated that the titrated voltages applied through the circuitry to the solenoids to produce the greater inhibitory effects on malignant cell growth was 4.3 V. Values below or above this precise number produced less or no suppression of malignant cell growth. When each solenoid was wrapped with copper foil the inhibitory effect upon malignant cells growth was completely abolished without affecting the intensity of the frequency-modulated, physiologically patterned magnetic field (Karbowski et al, 2016b). This reliable measurement suggested that the efficacy of time-varying magnetic fields reported by several authors (e.g., Karbowski et al, 2015) may involve variables sequestered within the domain of field intensity.

Zhadin et al (1998) succinctly demonstrated that DC magnetic fields applied orthogonally to time-varying fields produced differential effects. That stronger static fields and superimposed weaker, temporal fields should interact is not surprising. One of the most general phenomena in perceptual detection is Weber's Law which indicates that for a just noticeable difference to occur for a change in stimulus intensity there must be a specific (optimal) ratio between the intensity of the changing stimulus with respect to the background static (larger) stimulus. Many researchers assume that the resultant static magnetic field of the earth, upon and within which experimental magnetic fields are superimposed, is sufficient to describe immersive phenomena. However the total field is composed of three vector directions that can vary substantially while the resultant field remains more or less consistent. Each vector (plane) can display differential effects. As recently shown experimentally by Vares et al (2016) the human brain behaves as a dipole

whose shifts in microVoltage as measured by quantitative electroencephalography are precisely the difference in torque (energy) between either aligned or orthogonal orientation with the N-S component of the field only.

These eccentric changes in the intensities of the field parameters when time-varying fields are immersed within the 60 Hz fields of copper-jacked incubators may be more important than assumed. Buckner et al (2015), Karbowski et aI (2015) and several other groups of researchers have shown conclusively that appropriately patterned magnetic fields diminish the growth of several lines of malignant cells without affecting the growth of normal cells. This differential effect is qualitatively different from the effects of chemotherapy or radiation treatments that often kill both cancer and normal cells. Patterned magnetic field treatments penetrate the tissue and are not dependent upon vasculature for distribution within the tissue as is the case for chemotherapies. Here we present evidence: 1) of the importance of directionality and spatial plane in the production of the effective component of the applied field, 2) the differential effects of copper shielding of the solenoids that generate experimental magnetic fields, 3) how these fields inside of standard copper-shielded incubators results in marked alterations in the resulting intensity for exposures, and 4) that the Dicke model for quantum optics may serve as quantitative metaphor for central components of the magnetic field effects on malignant cell cultures.

METHODS AND MATERIALS

Our basic paradigm consisted of exposing a magnetometer sensor to a complex patterned electromagnetic field within a small exposure box typically used in experiments involving cancer cells. The box, equipped with solenoids, was placed within or outside of an incubator. The external surfaces of the solenoids were either partially covered or uncovered by copper wrapping which was designed to modify potential components within the electromagnetic field exposure (see Figure 29) . The magnetometer sensor was exposed to combinations of these experimental conditions in addition to different temporal increments of exposure and inter-exposure periods. We hypothesized that combinations of these variables would affect the intensity as well as other components of the field exposures in ways which might enhance or decrease the experimental effects associated with our various biological paradigms.

Magnetometer Measurements

A MEDA FVM-400 Vector Magnetometer sensor was placed into a cubed enclosure (4D box) with solenoids affixed to the center of each surface (Figure 30). The 4D box device is typically used to expose malignant cell lines to patterned (Karbowski et al, 2015; Murugan et al, 2014a) electromagnetic fields – a protocol which has demonstrated considerable anti- cancer effects (Hu et al., 2010). A Lenovo laptop computer with a Windows 7 operating system was programmed to, using custom

software, convert data strings into patterned current output which operated the 4D box solenoids (Koren et al, 2015). The standard decelerating frequency modulated, Thomas (a decelerating frquency modulated) electromagnetic field pattern (see Figure 31) which has been used in many experimental contexts in our laboratory was measured directly by the magnetometer and power meter.

The circuitry by which this pattern (and related patterns) are generated is a patented (Koren et al, 2015), custom constructed system (US Patent 7553272). In summary, the Thomas pattern is composed of 849 numbers each of which has a value between 0 and 256. They are converted by Digital to Analogue Convertors (DAC) to values between -5 and +5 V (127=0 V). The circuit is based upon a series of optocouplers and Triac components that allow photon transmissions across junctions to transform the input between -5 to +5 V. The potentials are delivered to appropproprite pairs of solenoids such that all three planes of space are occupied. The point duration which is the time each number between 0 and 256 are activated to produce the specific voltage has been found to be critical for the effect. When each of the points are ~3 ms the resulting magnetic field significantly reduces malignant cell growth and optimally affects calcium flux densities within cells (Buckner et al, 2015). Point durations less or greater than this value are not effective. The duration of one presentation of the pattern composed of 839 numbers at 3 ms each is 2.52 s. This is repeated for the duration of the experimental exposure.

Field intensity (nT) values were obtained in increments of 1 second (1 Hz) across three axes: X, Y, and Z. The X-axis consisted of the horizontal plane parallel with the bottom of the incubator, running from the front to the back of the incubator. The Y-axis

consisted of the same horizontal plane though the direction of the plane was perpendicular, running from one side (lateral wall) of the incubator to the other. The Z-axis was positioned within a plane perpendicular to both of the aforementioned planes, running from the bottom of the incubator to the top. The orientation of the magnetometer sensor was calibrated with respect to the X- axis at declination 20 deg. Consequently the orientation was slightly oblique. The exposure protocol was an A-B-A-B design where the field pattern was initiated and terminated multiple times within a trial. The time of each exposure (A) and the inter-exposure times (B) were always of equivalent temporal length. We selected four temporal increments of exposure: 5 sec, 10 sec, 20 sec, and 30 sec. This meant that, for example the Thomas field was activated for 10 s and deactivated for 10 s for 5 pairs of repetitions. Trials were repeated in triplicate in order to determine both internal variability and reliability.

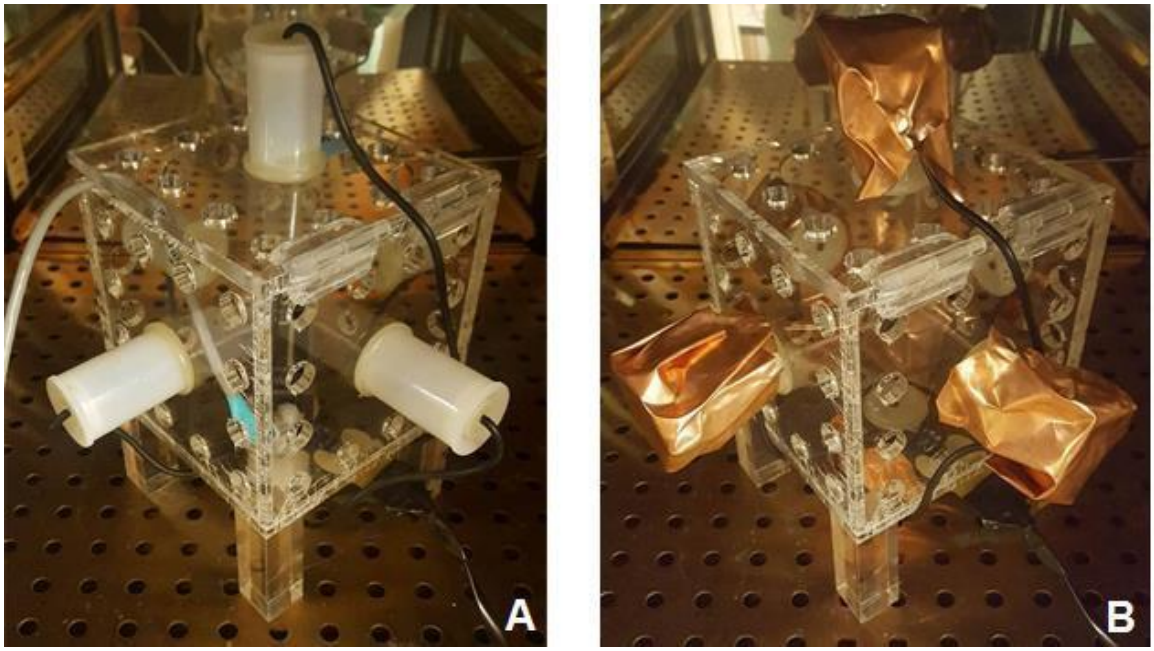

Figure 29. The 4D box within the incubator without (**A**) and with (**B**) copper-shielding surrounding the external surfaces of the solenoids.

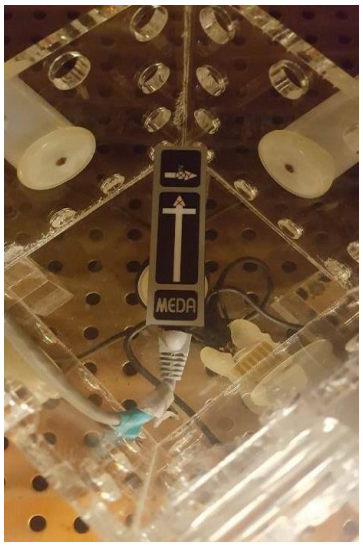

Figure 30. The FVM-400 sensor positioned within the 4D box within the incubator.

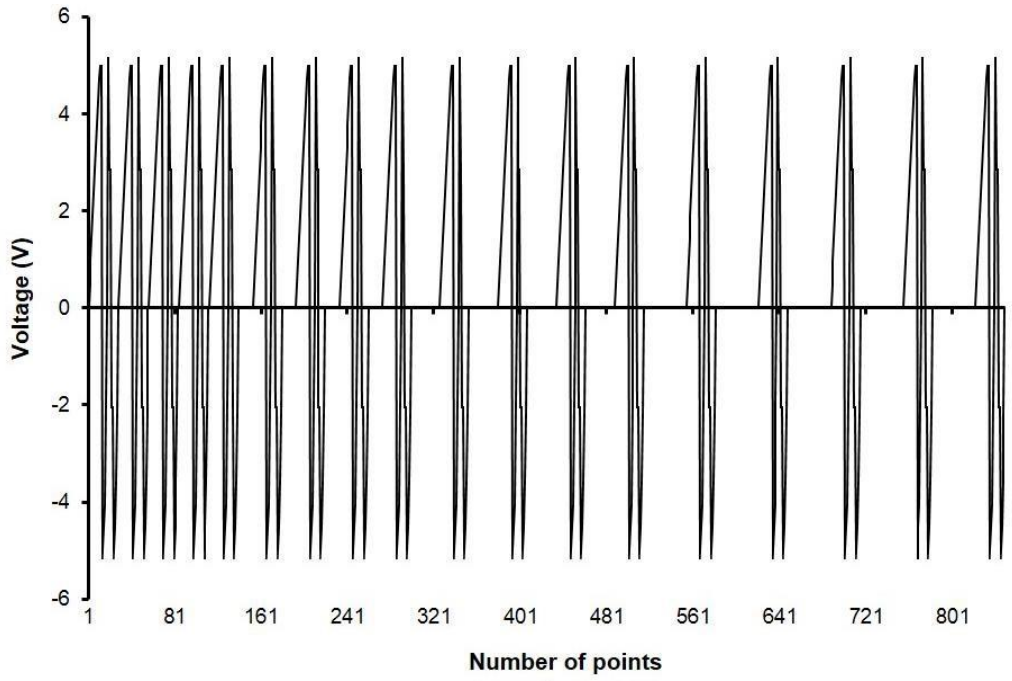

Figure 31. Pattern of the decelerating frequency modulated (Thomas) pattern that elicits more than 50% suppression of malignant cell growth in vitro. Vertical axis indicates voltage that was optimally ±4.3 V. Horizontal axis reflects time in 3 ms increments for a total of 859 points for a total of 2.58 s per cycle.

RESULTS

The measurements within and outside of the incubator when the copper wrapping of the solenoids were off or on are shown in Table 7. The data indicated that when the 4D box was placed within the incubator, the copper wrapping surrounding the solenoids attenuated the intensity of the background electromagnetic field (nT) by ~ 50% within the Y-axis relative to when the solenoids

were uncovered. This effect was not noted when the 4D box was placed outside the incubator ($p>.05$). Effects associated with the other axes were subtle, and required further detailed analysis.

Measurements of Y-axis (Figure 32) field intensity as a function of alternative exposure and inter-exposure temporal increments revealed consistency across most conditions where copper-shielded boxes were generally associated with decreased field intensity relative to non-shielded boxes when placed inside the incubator ($p<.05$). Copper-shielding did not influence field intensity if the 4D box was placed outside of the incubator ($p>.05$). An anomalous effect was noted for the repeated 20 second exposure condition wherein copper shielding did not demonstrate the same field intensity diminishments when the 4D box was placed within the incubator.

	Intensity					
	X-AXIS		**Y-AXIS**		**Z-AXIS**	
Condition	**Outside**	**Inside**	**Outside**	**Inside**	**Outside**	**Inside**
Copper OFF	10007.6	102459.9	10609.18	25301.82	39773.86	50887.76
Copper ON	10078.9	104980.9	10945.42	12518.41	39633.64	46723.92
	% Difference					
	1.00712	1.024605	1.031694	0.494763	0.996475	0.918176

Table 7. Average intensity measures for x-, y-, and z- axes as a function of 4D cell box exposure copper shielded vs non-shielded, and within or outside of the incubator. Note the 50% reduction in static field intensity for the y axis when shielded with copper field.

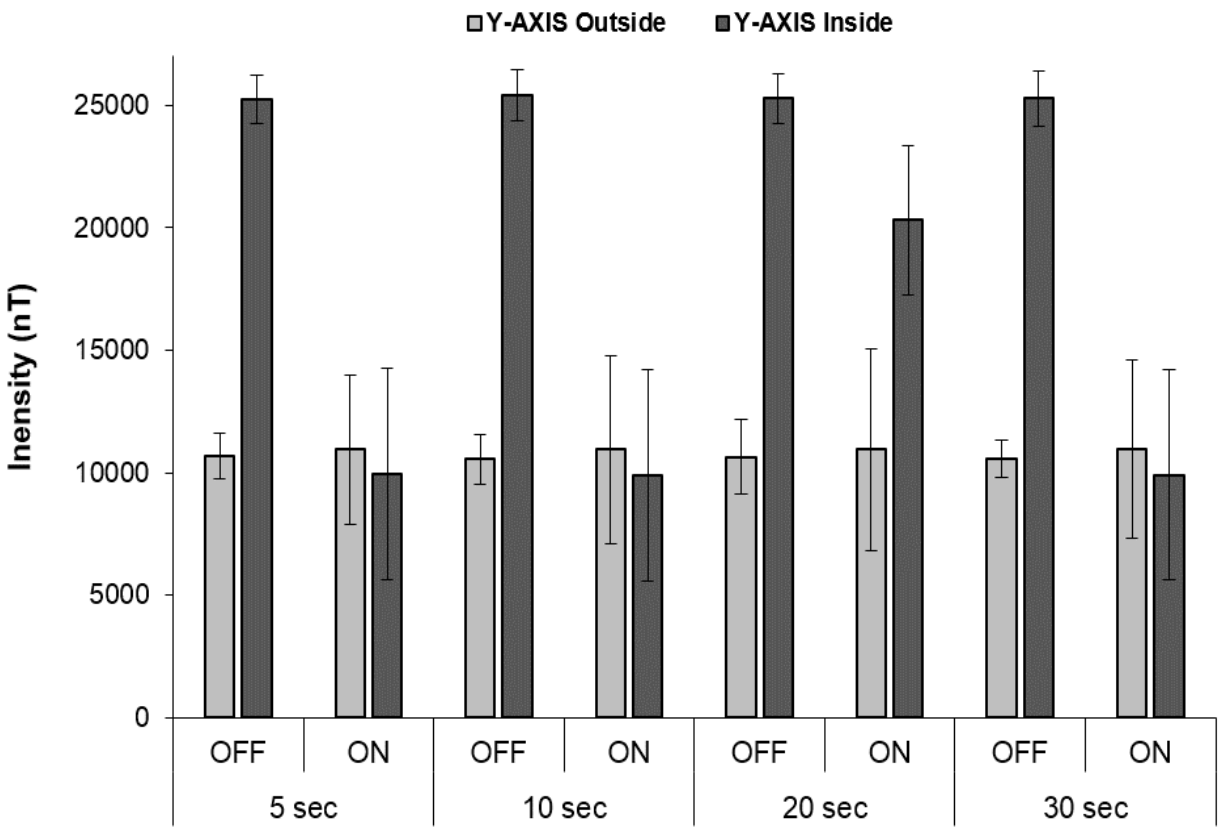

Figure 32. Comparison of the static magnetic field in 4D box shielded with (ON) and without (OFF) copper. It is apparent that application of copper shielding had the strongest effect inside of the incubator, where it reduced the background static magnetic field as compared to no shielding, in all time increments (except 20 seconds) where the copper weakened the effect.

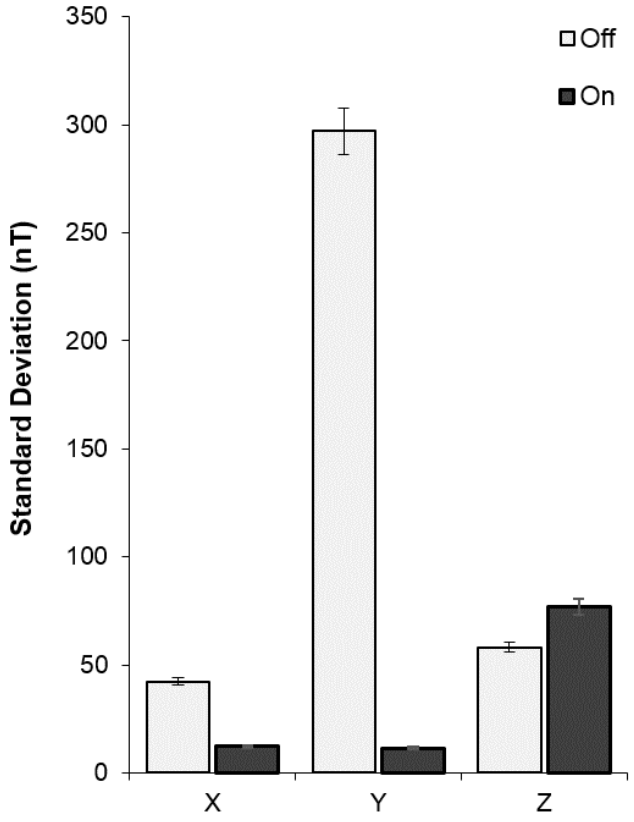

Figure 33. Standard deviation (variability) of field intensity (nT) as a function of X, Y, and Z planes as a function of whether the copper wrapping were either covering (On) or not covering (Off) the 4D box solenoids.

The solenoids were either covered (On) or uncovered (Off) by a copper wrapping. Clear increases in nT variability were noted for the uncovered solenoids relative to the copper-covered solenoids across the Y-axis of the probe [$t(78) = 26.65$, $p<.001$, $r^2 = .90$]. A similar increase in nT variability was noted for the uncovered solenoids relative to the copper-covered solenoids across the X-axis of the probe [$t(78) = 18.19$, $p<.001$, $r^2 = .81$]. However, an opposite effect was noted for the Z-axis where the uncovered solenoids were associated with significantly less nT variability relative to the copper-covered

solenoids [t(78) = -4.32, p<.001, r^2 =.19]. “Variability” within a “steady-state” component of the geomagnetic field contribution has been considered to be a latent source of signals and related potential information that can affect biochemical reactions (Rouleau and Persinger, 2015). Figure 34 reflects the unexpected shifts in the steady-state component of the Y axis of the geomagnetic field (primarily east-west) when the experimental magnetic field was switched on or off for fixed durations. The smaller amplitude dense lines reflect the effects of the Thomas pulse (Figure 31). The configuration is not discernable because of the time scale. When the field was deactivated, there was compensatory steady-state overshoots that remained present (and would affect cells immersed within it) until the experimental field was activated again. There was no systematic pattern with respect to the polarity of the steady-state shift.

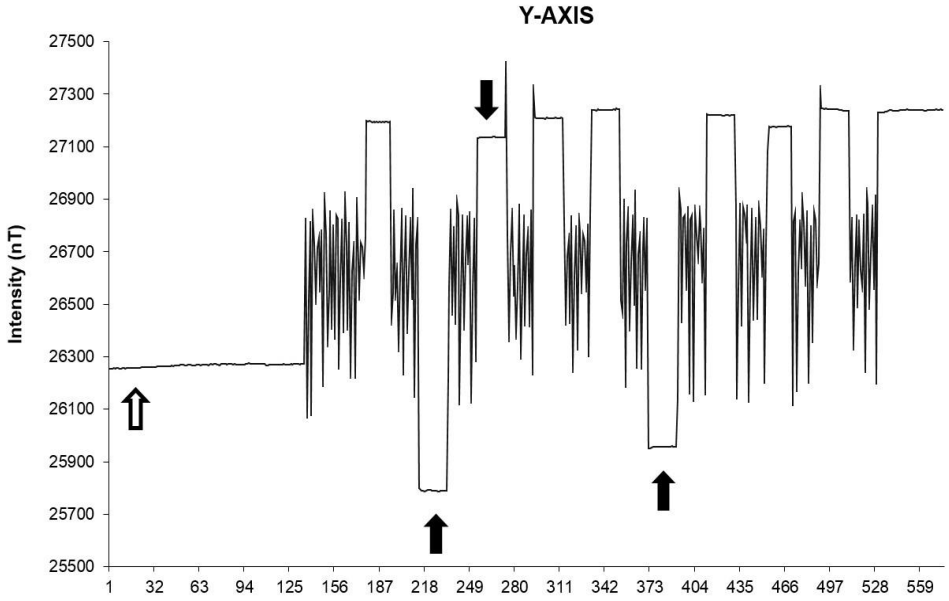

Figure 34. An example of field intensity directional reversals upon initiation and termination of the field exposure over time. The white arrow indicates baseline background field intensity measurements. The initiation of the first field exposure is

indicated by the sharp increase in field intensity at ~ 130 seconds and subsequent high-frequency fluctuations at equal intervals through the trial. The square-shaped deviations as indicated by the black arrows are inter- exposure periods wherein the solenoids were turned off. Note that the baseline or background field intensity reverses direction with respect to the relatively static intensity associated with the electromagnetic field exposure.

Figure 35 illustrates the number of directional reversals of the steady state (geomagnetic) field when the experimental field was activated or deactivated for different durations outside of the incubator. The durations were 5 s, 10 s, 20 s and 30 s. The numbers of pairs of activation-deactivation were between 10 and 15. There was marked consistency within a specific duration. Two effects were notable. First, the number of deviations varied across the different durations of activation and deactivation. Secondly, for one interval (20 s) the presence of copper shielding around the solenoids produced the opposite effect than the other three intervals. When the exposure chamber was placed inside the incubator (Figure 36) this anomaly was eliminated for the 20 s on-off field presentation when the copper shielding around the solenoids was present or not.

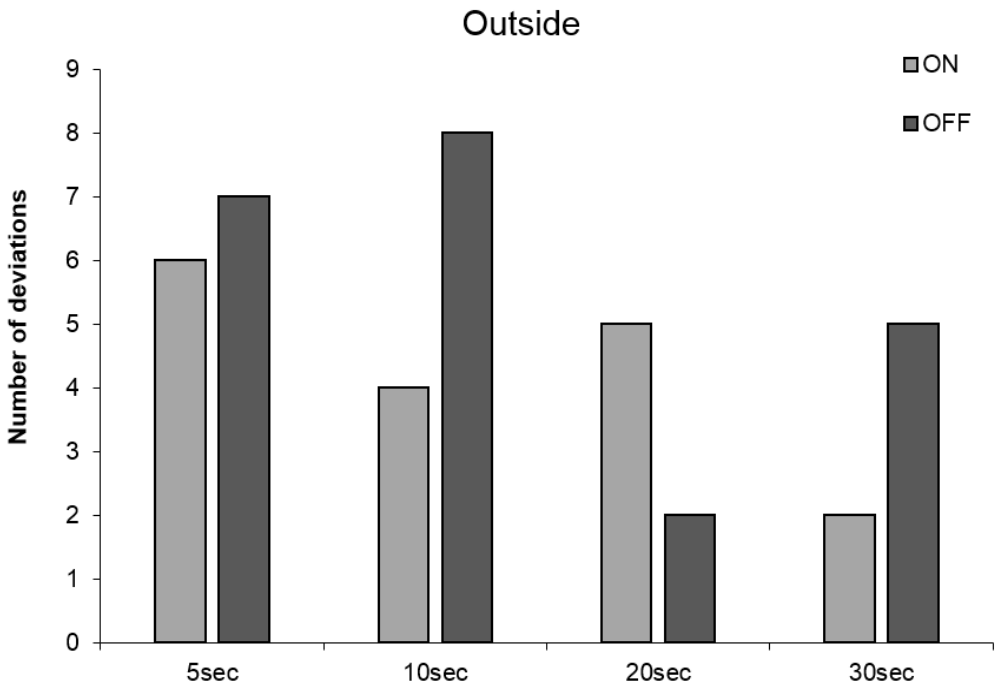

Figure 35. Number of directional reversals associated with field intensity changes (copper on or off) upon serial initiation and termination of the electromagnetic field as a function of the temporal increment of each exposure and inter-exposure period for trials completed within the 4D box positioned outside of the incubator.

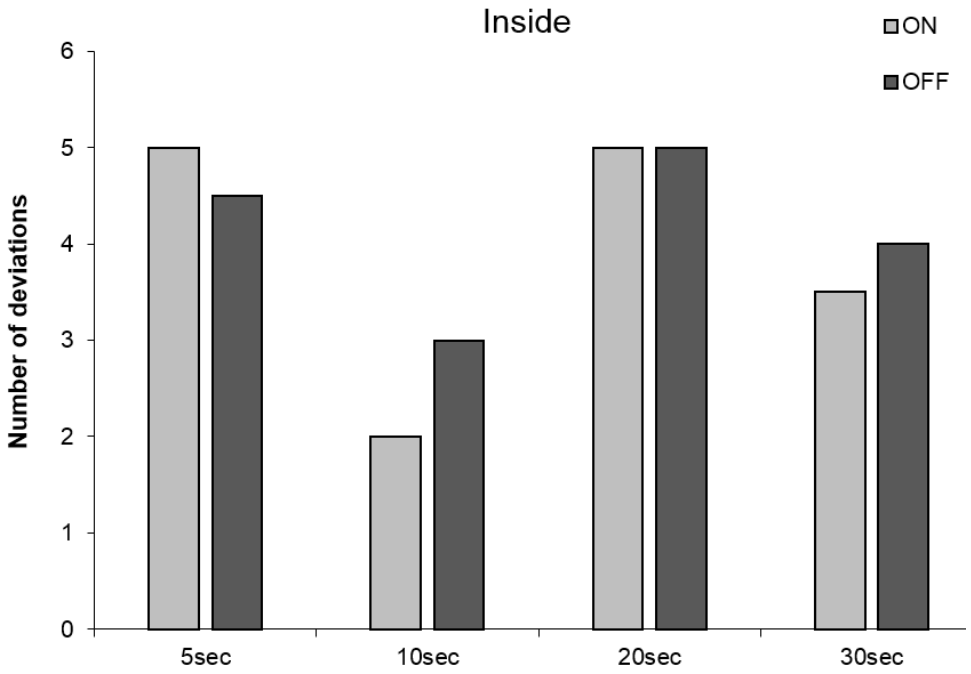

Figure 36. Number of directional reversals associated with field intensity changes (copper on or off) upon serial initiation and termination of the electromagnetic field as a function of the temporal increment of each exposure and inter-exposure period for trials completed within the 4D box positioned within the incubator.

DISCUSSION AND CONCLUSIONS

Researchers who study biochemistry or pharmacology are acutely aware of the importance of molecular structure. The specific spatial configuration of the molecule primarily determines its function although dynamics from the local environment contributes. The potential errors from assuming that all chemical structures behave the same because they share a phenol or indole ring despite different side chains or compositions would be obvious. However, some researchers over-include magnetic field

effects as homogenous phenomena such that electromagnetic fields created by different sources, with different intensities, various spatial application geometries, and different temporal shapes are all considered “magnetic fields” with the implicit assumption of convergent similarity. The results of the experiments reported here indicate that large and unusual shifts in magnetic field intensities within specific planes can occur when magnetic fields are immersed within magnetic fields. Such anomalies may help explain the challenges of replication of the effects of “magnetic fields” upon cellular dynamics in general and the specific inhibition of malignant cells in particular.

There were three major observations that are relevant to exploring the efficacy of applying physiologically-patterned magnetic fields to suppress malignant cell growth such as melanoma. First, wrapping the solenoids (between which the fields were generated) with copper foil did not affect the static magnetic field strength compared to when the solenoids are not wrapped outside of incubators within the normal laboratory environment. This would be expected. There was also no appreciable difference in the values for the Z (vertical) component when the copper metal was wrapped around the solenoid or not and the exposure device was either outside or inside the incubator. When the exposure box was placed within the incubator there was an increase in the intensity of the Y component by a factor of 2. Inside the incubator the presence of the copper around the solenoids markedly reduced this enhancement.

From our perspective the most revealing measurement was the attenuation of the standard deviation or variability of the magnetic field strength during the conditions that are associated with the maximum reduction of malignant cell growth in our experiments. Standard deviation can be employed as an inference of variability of the “signal” within

the field. As shown in Figure 34, activating and deactivating the Thomas pattern was associated with marked steady state shifts in the ambient geomagnetic field that was a greater intensity then the band of variation associated with the experimental magnetic field. We understand that these anomalous transients are generated by the circuitry of the Koren (Koren et al, 2015) digital-to-analogue system. However from the perspective of developing a reliable electromagnetic-field based technology to inhibit malignant cell growth, there are three potentially important observations and derivations.

First, the steady-state shift to produce either an enhanced or diminished geomagnetic ambient accompanied the termination of the experimental field and remained for the duration before the next pattern sequence was initiated. This could be considered the equivalents of “space-markers” containing information that facilitated the effect upon exposed cells. About 20 years ago, Litovitz et al (1997) completed a series of elegant experiments that have been unfortunately not appreciated for their profound significance. They found cells and central biochemical reactions associated with cellular processes such as ornithine decarboxylase activity demonstrated “temporal sensing”. There were critical intervals for disrupting the constantly presented extremely low frequency electromagnetic fields that completely abolished the responsiveness to these fields. If the interruptions were more than 100 ms the field-induced enhancement of ornithine decarboxylase activity was eliminated.

Second, the increased standard deviations in the steady-state transients that occurred when the “effective” experimental fields were off occurred in the horizontal plane (the X and Y components). This could explain an interesting discrepancy between the required spatial rotations associated with the malignant cell slowing effects required for

mice compared to cell cultures. Hu et al (2010) and Buckner (2012) showed that daily exposures of mice injected with melanoma cells required the spatial rotation of the experimental field across each of the three planes separately and then the simultaneous presentation in all three planes. In this context the switch from X to Y to Z to XYZ planes occurred every 0.5 s such that one duty cycle was completed every 2 s. However, for cell culture exposures, the condition employed in the present experiment, all three planes remained activated; the spatial rotation was not required. The discrepancy for maximum effectiveness between mouse and cell may simply reflect the three dimensional (bulk volume) of the mouse compared to the two dimensional (effectively a thin sheet) of cells in culture.

If the latter assumption is valid, then perhaps the mechanism for the malignant cell growth suppression occurs because the effective variability in signals is applied through the thin sheet of cells rather than across the large cross-sectional area. The diameter of the standard cell culture dish is ~6 cm and contains 2.5 cc of malignant cells in suspension. This means that as they proliferate over the typical experimental duration of 5 to 6 days before they approach 100% confluence, the activity occurs within a thin sheet with a thickness of ~1 mm. Unlike an effect from cross section application where individual cells would be influenced by the field independently, generation of the critical component through the thin horizontal plane would allow each cell to contribute the influence from the field to each adjacent cell such that the conditions for the Dicke model (Garraway, 2011) could be satisfied.

Implications of the Dicke Model at MacroQuantum Levels

The Dicke model was developed for quantum optics. However, our (Dotta and Persinger, 2012; Dotta et al, 2013) research suggests that the basic principles and patterns that exist at quantum levels display equivalents within magnetic field exposure systems that employ optocouplers as the primary means by which the circuit is generated (Koren et al, 2015). The physical system described by Dicke is composed of atoms cooperatively interacting with a single mode of an electromagnetic field that is radiating through space-time. This allows for entanglement among multiple particles. For this cooperation to occur one frequency must dominate relative to all others. The resulting rotating wave is an additive (sum) term for the frequency of the cavity in which the atoms occur and the resonant frequency of one of the atoms. According to Garraway's (2011) equations for very large samples of atoms, the uncoupling of the Dicke spin behaves similarly to a giant quantum oscillator. If the atoms are too close dipole-dipole interactions dominant and the symmetry of the Dicke model is compromised.

The containment of the critical components of the effective magnetic fields configurations in the same plane (horizontal) as the cells in culture might be considered a larger scale variant. Although the plate is 6 cm is diameter, with 2.5 cc of cells the thickness would be about 0.9 mm. This might be considered analogous to the "cavity" in the Dicke model. This means that the geometry of the distribution of cells within the magnetic fields is a large sheet where the length of the sheet is about 60 times that of its thickness. The horizontal magnetic fields would be propagated through this cavity. Several different experiments have indicated that the protons associated with hydronium

ion mediate a significant component of the effect. This is based upon the sensitivity of the magnetic field effect to the pH of the solution in which the cells are maintained. Assuming the typical diffusion constant of a proton through the density of cells which display the properties of water to be about ~$0.8 \cdot 10^{-4}$ $cm^2 \cdot s^{-1}$ (DeCoursey, 2003), the frequency associated with a cavity with a depth of 0.9 mm or $0.81 \cdot 10^{-2}$ cm^2 would be ~10^{-2} s or in the order of 1 to 2 min.

This latency is within the range Dotta et al (2014) measured for the emissions of photons from the same type of cell after this particular electromagnetic pattern was applied horizontally across the plates. From this perspective, the influence of the horizontal component containing the effective stimulus configurations from the applied fields upon the constituent cells and the coherence of the small dipoles of the cells through this plane by the Grothuss-like chain movements of protons through the thin sheet (cavity) of cells, may be instrumental in producing the state that promotes photon emissions from the cross-sectional surface. Stated alternatively, the photon emissions would be focused to be emitted perpendicular to the plane through which the charge carriers associated with the magnetic field are moving.

For the Dicke model to be applicable, one mode or frequency must dominate within the large numbers of dipoles (cells) while all others are suppressed. According to our present model the primary involvement of the horizontal plane or thin cavity would be conducive to this condition. The entry of the experimental magnetic fields generated between the two solenoids in the X and the two solenoids in the Y plane could result in generation of waves of protons that begin along the edges of the circular tissue dishes and move towards the center of the plate of cells. Within this focus interference waves

and cancellations would occur such that a dominant frequency would occur. Within this umbra the inhibitory effects of the experimental magnetic field on cell growth should be maximal. This is precisely what is observed by microscopic examination. The cell dropout or diminished cell growth is most apparent in the center of the exposed cell plate within a cross-sectional area that is about one- sixth of the area of the total plate.

According to the Dicke model, if the constituent dipoles are too proximal the symmetry is compromised and the coherence exhibits dissolution. The results of our multiple experiments are consistent with this macrospatial manifestation. We have noted that in those instances where the confluence of the cells were greater (i.e., the cell dipoles were statistically closer) at the beginning of the experiment and hence would accelerate the component of the proximal dipole magnitude, the effects of the applied experimental magnetic field were reduced conspicuously. In the Dicke atomic model reducing the volume, enhances coupling strength. At the level of the cell culture very small reductions in the volume containing the same numbers of melanoma cells, results in more consistent values of reduction in malignant cell proliferation (about 30%). The magnitude of the effect is less than the optimal applications (about 50% decrease cell growth).

The specific frequency that would be enhanced in the coherence between the dipoles of cells should exist as a rotating wave which is the sum of the frequency of the cavity mode ωc and the resonant frequency ωr of one of the constituents, i.e., a cell and the coupling constant, g, between the proximal cells within the cavity. If we ignore the latter or set the value at unity, the contribution of the voltage potential from which the magnetic field is generated becomes salient. Karbowski et al (2016a) indicated that most powerful diminishments of cell growth occurred when the application values were 4.3 V.

Larger values up to the maximum of 5 V or lower values displayed exponential diminishment to that of no field conditions. Assuming the typical value of $3.6 \cdot 10^{-3}$ cm^2 $V^{-1}s^{-1}$ for diffusion mobility (DeCoursey, 2003), the resulting frequency within the cavity $8.3 \cdot 10^{-3}$ cm^2 would be 1.9 s^{-1} or 0.5 s.

The resonant frequency of the constituents, the cells, might be inferred by the amplitude modulations revealed by the spectral power densities of the photons emitted from these cells. The most consistent spectral peak associated with these emissions is ~22 Hz. If the cavity mode is added the primary mode would be 22 to 23 Hz. This is an important number because it is the upper boundary of the frequency spectra for the experimental field when the point durations composing the field were 3 ms. Point durations that were shorter or longer did not produce the suppression of cell growth and did not enhance calcium transport across the cell membrane (Buckner et al, 2015). Within the Dicke model this interesting observation is rationalized because the 3 ms point duration (only) produced an upper boundary that was congruent with the rotating wave generated within the horizontal plane of cells. Experimental data pair the proton with a 3 ms quantum well-like effect derived from the application of Hubble's parameter (Persinger, 2013).

The importance of frequency mode and the temporal order of that mode should be critical to production of cellular effects. This has been verified by Buckner et al (2015). When the experimental (Thomas) field presentation was reversed (generated backwards) there was no inhibitory effect upon cell growth. If only the beginning (22 Hz) fragment or ending fragment (8 Hz) components were presented to the cells, there was also no effect. From the present perspective such precision must occur. The enhancement of a single

mode or frequency through the applied field that would produce the coherent interaction of the cells must occur first before any of the subsequent biochemical reactions and activation of molecular pathways would be initiated. Buckner et al (2015) demonstrated that the likely ion that mediates these effects is calcium through T-type channels. These channels in cell membranes are associated with the electromagnetic properties that govern the latency and thresholds for depolarization or altered resting membrane potentials. In some contexts these channels are associated with “burst firing”.

Such relationships had been found independently in the late 20th century by Pilla et al (1999) who investigated the effects of electromagnetic fields on Ca^{2+} CaM-dependent myosin phosphorylation during non-equilibrium stages of the reaction. The rate of the limiting step according to the Michaelis-Menton kinetics showed temporal sensitivities around 1.5 ms or the ½ wavelength equivalent of the optimal 3 ms point duration that is required to produce the malignant cell suppression effects. Two different rates for Ca^{2+} dissociation occurred in a broad range between 10 and 40 Hz which includes the 8 to 24 Hz spectral range of the experimental magnetic field and 300 to 500 Hz or 3.3 ms to 2 ms which again was the optimal point durations for the incremental voltage shifts that produced the magnetic field. They corresponded to the strong and weak Ca^{2+} binding sites on CAM.

Biochemical systems are highly correlative phenomena containing multivariate phenomena. As a result the actual cause may be obscured by shared temporal variances. Some of the more easily detected phenomenon, such as Ca^{2+} channels, may appear to be the controlling stimulus. However, it may not be the actual (recondite) cause. For example there are more proton channels within most plasma membranes than the sum

of all the other types of channels such as potassium or sodium (DeCoursey, 2003). Proton channels are very likely to be coupled to $Ca^{2=}$ channels in particular (Klockner and Isenberg, 1994; Zhou and Jones, 1996). The conductances of proton channels are strongly pH-dependent. If this is correct than altering the condition of the proton channels which would affect the concentration of H^{+} within the cell should affect the efficacy of the applied magnetic field. Our unpublished experiments have shown that an experimentally-induced pH shift extracellular fluid to 6.8 rather than pH 7.4 enhanced the impact of the field upon growth suppression of malignant cells (Murugan et al, 2016).

Photon Emission Coupling to Proton Related pH

Although the concept of quantum optics is a relatively novel application to cell-cell communication the fact that living systems emit photons has been known for decades. Both Popp (2002) and Persinger (2016) have suggested that photon emissions from cells and organisms represent some proportion of the total cumulative energy from flux density from the sun upon the earth's surface over the last 3 billion years. A first order calculation indicates that the total biomass of the earth is the mass-energy equivalence of this solar photon accumulation. Consequently the prominent role of photon emissions in cell-to-cell communication and as controls of biomolecular signalling pathways might be expected. Photon emissions from cell cultures occur during "disequilibrium" or "stress" to the cellular aggregate or system.

Murugan et al's (2016) experiments that showed more inhibition of melanoma growth rates when the extracellular pH was 6.8 compared to 7.4 also indicated the

enhanced emission of photons from these cells during the more acidic pH. The increase was equivalent to 250 photons per s from a plate of cells. If the inside of the cell displays a compensatory increase in hydroxyl groups then this emission might be associated with diminishment of proton availability. The digital photomultiplier unit was placed under the plate of cells such that photon emissions would be detected within the aperture. Assuming $4 \cdot 10^{-19}$ J per photon, this would be equivalent to 10^{-16} J per s. There are two solutions from this quantity that couple photons with the movement of protons from the hydronium ions that determine pH. The coupling of the two entities might be considered a condition for the Dicke model to be applied as a macroscopic variant of quantum optics.

First, the typical numbers of melanoma cells within a standard dish is about 0.5 million. The area of the dish is 28 cm^2 while the aperture of the photomultiplier unit is not more than 4 cm^2. Consequently the actual number of cells for which the photons were detected would have been in the order of 10^4 cells. This would mean that for each cell the photonic energy would average about 10^{-20} J per s (Persinger, 2010). This unit of energy is associated with resting membrane potential of cells as was the sequestering of ligands to receptors. One interpretation is this precise range of photon emissions represents the enhanced photon emissions associated with decreased Grotthuss chain movement of protons.

The second calculation involves the number of protons that would be more prominent within the extracellular pH. The difference between pH 7.4 and 6.8 is ~$7.2 \cdot 10^{16}$ protons. Assuming the typical volume of a melanoma cells (which is relatively flat in vitro) is 10^{-10} cc, then the displacement outward with the compensatory increase in intracellular pH would be about 10^4 protons per cell. Given the energy for transport of protons through

aqueous phases according to DeCoursey (2003) is about 10^{-20} J, the total energy involved per cell would be 10^{-16} J. This is the photon power measured from the approximately 10^4 cells within the photomultiplier unit's aperture. That the same quantity of energy occurs with the movement of protons within a given cell whose numbers and energies match the numbers of total cells contributing to field is one property of a hologram. In this optic phenomenon the sum of the whole is often equal to the basic unit. This can be considered a form of coherence that is very similar to the properties of a condensate that is usually reserved for very low Kelvin-level temperatures.

Although these quantitative solutions do not prove that the proton movement through the thin layer cavity of sheet of cells is the primary process by which the specific temporal signals within the horizontal components of the applied fields are mediating their cancer- inhibiting effects, the convergent solutions indicate that very small energies and optimal densities of the matter (the protons) contribute to coherence and cooperative interaction. The direct involvement of photons could create the conditions for multi-partite entanglement such that non-local effects could occur across the cells in response to applied magnetic field that would increase the disruption of their growth.

The Role of Copper Metal in Diminishing Beneficial Magnetic Field Effects

The third important result from the direct measurement of the fields is that copper shielding of the solenoids diminished the numbers of excursions within the static magnetic field within the cell exposure area. If these excursions are the essential component that produces the malignant cell suppression, then the recent results reported by Karbowski

et al (2016b) are rational. They found that wrapping specific portions of the external area of the solenoids with copper foil completely eliminated the suppression effects of the experimental fields without altering the intensity of the magnetic field within the exposure areas. There are recent calculations that strongly support the ubiquitous role of the Aharanov-Bohm effect in tuned magnetic field-cell electron interactions (Persinger and Koren, 2016).

In addition these researchers found that the relative distance of the exposure chambers (Figure 29) within incubators that contained copper lining or copper shelving was directly related to the efficacy of the experimental (Thomas) field to produce suppression of melanoma growth. Elevating the exposure chambers closer to the copper shelving diminished the effectiveness. Yet in most laboratories these variables are rarely considered. In our experience the physical properties of incubators for cell culture research, which is the dominant method of examination in contemporary biomolecular sciences, are rarely reported. We have measured substantial ranges in the magnetic fields generated within different types of water- or copper-jacketed incubators that can be as intense as the microTesla-level fields employed by experimenters to assess their effects upon cells. This typically non-documented variable could account for the incubator differences and laboratory differences that contribute to the capacity to replicate or not replicate these phenomena.

Murugan et al (2015) had shown that water exposed in the dark to the patterned field employed in the melanoma studies and in the present measurement of parameters resulted in an enhancement of a specific band of photons between 270 and 305 nm. Aluminum or plastic wrapping of the quantities of spring water during the exposures did

not affect this emission. However those quantities of spring water wrapped by copper sheets did not display this emission band. That the effect was specific to ion-containing water, that is spring water that simulates the physiological condition of cells, was demonstrated by the absence of any magnetic field effect upon differential photon emissions when double-distilled water was exposed to the same field conditions. When only spring water was exposed to the malignancy-slowing, patterned magnetic fields serial shifts in pH occurred within increments of 20 ms to 40 ms (Murugan et al, 2014b) which is remarkably similar to the stacking latency of base nucleotides upon a synthesizing DNA strand.

This band overlaps with the spectroscopic studies of solutes in aqueous solutions reported by Chai et al (2008). They were investigating the long-range interactions between substrates and solvents and discovered the presence of solute free zones near boundaries conditions, exclusion zones, which differentiated this interfacial water from bulk water (Pollack, 2003). The former more typically represents the condition of the cell membrane- water interface. These researchers found an absorption peak within these zones between 250 to 310 nm and fluorescence when excited by 270 nm. Electromagnetic fields can be trapped within atomic aggregates that oscillate in phase with atomic transmissions between ground and excited states reflected by the gap energy (Del Giudice and Preparata, 1994). Karbowski et al (2016c) verified their calculations experimentally. Complex-shaped temporally patterned magnetic fields coherently coupled with (LED) light flashes produced representations of photonic energy within the aqueous suspension of malignant (melanoma) cells. The photons were re-emitted within the subsequent hour after the termination of the field. The total flux power density was

directly proportional to the intensity of the magnetic field presented with the light flashes during the first component of the experiment. Interference with the singular modalities that promote theses coherent domains by copper shielding during magnetic field exposures would be expected to eliminate the modality and hence disrupt the coherence.

If the copper shielding eliminated the emission of the marker for the exclusion zone (EZ) pursued by Pollack over the last three decades (2003), then two implications arise. First, the parallel single modality within the optic range for the Dicke model would involve the 270 nm wavelength. If it is blocked by the quantum consequences of copper shielding then the cooperative dipole coherence between the cells would not occur. Interfacial water has a number of characteristics that could promote cooperation between adjacent cells within the cavity. First adjacent to the surface (such as the membrane) there is a 10 fold increase in viscosity. Very specific physical chemistry within water would set the condition for enter of zero point potential oscillations into the local reaction (Persinger, 2015). Second, and most critically, the separation between the EZ and bulk water near a surface contain a sheet of concentrated protons. The potential difference associated with this sheet ranges in the order of 100 mV which is the same order of magnitude as the plasma cell membrane. Thus the presence of the high density of protons within interface between interfacial and bulk water might be considered a cavity through which further coherence would occur across the cells in the same plane as the horizontal magnetic field.

To date there are only two major means by which to treat and to diminish cancer growth. They are intense ionizing radiation and chemical therapies. Both destroy or disrupt normal cells as well as cancer cells. Both are intrusive, disruptive techniques that

operate primarily upon those cells with the greater division rates or metabolic activity. The potential of the third option, temporally-patterned magnetic fields applied to the entire organism, is that only malignant cells are affected while normal cells are not. The third treatment is not dependent upon blood flow or technology to focus irradiative beams within the volume of the body. However what the third treatment does require is the precise information to switch on and switch off molecular pathways that is comparable to the precision and discrete energies that define quantum phenomena.

References

Adair, R. K. (1991). Constraints on biological effects of weak extremely-low-frequency electromagnetic fields. Physical Review A, 43(2), 1039.

Adey, W. R. (1981). Tissue interactions with nonionizing electromagnetic fields. Physiological Reviews, 61(2), 435-514.

Afsharimani, B., Cabot, P., and Parat, M. O. (2011). Morphine and tumor growth and metastasis. Cancer and Metastasis Reviews, 30(2), 225-238.

Berg, H. (1999). Problems of weak electromagnetic field effects in cell biology. Bioelectrochemistry and Bioenergetics, 48(2), 355-360.

Buckner, C. (2012). Effects of electromagnetic fields on biological processes are spatial and temporal-dependent. Library and Archives Canada.

Buckner, C. A., Buckner, A. L., Koren, S. A., Persinger, M. A. and Lafrenie, R. M. (2015). Inhibition of cancer cell growth by exposure to specific time-varying electromagnetic field involves T-type channels. PLOS ONE, DOI: 10.1371.

Burke, H. E. (1986). Handbook of magnetic phenomena. Van Nostrand Reinhold: N.Y.

Chai, B-h, Zheng, J.-m., Zhao, Q., and Pollack, G. H. (2008). Spectroscopic studies of solutes in aqueous solution. Journal of Physical Chemistry, 112, 2242-2247.

DeCoursey T.E. (2003). Voltage-gated proton channels and other proton transfer pathways. Physiol. Rev. 83, 476-579

Del Giudice, E. and Preparata, G. (1994). Coherent dynamics in water as a possible explanation of biological membranes formation. Journal of Biological Physics, 20, 105-116.

Dotta, B. T. and Persinger, M. A. (2012). “Doubling” of local photon emissions when two simultaneous, spatially separated, chemiluminescent reactions share the same magnetic field configurations. Journal of Biophysical Chemistry, 3, 72-80.

Dotta, B. T., Murugan, N. J., Karbowski, L. M. and Persinger, M. A. (2013). Excessive correlated shifts in pH with distal solutions sharing phase-uncoupled angular accelerating magnetic fields: macro-entanglement and information transfer. International Journal of Physical Sciences, 8, 1783-1787.

Dotta, B. T., Lafrenie, R. M., Karbowski, L. M., and Persinger, M. A. (2014). Photon emission from melanoma cells during brief stimulation by patterned magnetic fields: is the source coupled to rotational diffusion within the membrane. General Physiology and Biophysics, 33, 63-73.

Garraway, B. M. (2011). The Dicke model in quantum optics: Dicke model revisited. Philosophical Transactions of the Royal Society A, 369, 1137-1155.

Hu, J. H., St-Pierre, L. S., Buckner, C. A., Lafrenie, R. M., and Persinger, M. A. (2010). Growth of injected melanoma cells is suppressed by whole body exposure to specific spatial-temporal configurations of weak intensity magnetic fields. International journal of radiation biology, 86(2), 79-88.

Karbowski, L. M., Harribance, S. L., Buckner, C. A., Mulligan, B. P., Koren, S. A., Lafrenie, R. M. and Persinger, M. A. (2012). Digitized quantitative electroencephalographic patterns applied as magnetic fields inhibit melanoma cell proliferation in culture. Neuroscience Letters, 523(2), 131-134.

Karbowski, L.M., Murugan, N.J., Koren, S. A. and Persinger, M.A. (2015a). Seeking the source of transience for a unique magnetic field pattern that completely dissolves cancer cells in vitro. Journal of Biomedical Science and Engineering, 8, 531-543.

Karbowski, L.M., Murugan, N.J., Lafrenie, R.M., and Persinger, M.A. (2016a). Experimental demonstration that Aharanov-Bohm phase shift voltages in optical coupler circuits of tuned patterned magnetic fields is critical for inhibition of malignant cell growth. Journal of Advances in Physics, 11(7), 3557-3563.

Karbowski, L. M., Murugan, N. J., Lafrenie, R. M. and Persinger, M. A. (2016b). Elimination of growth inhibition of malignant cells by specific patterned magnetic fields when source solenoids are wrapped with copper: implications for quantum (Aharanov-Bohm) effects (in submission).

Karbowski, L. M., Murugan, N. J. and Persinger, M. A. (2016c). Experimental evidence that specific photon energies are “stored” in malignant cells for an hour: the synergism of weak magnetic field-LED wavelength pulses. Biology and Medicine, 8:1.

Klockner, U. and Isenberg, G. (1994). Calcium channel current of vascular smooth muscle cells: extracellular protons modulate gating and single channel conductance. Journal of General Physiology, 103, 665-678.

Koren, S. A., Bosarge, W. E. and Persinger, M. A. (2015). Magnetic fields generated by optical coupler circuits may also be containment loci for entanglement of PN junction-plasma cell membrane photons within exposed living systems. International Letters of Chemistry, Physics and Astronomy, 3, 84.

Litovitz, T. A., Penafiel, M., Krause, D., Zhang, D. and Mullins, J. M. (1997). The role of temporal sensing in bioelectromagnetic effects. Bioelectromagnetics, 18, 388-395.

Martin, L. J., Koren, S. A. and Persinger, M. A. (2004). Thermal analgesic effects from weak, complex magnetic fields and pharmacological interactions. Pharmacology, Biochemistry and Behavior, 78, 217-227.

Murugan, N. J., Karbowski, L. M. and Persinger, M. A. (2014a) Weak burst-firing magnetic fields that produce analgesia equivalent to morphine do not initiate activation of proliferaition pathways in human breast cells in culture. Integrative Cancer Science and Therapeutics, 1, 47-50.

Murugan, N. J., Karbowski, L. M. and Persinger, M. A. (2014b). Serial pH increments (20 to 40 milliseconds) in water during exposures to weak, physiologially-patterned magnetic fields: implications for consciousness. Water, 6, 45-60.

[Murugan, N. J., Karbowski, L. M., Lafrenie, R. M. and Persinger, M. A. (2015).Maintained exposure to spring water but not double distilled water in darkness and thixotropic conditions to weak (1 microTesla) temporally patterned magnetic fields shift photon spectroscopic wavelengths: effects of different shielding materials. Journal of Biophysical Chemistry, 6, 14-28.

Murugan, N. J., Karbowski, L. M., Lafrenie, R. M. and Persinger, M. A. (2016). Small shifts in extracellular pH in melanoma cells elicit marked increases photon emission: a potential role for proton channels. (in submission).

Murugan, N. J., Karbowski, L. M., & Persinger, M. A. (2014). Serial pH Increments (~ 20 to 40 Milliseconds) in Water during Exposures to Weak, Physiologically Patterned Magnetic Fields: Implications for Consciousness.Water, 6, 45-60.

Persinger, M. A. (2010). 10-20 Joules as neuromolecular quantum in medicinal chemistry: an alternative approach to myriad molecular pathways. Current Medicinal Chemistry, 8, 1957-1969.

Persinger, M. A. (2013). Experimental evidence that Hubble's Parameter could be reflected in local physical and chemical reactions: support for Mach's principle of imminence of the universe. International Letters of Chemistry, Physics and Astronomy, 11, 86-92.

Persinger, M. A. (2015). Thixotropic phenomena in water: quantitative indicators of Casimir-magnetic transformations from vacuum oscillations (virtual particles). Entropy, 17, 6200-6212.

Persinger, M A. (2016). Spontaneous photon emissions in photoreceptors: potential convergence of Arrhenius reactions and the latency for rest mass photons to accelerate to Planck unit energies. Journal of Advances in Physics, 11, 3529-3537.

Persinger, M. A. and Koren, S. A. (2016). The Aharanov-Bohm phase shift and magnetic vector potential A could accommodate for optical coupler, digital-to-analogue magnetic

field excess correlations of photon emissions within living aqueous systems. Journal of Advances in Physics, 11, 3333-3339.

Pilla, A. A., Muesham, D. J., Markov, M. S. and Sisken, B. F. (1999) EMF signals and ion/ligand binding kinetics: prediction of bioeffective waveform parameters. Bioelectrochemistry and Bioenergetics, 48, 27-34.

Pollack, G. H. (2003). The role of aqueous interfaces in the cell. Advanves of aqueous interfaces in the cell. Advances in Colloid and Interface Science, 103, 173-196.

Popp, F. A., Chang, J. J., Herzog, A., Yan, Z. and Yan, Y. (2002). Evidence of non-classical (squeezed) light in biological systems. Physics letters A, 293(1), 98-102.

Rouleau, N. and Persinger, M. A. (2015). Local electromagnetic fields exhibit temporally non-linear, east-west oriented 1-5 nT diminishments with a toroid: empirical measurements and quantitative solutions indicating a potential mechanism for excess correlation. Journal of Electromagnetic Analysis and Applications, 7, 19-30.

Rouleau, N., Carniello, T. N. and Persinger, M. A. (2016). Identifying Factors Which Contribute to the Magnitude of Excess Correlations between Magnetic Field-Paired Volumes of Water. Journal of Signal and Information Processing, 7(03), 136.

Tonomura, A., Osakabe, N., Matsuda, T., Kawasaki, T., Endo, J., Yano, S. and Yamada, H. (1986). Evidence for Aharonov-Bohm effect with magnetic field completely shielded from electron wave. Physical Review Letters, 56(8), 792.

Vares, D.A.E., Corradini, P.L. and Persinger, M.A. (2016). MicroVolt variations of the human brain (quantitative electroencephalography) display differential torque effects during West-East vernus North-South Orientation in the geomagnetic field. Journal of Advances in Physics, 12(2), 4255-4259.

Zhadin, M. N., Novikov, V. V., Barnes, F. S. and Pergola, N. F. (1998). Combined action of static and alternating magnetic fields on ionic current in aqueous glutamic acid solution. Bioelectromagnetics, 19, 41-45.

Zhou, W. and Jones, S. W. (1996). The effects of external pH on calcium channel currents in bullfrog sympathetic neurons. Biophysical Journal, 70, 1326-1334.

Chapter 10 - Conclusions & Future Directions

The collective studies presented here are demonstrative of a common thread which links electromagnetic fields, light, and biological systems: patterns. At all levels of discourse, from proteins to cells to tissues and organs (whether they be chemical active or not), patterns reveal themselves as deeply engrained within the very fabric of nature. This principle was evident whether we used exclusion filters to discriminate cancerous and non-cancerous cells based upon photon emissions with specific wavelengths or pulsed light coupled with magnetic field patterns to selectively modify melanoma cell proliferation and planarian regeneration. Temporal ordering, wavelength, frequency, inter-stimulus duration, refresh rate, and spatial plane of exposure all proved to be relevant across the various light and electromagnetic field applications.

Having established connections between spectral resonances of proteins involved in typical biomolecular pathways and their photon emission spectra, it was logical to pursue applications of RRM to predict the lethality or spatial prevalence of microorganisms. Even the classification of malignancy could be determined based upon inferences derived from RRM. Re-applying light and electromagnetic fields to cancer cells and planaria demonstrated the utility of RRM, demonstrating reliable modulations of proliferation, regeneration, and even learning. Applied circumcerebrally to human participants, our photostimuli suppressed and enhanced brain activity contingent upon focal points of exposure and wavelength. This was observed even within biological tissue fixed in its spatial and temporal configurations. Finally, a thorough examination of temporal electromagnetic anomalies using either physical (e.g. copper shielding) or

chemical means (e.g. pH manipulation) within the context of cancer treatment was provided. These means of EM alterations are an important parameters that need to be seriously considered when designing EM applications for biomedical uses, as we have shown any alteration in the applied electromagnetic fields properties can enhance, inhibit or negate a response within a biological source. This is analogous to epigenetic mechanism that are responsible for proper protein formation and functioning, any deviation from proper nucleotide sequence translation or transcription can be detrimental to the overall system's functioning.

This thesis describes how a novel bioinformatics tool, the Cosic Recognition Model, can be used to predict the role of a cell's functioning or viral transmission based on the electronic properties of the proteins that encompass them. The emission spectra of these biomolecules indicate that relationships/reactions can be made among other elements that share the same electronic resonance. This implies the static electronic properties of molecules makes them susceptible to fields or the interaction with neighboring molecules with similar electronic properties. The EMF/light exposure studies are a means to activate resonance in these molecules by acting their electronic spectra and consequently alter the biologicals systems functioning.

Future directions should include pursuits from both the observational and manipulative perspectives. This thesis provides a basis for detection of photon signatures which could be ultimately used to diagnose cancers much earlier than is currently possible by means of biopsy or nuclear imaging. Future projects should attempt to increase the classification accuracy of the photo-detection paradigms by including currently untapped variables. Different filters, the use of multiple PMTs, different signal processing methods,

the use of specialized probes, and other innovations would surely move the detection paradigms forward. In addition, harvesting these photonic signatures from healthy cells can be re-applied a as a feedback mechanism into a malignant system to try and “poke the bull” to induce emissions, which can subsequently be used an early detection mechanism. These techniques and experiments can be expanded into the field of neuroscience, where neuropathologies, which stem from dysfunctional patterns of electrical firing, can be treated using applied electromagnetic field therapy if we can “listen” to the problem. Particular advancements in this area could be sufficient to bring the technology to a clinical setting – a possibility which remains urgent in the minds of those expecting novel, non-invasive imaging methods in oncology. Perhaps as significant as a source of concern is the need for a thorough appraisal of RRM as a precise tool to target biomolecules. Future projects should attempt to target well-characterized molecular pathways, systematically targeting signalling proteins which trigger particular events within the cell. Methods of influence should be able to inhibit as well as activate pathways contingent upon target molecules predicted by RRM.